Master's thesis
Astronomy

Parametric studies of galaxy structure and morphology using GALFIT

Antton Jaakko Ilmari Luoma

January 4, 2018

Tutor: prof. Alexis Finoguenov

Censors: prof. Alexis Finoguenov
doc. Hannu Kurki-Suonio

UNIVERSITY OF HELSINKI
Department of Physics

PL 64 (Gustaf Hällströmin katu 2)
00014 Helsingin yliopisto

HELSINGIN YLIOPISTO — HELSINGFORS UNIVERSITET — UNIVERSITY OF HELSINKI

Tiedekunta — Fakultet — Faculty	Laitos — Institution — Department
Faculty of Science	Department of Physics

Tekijä — Författare — Author
Antton Jaakko Ilmari Luoma

Työn nimi — Arbetets titel — Title
Parametric studies of galaxy structure and morphology using GALFIT

Oppiaine — Läroämne — Subject
Astronomy

Työn laji — Arbetets art — Level	Aika — Datum — Month and year	Sivumäärä — Sidoantal — Number of pages
Master's thesis	January 4, 2018	102 pages

Tiivistelmä — Referat — Abstract

The visual structure of galaxies, their morphologies, reveal a lot of information about the ongoing physical processes in galaxies. Galaxies interact gravitationally with each other, so the effects of the environment can be studied via galaxy structure. Galaxy structure can be studied by fitting analytical light profile functions to the observed images. The fitting is based on an assumption that the shape of the galaxy can be described by certain analytical forms. This kind of parametric studies can be done using the GALFIT software. As a result, these fitted models give values for the fundamental parameters describing galaxy size, shape and brightness.

In this Master's thesis I introduce GALFIT as a tool for structural studies and morphological classifications of galaxies. I have gathered a sample of group member spiral galaxies in multiwavelength Hubble Space Telescope CANDELS survey data. I have completed detailed multicomponent and multiwavelength fits for 9 galaxies from the sample of 73 galaxies. The results are used to study stellar mass-to-light ratios and star formation using galaxy colors. Also a variety of asymmetry measurements are calculated for a subsample of these 9 galaxies. The results imply that the fitting process should be unified to measure similar comparable parameters for the entire sample.

I have used my knowledge in GALFIT in a study of galaxies in the infalling groups observed in LoCuSS survey by completing bulge-to-disk decomposition fitting for a sample of several hundred galaxies. The sample galaxies are classified based on the Sérsic indices from my fits and tests verify the classification. The results imply that the effect of mass-quenching is negligible in the infalling galaxy groups. The results also imply that the star-forming galaxies are more elongated than the passive ones, and that the bulge luminosity of the star-forming galaxies rise towards the center of the cluster, however with a low statistical significance.

GALFIT is capable of producing images based on the initial input parameter values if it's not used to fit existing data. I have applied this feature to simulate mock observational data of fields covered in galaxies for the Euclid mission. The images accompanied with catalogs of coordinates, magnitudes and position angles of the objects are used by the Euclid group in Helsinki as independent test data for developing validation tools for Euclid data simulations.

Avainsanat — Nyckelord — Keywords
Galaxies: Fundamental Parameters – Galaxies: Structure – Galaxies: Morphology – Methods: Fitting

Säilytyspaikka — Förvaringsställe — Where deposited

Muita tietoja — övriga uppgifter — Additional information

Contents

List of abbreviations

ACS	Advanced Camera for Surveys
ADU	Analog-to-Digital Units
AGN	Active Galactic Nucleus
CANDELS	Cosmic Assembly Near-infrared Deep Extragalactic Legacy Survey
CCD	Charge-Coupled Device, an electronic light sensor
COSMOS	The Cosmic Evolution Survey
EGS	Extended Groth Strip
FWHM	Full Width at Half Maximum
GAMA	Galaxy And Mass Assembly
GOODS-N	The Great Observatories Origins Deep Survey North
GOODS-S	The Great Observatories Origins Deep Survey South
HST	Hubble Space Telescope
IRAF	Image Reduction and Analysis Facility
LoCuSS	Local Cluster Substructure Survey
PSF	Point Spread Function
SAOImage DS9	Astronomical data visualization and imaging tool developed at Smithsonian Astrophysical Observatory
SDSS	Sloan Digital Sky Survey
SED	Spectral Energy Distribution
SFR	Star Formation Rate
STSCI	Space Telescope Science Institute
WFC3	Wide Field Camera 3
WFPC2	Wide-Field Planetary Camera 2

1. Introduction

1.1 Galaxy structure and galaxy evolution

Galaxy structure has been studied since the first galaxies were observed and it is one of the main methods of describing galaxy properties. Classifications based on the visual morphology of galaxies divide them also to physically different classes. For example spiral galaxies form significantly more stars than elliptical galaxies.

Striking galaxy images are beautiful to look at, but they also present a variety of physical events and features. Bluer clumps in an image of a spiral galaxy reveals places where new, young stars are born. Long winding tidal tails expose the gravitational interactions between galaxies. Signs of light bended by the gravitational lenses lead us to the traces of unseen mass, the dark matter, which encloses the visible parts of galaxies to its haloes.

Evolution of galaxies is studied via galaxy structure. Galaxies and their evolution through cosmic time is a large piece in a puzzle called the Universe, and understanding them plays a major role in understanding the Universe we live in. Our own galaxy Milky Way is a disk galaxy with spiral-like structure. At the center of the Milky Way, there is a bulge of old stars, and at the very center there lies a supermassive black hole. However, Milky Way has not always been exactly like it is today. It's under constant evolution. There are signs of past merger events with smaller galaxies, and we are on the collision course with our largest neighbour

galaxy, the Andromeda.

1.2 Historical overview

The first published detections and descriptions of galaxy structure and morphology were in the tenth century, when the Andromeda was described as a "small cloud" [Kepple and Sanner, 1998]. According to Conselice [2014] galaxies were mainly classified and catalogued during the time before photography. The most noted achievements in cataloguing of galaxies were made by Messier, John Herschel and William Herschel. The third Earl of Rosse, William Parsons was first to describe morphology of a galaxy with a term spiral [Bailey et al., 2005].

After the photography made possible to study galaxy morphologies and structure more conveniently, the most significant development in morphology-based galaxy classification was made by Edwin Hubble [Conselice, 2014]. The Hubble classification is still used in modern astronomy. It was first published in 1926, and established to its final form by Hubble [1936] and Sandage [1961]. Later De Vaucouleurs revised the classification and added criteria e.g. bars and spirals [Conselice, 2014]. From 1960 to late 1980s studies included classification of galaxies based on the form of spiral arms and clumpiness of the light in the arms [van den Bergh, 1960, 1976; Elmegreen and Elmegreen, 1987].

The morphology is not used only for the visual classifications, but there is physics relevant to galaxy formation behind it. Spectroscopy and photometric photometry have proven to be potent tools for quantitative study of structural properties as the technology has advanced [Conselice, 2014].

De Vaucouleurs [1948] proved that elliptical galaxies follow roughly the same light distribution and then Sérsic [1963] formulated general form (Eq. 1.8) of light distribution where de Vaucouleurs profile is embedded as one form of it ($n = 4$). The light profiles can be used to derive bulge and disk components of galaxies, and

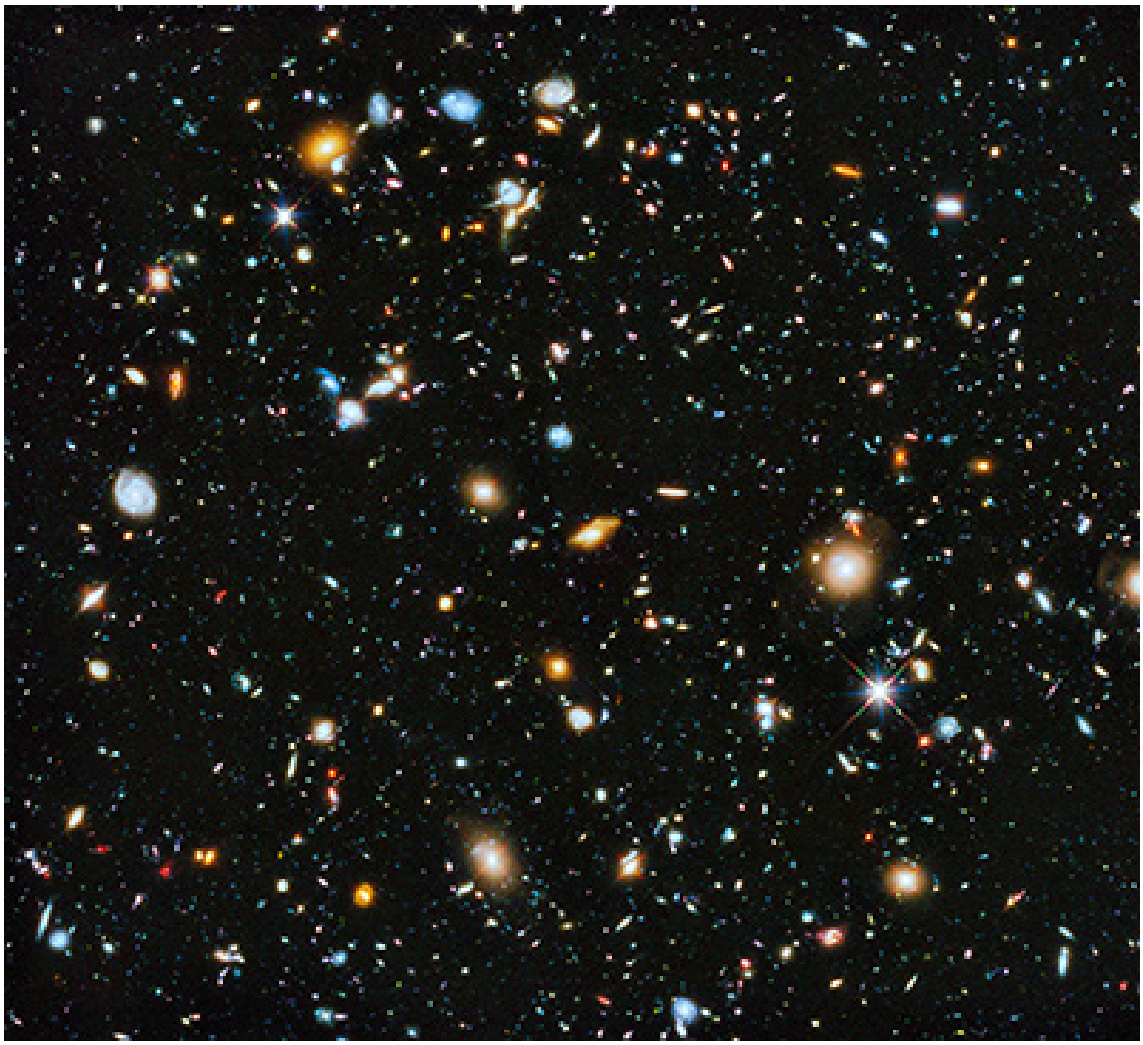

Figure 1.1: Hubble Ultra Deep Field 2014 is a composite of multiple observations by Hubble Space Telescope. The deep image reveals galaxies at high redshifts, i.e. galaxies of the early Universe. The image courtesy of NASA/ESA and STSCI.

light distributions are used in study of internal structure of elliptical galaxies and structure of central bulges, bars and disks of spiral galaxies [Conselice, 2014].

Modern theories describe several non-exclusive ways of galaxy formation: Galaxies can form either by accretion of intergalactic gas or via in situ star formation in collapsed galaxy or through mergers [Conselice, 2014]. After the formation, galaxies evolve through time. This has been observed as the mass density of galaxies changes quickly at $1 < z < 3$ and $\sim 50\%$ of stellar mass is formed by $z = 1$ [Bundy et al.,

2005; Mortlock et al., 2011]. The galaxy structure is clearly different now than e.g. at the highest observed redshift z = 8.

The Hubble Space Telescope (HST) has provided images of thousands of galaxies at redshift z > 1 with its Deep Field observations, and Sloan Digital Sky Survey (SDSS) and Millenium Galaxy Catalog surveys cover vast number of nearby galaxies with both spectroscopic and imaging data [Conselice, 2014]. The comparison of the galaxies at different redshifts is the key in the study of galaxy evolution.

1.3 Methods of structural measurement

The methods of measuring and quantifying structure properties that can be compared between galaxies at different redshifts are introduced in this section.

Visual morphology

Visual morphology is the most classical approach of studying galaxies. Using the Hubble sequence, distant galaxies can be classified to limited classes such as ellipticals, spirals and peculiars or irregulars. The spirals are divided into barred and normal spirals. Many irregular galaxies are too faint and can't be detected at high redshifts [Conselice, 2014]. According to Conselice distant galaxies may not share the same characteristics as nearby galaxies of the same visual morphological type.

Nonparametric measurements

The methods that quantify structure without making assumptions of underlying structure are called nonparametric methods [Conselice, 2014]. So called CAS system (Consentration, Asymmetry and Clumpiness) is the most common of nonparametric methods according to Conselice. These parameters are measurable also at high redshifts [Conselice, 2014].

Often used radius in these measurements is the Petrosian radius defined as the distance where the following ratio $\eta(R)$ reaches some value (usually $\eta(R) = 0.2$):

$$\eta(R) = \frac{I(R)}{\langle I(< R)\rangle}, \tag{1.1}$$

where $I(R)$ is the surface brightness at radius R and $\langle I(< R)\rangle$ is the surface brightness inside that radius [Petrosian, 1976].

Asymmetry index: Asymmetry is measured by comparing the original galaxy image to the same image rotated around the center of the galaxy light [Abraham et al., 1996]. Abraham et al. determine the center by smoothing the image first with a Gaussian kernel and then picking the brightest pixel as the center. Conselice et al. [2000] choose the center by an iterative process that finds the center resulting a global minimum of A. The mathematical form of this asymmetry index is

$$A = \min\left(\frac{\sum |I_0 - I_{180}|}{\sum |I_0|}\right) - \min\left(\frac{\sum |B_0 - B_{180}|}{\sum |I_0|}\right), \tag{1.2}$$

where B_0 and B_{180} are the pixel values of a blank background area, I_0 and I_{180} are the pixel values of the galaxy and subscript 0 stands for the original image and 180° indicates the rotated image [Conselice et al., 2000].

Light concentration: The amount of light concentrated in the galaxy center is measured by using two (often Petrosian, Eq. 1.1) radii which contain fractions of total flux of the galaxy

$$C = 5 \times \log\left(\frac{R_{\text{outer}}}{R_{\text{inner}}}\right) \tag{1.3}$$

[Conselice, 2014]. The most common fraction sizes are 20% with 80% and 30% with 70% according to Conselice. Values of C get higher when larger amount of light is within the inner region. C is strongly correlated with Sérsic index n which also indicates the concentration of light as Conselice [2014] notes.

Clumpiness: Actively star-forming galaxies have clumpy structure. Parameter S describes the fraction of light concentrated to these clumps [Conselice, 2014]. The most common form is

$$S = 10 \times \left[\sum_{x,y=1,1}^{N,N} \left(\frac{(I_{x,y} - I^{\sigma}_{x,y})}{I_{x,y}} \right) - \sum_{x,y=1,1}^{N,N} \left(\frac{(B_{x,y} - B^{\sigma}_{x,y})}{I_{x,y}} \right) \right], \tag{1.4}$$

where $I_{x,y}$ is pixel value of the original image at (x, y), $I^{\sigma}_{x,y}$ is pixel value at (x, y) in a secondary image produced by blurring the original one, and N is the size of the galaxy in pixels [Conselice, 2003]. The multiplication by 10 normalises values of S to a similar level with the other CAS parameters C and A. The smoothing kernel size σ is defined as a function of radius. According to Conselice [2003] the best value for nearby galaxies is $\sigma = 0.3 \times 1.5R(\eta = 0.2)$, where $1.5R(\eta = 0.2)$ is an usual way of using the Pertosian radius with a small multiplier.

Other coefficients: Conselice [2014] introduces Gini/M_{20} parameter which measures the relative distribution of light within pixels. Calculating this coefficient doesn't involve subtraction what makes it less sensitive to high noise levels than the CAS parameters [Conselice, 2014].

Conselice [2014] explains that Gini parameter is originally used in economics to calculate the distribution of wealth within a population. Small values (~ 0) indicate even distribution whereas Gini = 1 means that all light is in one pixel. The Gini parameter is measured by first sorting the pixels into increasing order by their fluxes and then calculating

$$G = \frac{1}{|\bar{f}|n(n-1)} \sum_{i}^{n} (2i - n - 1)|\bar{f}|, \tag{1.5}$$

where $\bar{f}$ is the average pixel flux value, n is the number of pixels, pixel i has flux f_i and $i \in [1, n]$ [Lotz et al., 2004].

M_{20} parameter describes whether the light is concentrated in the image or not. Compared to the parameter C, it does not imply the location of the concentration.

The mathematical form is

$$M_{20} = \log_{10}\left(\frac{\sum_i M_i}{M_{\mathrm{tot}}}\right), \text{ while } \sum_i f_i < 0.2 f_{\mathrm{tot}}, \tag{1.6}$$

where f_{tot} is the total flux and M_{tot} has form

$$M_{\mathrm{tot}} = \sum_i^n M_i = \sum_i^n f_i[(x_i - x_C)^2 + (y_i - y_C)^2] \tag{1.7}$$

[Lotz et al., 2004]. Coordinates of the galaxy center are x_C and y_C.

Conselice mentions one more parameter, the multiplicity index Ψ. It measures potential energy of the light distribution. Newer parameters by Freeman et al. [2013], light profile's multimode (M), intensity (I) and deviation (D) are used in the study of mergers.

Parametric Measurements

Whereas the nonparametric methods do not assume any specific structure of the objects, the parametric methods are based on fitting known profile shapes to the data. The integrated light profiles are used in quantification of galaxy structure [Conselice, 2014]. The aforementioned Sérsic profile by [Sérsic, 1963] has form

$$I(R) = I_0 \times \exp\left(- b(n) \times \left[\left(\frac{R}{R_e}\right)^{1/n} - 1\right]\right), \tag{1.8}$$

where n is Sérsic index and $b(n)$ is a function of n which describes the shape of the light profile so that R_e is the effective radius which encloses half of the galaxy's light [Conselice, 2014].

The most important parameters of galaxy structure are n and R_e [Conselice, 2014]. The effective radius is used to quantify the size of the galaxy. Sérsic index describes the galaxy shape and morphology: elliptical galaxies have $n \approx 4$ which corresponds to the de Vaucouleurs profile and disk galaxies have smaller n since $n = 1$ describes the exponential profile.

GALFIT software, also used in my work, is a tool for fitting two-dimensional profiles to data images. The chapter 2 introduces GALFIT in more details. Another

fitting software for 2D imaging data is the IRAF package GIM2D by [Simard, 1998]. It can be used e.g. in bulge-to-disk decompositions similar to the work presented in chapter 4.

1.4 Aims of the thesis

This thesis introduces three projects in which I worked during summers of 2016 and 2017 as a research assistant in the Observational Extragalactic Astronomy Group in the Department of Physics in University of Helsinki. The aim is to present the goals and the results of the work, to point out the scientific relevance of each project, and showcase GALFIT as a diverse tool for parametric studies of galaxy morphology.

Project of multiwavelength studies of disk galaxies in groups and clusters at different redshifts aims to acquire better understanding of spiral galaxy evolution over cosmic time. The work includes detailed multicomponent light profile fitting with GALFIT. Observational data from the deep HST fields is used to select the sample of spiral galaxies with data in multiple wavebands.

Gained knowledge of GALFIT is applied to a larger data set in a study of structural and morphological parameters of galaxies in clusters and infalling groups. The aim is to study the effects of the dense environment in the evolution and morphology of the galaxies in the infalling groups. My part is to fit two component fits using GALFIT to gain parameter values that can be used in galaxy classification and further analysis.

The aim of the third project is to produce simulated galaxy field images along with the catalogs for data processing tool validation for the Euclid satellite mission. The goal is to adapt GALFIT to produce mock images instead of fitting. This project also introduced me to the Euclid mission and to the possibilities to use my knowledge in profit of the mission.

The structure of the thesis is as follows: Chapter 2 introduces the light profile

fitting software GALFIT. After gaining basic understanding on GALFIT, chapters 3 to 5 contain a detailed desription of studies which are based on GALFIT fitting. Work described in chapter 3 was done mainly during summer 2016 when I was studying spiral galaxies of CANDELS (Cosmic Assembly Near-infrared Deep Extragalactic Legacy Survey) fields. The following chapters address projects I worked in during summer 2017: bulge-to-disk decomposition for group and cluster galaxies in LoCuSS (Local Cluster Substructure Survey) and modeling galaxy images for data reduction tool validation for Euclid satellite project. Finally chapter 6 contains conclusions and a brief overview on future work.

2. GALFIT – 2D light profile fitting

2.1 Brief introduction to GALFIT

As described in [Peng et al., 2002, 2010a] and in the most updated document the GALFIT User's Manual [Peng, 2002], GALFIT is a tool for data analysis that fits analytical functions to observed images. It can model objects from point sources to galaxies with complicated structure with e.g. truncations, spiral arms or irregular, curved shapes. The models are used to extract information from the objects [Peng, 2002].

Installation of GALFIT is really easy as the most recent version of the software is provided only in a binary form in the GALFIT home page [Peng, 2014]. It is explained in the website, that due to copyrighted algorithms used in GALFIT, the source code is not provided publicly.

GALFIT is downloadable for several operating systems as a tar.gz file. The file just needs to be downloaded and extracted to get GALFIT operational. The manual [Peng, 2002] advises to try the first run with the example ready in the `galfit/EXAMPLE` directory. The example is run by the command

`./galfit galfit.feedme`,

where the `galfit.feedme` is the pre-formatted template input file.

The input file of GALFIT is a template file where is a list of all the functions ought to be fitted, the initial parameters for the functions, the input image name, the result image block name, possible constraints file and several other parameters [Peng, 2002]. An example input file is shown in Appendix A.1.

The initial fitting parameters are organized in columns where the first column indicates the parameter number. The second column is for parameter values: The parameter 0 has the function name. Parameters from 1 to 10 have the initial values. Parameter C0 describes the diskiness/boxyness and has values which are negative for disky and positive for boxy models [Peng, 2002]. Parameter Z defines whether the model is subtracted from the data to create residual image (value = 0) or is the model left without subtraction (value = 1).

The third column determines whether the parameter is allowed to vary or not [Peng, 2002]. Number 1 means that the value can be varied and 0 that it can't. Fourth column consists of comments explaining the parameters. All the parameters and the fitting functions are introduced in the manual [Peng, 2002] in detail. That information combined with the comments in the example template file from the GALFIT home page helps to understand how these parameters affect the model.

Running GALFIT in terminal is done by aforementioned command `./galfit` with the input file [Peng, 2002]. GALFIT prints parameter values of each iteration in the terminal during the fitting, so the fitting process can be monitored. Seeing how the parameters change between the iterations gives insight on the convergence of the fit. Even when some of the parameters cause the fit to crash it is helpful to see where the other parameters converge. Adjusting the converging parameters closer to the final values could help with the problematic parameters as well.

GALFIT generates three output files during the run. The `fit.log` text file stores the final parameter values and the errors for the fit [Peng, 2002]. Another file generated is `galfit.NN` where the `NN` is increasing number so output never

overwrites the previous fit. This file contains all of the best fit parameters [Peng, 2002]. The last output file is the data image block which has four extensions: [0] is a blank image, [1] shows the region of data image sized with convolution box size, [2] displays the final model and [3] is the residual image made by subtracting [2] from [1] [Peng, 2002].

GALFIT generates a model image based on the input parameters with exposure time of one second, if the input image name is not given [Peng, 2002]. Then the output .fits file has only one extension: the model. This feature of the GALFIT is used in the project described in chapter 5.

GALFIT uses a map of standard deviations of the data to give relative weights to the pixels during the fitting. If user doesn't provide this sigma image in the input file, GALFIT generates it by itself. For this, GALFIT requires some .fits keywords in the image header [Peng, 2002]. The GALFIT User's Manual states that the `GAIN` and the `RDNOISE` parameters are used in the sigma image generation and the data image should be in units of ADU counts. GALFIT takes the exposure time from the `EXPTIME` header and if it's not found, exposure time of one second is assumed [Peng, 2002]. It is important to check that the exposure time reflects the units of the data.

2.1.1 Analytical light profile functions

GALFIT is a light profile fitting software which has variety of analytical functions to be fitted on data. The available functions are Sérsic, de Vaucouleurs, exponential disk, Gaussian, modified Ferrer, empirical King, Moffat, Nuker, edge-on disk and PSF profiles, and the background sky component [Peng, 2002].

Already introduced Sérsic profile (Eq. 1.8) is really flexible and useful profile, since all de Vaucouleurs, Gaussian and exponential disk profiles are special cases of this function. The Sérsic profile describes de Vaucouleurs profile when Sérsic

index $n = 4$, Gaussian profile when $n = 0.5$ and exponential disk when $n = 1$ [Peng et al., 2002]. However, GALFIT has these functions separately partly because of the historical reasons and partly because of the difference of the size parameters [Peng, 2002].

The exponential disk profile has a size parameter called scale length r_s. The scale length and the effective radius r_e presented in the Sérsic profile have following relation, when $n = 1$ [Peng, 2002]:

$$r_e = 1.678 r_s. \tag{2.1}$$

The exponential disk profile itself has form:

$$\Sigma(r) = \Sigma_0 \exp\left(-\frac{r}{r_s}\right), \tag{2.2}$$

where Σ_0 is the central surface brightness [Peng et al., 2002]. The size parameter of the Gaussian profile is the full width at half maximum (FWHM). The function has form:

$$\Sigma(r) = \Sigma_0 \exp\left(-\frac{r^2}{2\sigma^2}\right), \tag{2.3}$$

where σ is the standerd deviation and FWHM $= 2.354\sigma$ [Peng et al., 2002].

The edge-on disk profile describes a disk galaxy seen parallel to the plane of the disk. The light distribution of a disk component depends strongly on the distance from the center of the disk. The surface brightness distribution of the edge-on disk component has form:

$$\Sigma(r, h) = \Sigma_0 \left(\frac{r}{r_s}\right) K_1 \left(\frac{r}{r_s}\right) \mathrm{sech}^2 \left(\frac{h}{h_s}\right), \tag{2.4}$$

where r_s is the scale length of the major axis, h_s is the scale height from the plane of the disk, Σ_0 is the central surface brightness and K_1 is a Bessel function [van der Kruit and Searle, 1981]. This component uses the central surface brightness as the flux parameter to be fitted:

$$\mu_0 = -2.5 \log_{10}\left(\frac{\Sigma_0}{t_{\exp} \Delta x \Delta y}\right) + \text{mag zpt}, \tag{2.5}$$

where t_{exp} is the exposure time from .fits header, Δx and Δy are the plate scale [arcsec] and mag zpt is the magnitude zeropoint value given by user [Peng, 2002].

The background component is assumed to be flat in GALFIT [Peng, 2002]. The flat plane can be tilted in x and y directions around the central point of the image. User gives a value for the background sky in the center of the image [Peng, 2002]. The background sky value in the center of the galaxy, which most often is not at geometric center of the image, is calculated by:

$$\mathrm{sky}(x, y) = \mathrm{sky}(x_0, y_0) + (x - x_0)\frac{d\mathrm{sky}}{dx} + (y - y_0)\frac{d\mathrm{sky}}{dy}, \tag{2.6}$$

where x_0 and y_0 are the center coordinates, and $\frac{d}{dx}$ and $\frac{d}{dy}$ are the gradients of the sky in x and y directions [Peng et al., 2010a].

The point spread function (PSF) component is not in an analytical function form in GALFIT, but as a convolution PSF image [Peng et al., 2010a]. User provides an image in .fits format that has a PSF flux peak in the center of the image, and the image contains all of the light from the PSF [Peng et al., 2010a].

The rest of the functions GALFIT offers are not used in my work. The modified Ferrer profile is used to fit lens galaxies and central bars [Peng et al., 2010a]. The Ferrer profile has steep outer truncations and flattened core [Binney and Tremaine, 1987]. The King profile is an empirically found function that fits light profiles of the globular clusters [King, 1962]. The Moffat profile [Moffat, 1969] is not widely used in galaxy fitting, but it describes well HST WFPC2 point spread function [Peng et al., 2010a]. The Nuker profile describes the shape of the light profiles at the center of the galaxies with cores [Lauer et al., 1995].

2.1.2 Non-classical fitting parameters

Basis of the GALFIT fitting is the generalized ellipse introduced by Athanassoula et al. [1990]. This elliptical shape has the radial coordinate implemented in GALFIT

as

$$r(x,y) = \left(|x - x_0|^{C_0+2} + \left| \frac{y - y_0}{q} \right|^{C_0+2} \right)^{\frac{1}{C_0+2}}, \tag{2.7}$$

where (x_0, y_0) is the center of the ellipse, q is the axis ratio b/a, where b is semi-minor axis and a is semi-major axis, and C_0 governs the boxiness and diskiness of the isophotes [Peng et al., 2010a]. The shape is a pure ellipse when $C_0 = 0$.

The galaxy fitting requires more than only ellipsoidal shapes. In addition to the C_0 parameter GALFIT has Fourier mode, truncation, coordinate rotation and bending mode parameters to fit realistically different kinds of galaxies from ellipse galaxies to barred spirals and irregulars [Peng et al., 2010a].

The Fourier modes add perturbations to the generalized shape (Figure 2.1). These perturbations have following form:

$$r(x,y) = r_0(x,y) \left(1 + \sum_{m=1}^{N} a_m \cos(m(\theta + \phi_m)) \right), \tag{2.8}$$

where m is positive integer indicating the Fourier mode and a_m is its amplitude, $\theta = \arctan((y - y_0)/((x - x_0)q))$, $r_0(x,y)$ is the radial coordinate of the traditional ellipse and ϕ_m is the phase angle that describes the alignment of the mode from the position angle of the generalized ellipse [Peng et al., 2010a].

The bending modes add curvatures to the model. The curvatures are attained by coordinate transformation that changes the y-axis as

$$y' = y + \sum_{m=1}^{N} a_m \left(\frac{x}{r_{\text{scale}}} \right)^m, \tag{2.9}$$

where r_{scale} is model's scale radius (e.g. r_e for Sérsic profile or r_s for exponential disk) and $x' = x$ [Peng et al., 2010a]. The bending mode $m = 1$ is described as a shear term, the mode $m = 2$ bends the model to U-shape and the mode $m = 3$ folds the model to S-like shape [Peng, 2002].

The structure of spiral galaxies can be fitted with GALFIT because of its coordinate rotation features. The coordinate rotation means that when the image is divided to circular rings around the object, the fluxes within the rings are rotated as

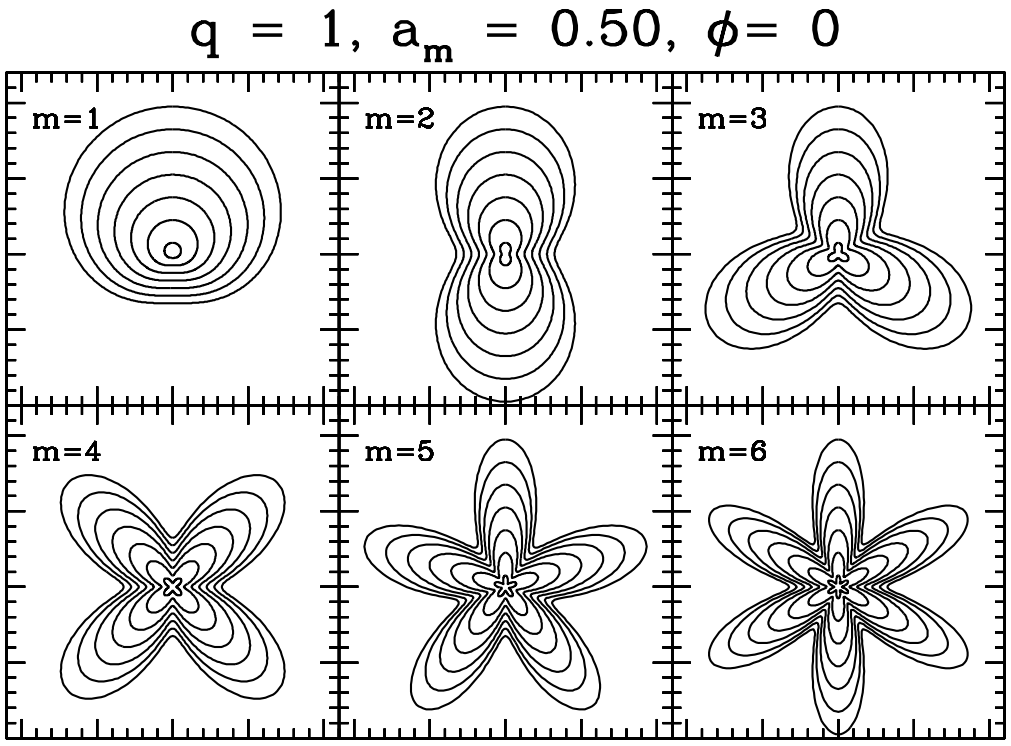

Figure 2.1: Examples of the effects of Fourier modes to a round (axis ratio $q = 1$) generalized ellipse model [Peng et al., 2010a].

some function of radius, $\theta = f(r)$ [Peng et al., 2010a]. GALFIT has two functions for this: The power-law-hyberbolic tangent (α-tanh), which is schematically

$$\theta(r) = \theta_{\rm out}\tanh(r_{\rm in}, r_{\rm out}, \theta_{\rm incl}, \theta^{\rm sky}_{\rm P.A.}; r) \times \left[\frac{1}{2}\left(\frac{r}{r_{\rm out}} + 1\right)\right]^{\alpha}, \tag{2.10}$$

and the logarithmic-hyberpolic tangent (log-tanh), which has schematic form

$$\theta(r) = \theta_{\rm out}\tanh(r_{\rm in}, r_{\rm out}, \theta_{\rm incl}, \theta^{\rm sky}_{\rm P.A.}; r) \times \left[\log\left(\frac{r}{r_{\rm ws}} + 1\right) / \log\left(\frac{r_{\rm out}}{r_{\rm ws}} + 1\right)\right], \tag{2.11}$$

where $r_{\rm in}$ is inner radius where the rotation is 20°, $\theta_{\rm out}$ is the rotation angle at the outer radius $r_{\rm out}$, $\theta_{\rm incl}$ is the inclination angle from the line of sight, $\theta^{\rm sky}_{\rm P.A.}$ is the position angle and $r_{\rm ws}$ is the winding scale radius [Peng et al., 2010a]. Peng et al. introduce the full form of these functions in the appendices of their article.

The truncation functions can be used to restrict the brightness of the model either at the inner part or at the outer region, or both inner and outer parts [Peng

et al., 2010a]. An example case of the need of truncation is a prominent dust lane across the galaxy. The shape of the truncation can be modified with the Fourier modes, bending modes and coordinate rotations [Peng et al., 2010a]. However Peng et al. warn that the truncations should be used carefully and only for objects that has clear truncations, because of the degeneracies between the edge of the truncation and the size of the galaxy might cause numerical problems.

2.1.3 Goodness of fit

GALFIT uses the Levenberg-Marquardt technique to optimise the fit and calculates χ^2 to measure the goodness of fit [Peng et al., 2010a]. The optimization method is an improved least squares fitting procedure by Levenberg [1944] and Marquardt [1963] that can be used for non-linear problems.

GALFIT informs the goodness of fit by the normalized or reduced χ^2_ν [Peng, 2002]. It has form:

$$\chi^2_\nu = \frac{1}{N_{\mathrm{DOF}}} \sum_{x=1}^{N_x} \sum_{y=1}^{N_y} \frac{(f_{\mathrm{data}}(x,y) - f_{\mathrm{model}}(x,y))^2}{\sigma(x,y)^2}, \tag{2.12}$$

where N_{DOF} is the degree of freedom, $f_{\mathrm{data}}(x,y)$ is the input image, $\sigma(x,y)$ is the sigma image either created internally or given as an input, and $f_{\mathrm{model}}(x,y)$ is the model image [Peng, 2002]. Also the χ^2 value is saved to the header of the output .fits file.

In the reduced χ^2 test, the expectation value is $\langle \chi^2_\nu \rangle = 1$ [Bevington and Robinson, 2003]: The fitted model matches the data when $\chi^2_\nu = 1$. When $\chi^2_\nu \gg 1$ the model fits the data poorly. Also values of $\chi^2_\nu < 1$ imply problems with the fit. Very small values indicate that the uncertainties of the fitted parameters are estimated incorrectly [Bevington and Robinson, 2003].

3. Multiwavelength studies of cluster galaxies in CANDELS fields

3.1 Scientific motivation

Magnitude is a fundamental characteristic of galaxies. They are extended objects with no clear edge or boundary where the galaxy ends, so the total brightness is hard to measure from the image data. The total integrated magnitude can be measured by fitting analytical light profiles to the data by using for example GALFIT. Total magnitude and magnitudes in different wavebands, colors, can be used as indicators of a variety of galaxy properties.

The ratio of galaxy stellar mass and galaxy total light can be estimated using magnitudes in g and i bands to calculate the $(g - i)$ color of the galaxy [Taylor et al., 2011]. Also stellar masses can be estimated by using the magnitudes and the empirical relation by Taylor et al.. These estimation methods are introduced in section 3.5.1.

The u and r band magnitudes are used to measure the $(u-r)$ colors of galaxies. It indicates the amount of the galaxy's star formation. This color is also used to classify galaxies to star-forming and non star-forming galaxies [Strateva et al., 2001].

These measurements are presented in section 3.5.2.

Multiwavelength data reveals the internal structure of galaxies as different types of stars are prominent in different wavebands. The stellar populations of galaxies can be resolved using spectral energy distribution (SED) fitting to the multiwavelength data [Conselice, 2014]. SEDs can be fitted to different parts of the galaxy using suitable apertures or even to the entire galaxy pixel by pixel. Detailed multicomponent GALFIT fits can be used to define the aperture shapes and sizes, or the SED fitting can be done to the GALFIT models which have the sky subtracted.

The deep HST images provide information from a wide range of redshifts. The redshift information is important in the galaxy evolution research. Each observation is a snapshot of a galaxy at one point of time. Since following observationally the evolution of a single galaxy is impossible due to long time scales, series of snapshots of galaxies in different redshifts are needed to trace the galaxy evolution. Inspection of the stellar mass estimates and the star formation rates as a function of redshift, shows the evolution of star formation and stellar content of the spiral galaxies in clusters.

The sample consists of spiral galaxies in galaxy clusters. Studying spiral galaxies and their evolution gives understanding of the physical processes that affect also the Milky Way. By selecting cluster galaxies, the environmental effects can be studied as well. Galaxies interact with each other and in dense environments their morphology can be strongly affected by galaxy-galaxy interactions. GALFIT fitting can be used to measure the asymmetries of the galaxies. The GALFIT models can be used also to measure the ratio of symmetric and asymmetric components of the galaxies. The asymmetries of the galaxies can be plotted as a function of distance to the cluster center, to inspect the effect of the location in the cluster to the morphology.

3.2 Gathering the sample

The galaxy sample is gathered from the CANDELS [Grogin et al., 2011] multiwave-band observations with HST. The survey observes the evolution of galaxies and black holes up to $z \sim 8$ and detects high redshift Type Ia supernovae to probe dark energy [Koekemoer et al., 2011]. The CANDELS data [Koekemoer et al., 2011] of four different fields COSMOS, EGS, GOODS-S and GOODS-N, is used to collect the spiral galaxies covered in several bands. The images are from observations obtained with ACS (Advanced Camera for Surveys) and WFC3 (Wide Field Camera 3) detectors of the HST. The sample galaxies are part of the catalog used in [Erfanianfar et al., 2014]. They are identified to be members of X-ray galaxy groups.

The galaxies are checked visually with SAOImage DS9 software to be visible in multiple images taken with different filters. The large survey images are opened in DS9. Galaxy coordinates are saved to a region file which is used to load circles to mark the catalog galaxies to the open image in DS9. The marked coordinates are inspected and flagged if there is a spiral galaxy visible in that image. No elliptical galaxies are selected to the sample. Because of the visual galaxy classification some of the selected galaxies might be mergers, irregulars or edge-on S0 galaxies rather than lone spiral galaxies.

Overall 73 objects are visible in at least two images with different filters. 5 are in three, 21 in four, 4 in five and 11 in six images.

Filter name	Central λ [nm]	Filter name	Central λ [nm]
F160W	1537	F850LP	945
F125W	1249	F814W	833
F105W	1055	F606W	591

Table 3.1: The filter set used in the observations. Filters of WFC3/IR are on the left column and filters of ACS/WFC are on the right.

3.3 Data reductions using IRAF

IRAF (Image Reduction and Analysis Facility) is a software for image reductions and analysis of astronomical imaging and spectral data. It has a vast number of tools for different kinds of operations astronomers need to use for data. IRAF consists of packages that contain the commands, tasks. The tasks can be operated from the IRAF command line or they can be gathered in to a IRAF Command Language (CL) script. PyRAF offers Python-based user interface for running the IRAF commands.

3.3.1 Cropping the images from the mosaics

Survey images are compositions of multiple images, mosaics of exposures, that cover wide fields of sky. Working with these huge images (.fits files with size ranging approximately from 5 to 25 GB) is terribly slow and most of the image area is not used at all, so the objects are cropped first to $10" \times 10"$ sized separate images. This is done by selecting the object from the survey image and putting the object's central coordinates to a Fortran script that calculates the coordinates for the small image corners. The script's output is formatted to match the cutting coordinate input of the IRAF task `imcopy`.

`imcopy input_image_drz.fits[xmin:ymin,xmax:ymax] output_image.fits`,

where `xmin:ymin` and `xmax:ymax` are the pixel coordinates of the lower left and the upper right corner of the area being copied to the output image. The IRAF tasks are written into a CL script so all of the sample objects are cut when the script is run.

3.3.2 Pixel scale

The pixel scale for calibrated WFC3/IR images is 60 mas/pixel (milliarcseconds per pixel) and 30 mas/pixel for ACS/WFC data [Koekemoer et al., 2011]. This means

that the WFC3/IR and ACS/WFC 10" × 10" images cropped out of the wide survey images have different size. This prevents the combination of these images by IRAF, if the pixels are not rescaled.

The IRAF task `magnify` is used to rescale the pixels of the WFC3/IR images. The parameters of the task are given with `epar magnify`: input = @input_image.list, output = @output_image.list, xmag = 1.995 (or 2), ymag = 1.995 (or 2), (interpolation) = linear and (boundary) = nearest.

3.3.3 Unit transformation to ADU counts

The HST images available in the CANDELS website [CANDELS, 2013] have gone through several reduction steps explained in [Koekemoer et al., 2011]. The final results are calibrated to units of electrons per second. The images need to be converted to different units, because GALFIT takes input in units of ADU counts [Peng et al., 2002].

The images are multiplied with their exposure times using IRAF task `imarith`. After this the images are in units of electrons. The `EXPTIME` header keyword values explained in 3.3.4 are used as exsposure times.

When the images are in units of electrons, the last conversion to the ADU counts has form:

$$\texttt{number of counts} = \frac{\texttt{number of electrons}}{\texttt{gain}}, \tag{3.1}$$

[Richmond, 2010]. This conversion is again achieved using `imarith`. Gain is a scaling factor in a detector software that governs the relation of number of electrons collected to a pixel and value of ADU counts in that pixel [Richmond, 2010]. Usually gain factor is selected so that the maximum ADU count value corresponds the maximum number of electrons the CCD is capable of collecting into one pixel. The gain value is taken from `GAIN` header keyword. The origin of the `GAIN` values is explained in section 3.3.4.

These unit conversions are run with a script to all of the images per each field. In writing and running IRAF scripts the parameter `verbose` is set to 'yes', so the results of the operations are printed in the terminal and the results can be checked for possible errors.

3.3.4 Fits headers

GALFIT expects the image .fits files to contain `EXPTIME`, `GAIN` and `NCOMBINE` keywords in the .fits headers. `EXPTIME` is used to calculate the magnitude, and `GAIN` and `NCOMBINE` are used in the calculation of the σ-image. The survey images do not have these keywords in the file headers, but the information is found elsewhere.

The header keywords can be uploaded to the fits header with IRAF task `hedit`. The commands are gathered to scripts which go through every object subdirectory within the field directory. The commands have form:

```
hedit *filtername.fits KEYWORD "value" add+,
```

where `filtername` indicates the filters used in observations, `KEYWORD` is the header keyword (e.g. `EXPTIME`) and `value` is the value wanted to be uploaded to the header.

Exposure times, i.e. the values for the `EXPTIME` keyword are found in the CANDELS website [CANDELS, 2013] in the Readme documents. There is own Readme file for each epoch in each field. The exposure times of the object images are chosen according to the data file they are cropped from, i.e. its epoch. The ACS exposures overlap each other so they effectively double the depth of the exposures. These values of effective exposure time are used in the unit conversions and uploaded to the fits header. The exact effective exposure time values are given for images from COSMOS, EGS and GOODS-N fields and for GOODS-S ACS/WFC images. The GOODS-S WFC3/IR images are cropped from the mosaics made with the images from all epochs. For those the effective exposure time is given as a time range e.g. 2700s – 8100s. I use the average values for the `EXPTIME` keywords. This causes some

errors to the results of the objects in the GOODS-S field.

Keyword `NCOMBINE` tells the number of images used to compose the image file, for example composition of three images would have `NCOMBINE` value of 3. For the used image files the `NCOMBINE` values are already in the headers as 1. In the case that GALFIT doesn't find keyword `NCOMBINE` in the header, the default value 1 is used [Peng, 2002].

The `GAIN` value for the ACS/WFC images is 2 electrons/counts [Koekemoer et al., 2011]. For the WFC3/IR data, the `GAIN` value is 2.5 electrons/counts retrieved from STSCI website [STSCI, nda]. The `GAIN` values were also added by a script with task `hedit`.

3.4 GALFIT

3.4.1 Fitting

After moving the data image to GALFIT's directory, fitting of the model to the data with GALFIT works basically in a following sequence: 1) Setting up the GALFIT input file by adding the input data image name, the result image name and setting the initial values to parameters: functions, coordinates, position angles and so on. 2) Running GALFIT with command `./galfit input.file`. 3) Inspecting the fitting iterations in the terminal. 4) Checking the model visually with DS9. 5) Adjusting the parameter values using the best fit values from `fit.log` file or adding more complex components like bending or Fourier modes. 6) Running GALFIT again.

The manual [Peng, 2002] and the instructions in the GALFIT home page [Peng, 2014] suggest that the models should be started first as simple ellipsoids and the more complicated structure such as spiral arms and Fourier modes should be introduced later at the last step. GALFIT is capable of fitting irregular and complicated structures, but bad initial values and ill-suited models can cause bad solutions

[Peng, 2002]. The selection of fitting profiles is made based on the appearance of the object i.e. edge-on disk function to object which has clear edge-on component and exponential disk profile with coordinate rotation function to object with clear face-on disk with spiral arms.

3.4.2 Fitted models

The GALFIT models are fitted to 9 objects in all of the filters they have data. Figure 3.1 shows the GALFIT output images of the object 29_3 in 5 different bands. Similar images for all of the rest fitted objects are in the Appendix A.3.2. The objects' magnitudes can be calculated using the integrated magnitudes of the models' components (as shown in section 3.6.1).

Table 3.2 presents the goodnesses of the fits. As discussed in section 2.1.3, the ideal χ^2_ν value for the fits would be 1. Most of the fits in column F606W are reasonably close to this indicating that the models represent the data fairly well. In F814W, 29_3 has its best fit, but models of the other objects lie further from the data. In addition, all fits in columns F125W and F160W have $\chi^2_\nu < 1$. This indicates that the models in these bands systematically misinterpret errors or noise, or both of them.

3.5 Colors and structure

Colors of the galaxies depend on the types of stars dominating the light of the galaxy [Strateva et al., 2001]. The color of stars depend on their mass and metallicity. Old low mass stars are red compared to more massive stars, which die younger since they are hotter and brighter, and therefore use their fuel faster.

The filters corresponding best the u, g, r and i bands are checked by calculating

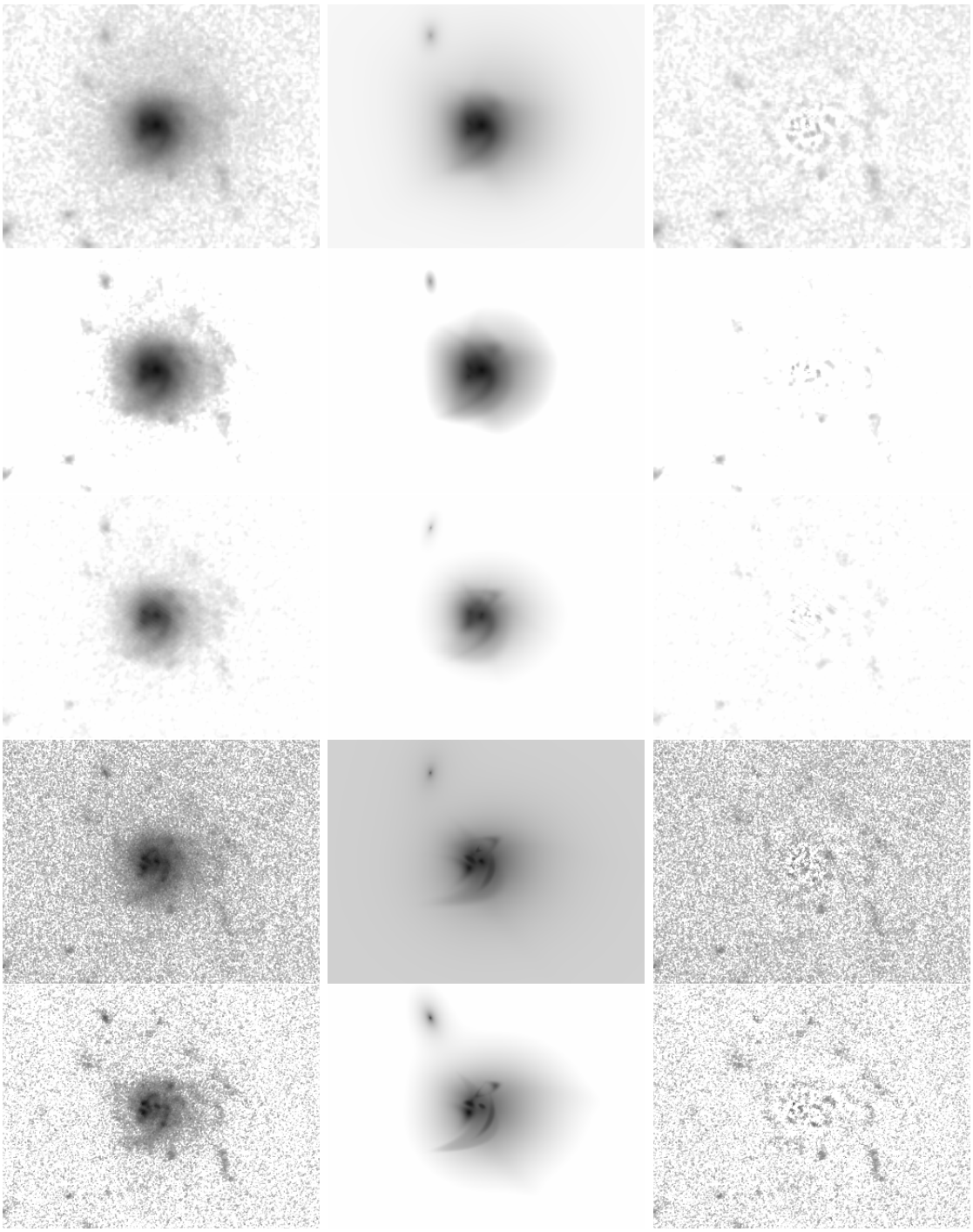

Figure 3.1: The observed images of the object 29_3 are displayed in the left column. The middle column is the GALFIT models obtained with several Sérsic components and the sky estimate. The right column shows the residual image. The used filters are in the following order from top to bottom: F160W, F125W, F105W, F814W and F606W.

The goodness of fit (χ^2_ν)

Obj. ID	F105W	F125W	F160W	F606W	F814W	F850LP
29_3	0.9073763	0.7500263	0.731443	1.174929	1.054925	-
3124_3	-	0.7900451	0.8722909	1.564675	2.644456	-
3124_5	-	0.7887784	0.8042713	1.484647	2.778944	-
3124_6	-	0.7807376	0.7478507	1.370882	2.739916	-
3124_8	-	0.4355423	0.3709593	2.037442	1.874893	-
3124_11	-	0.3552772	0.2767377	1.673889	3.662475	-
3167_2	-	0.7600534	0.7061687	1.421983	6.510676	-
3167_4	-	0.8473853	0.8343813	1.700695	4.808036	-
3167_6	-	0.7528951	0.8086987	1.561793	3.706711	-

Table 3.2: The table shows the χ^2_ν values (Eq. 2.12) of the GALFIT fits to the images observed in different bands.

first the redshifted u, g, r and i wavelengths for all of the sample galaxies:

$$\lambda_{\text{observed}} = (z_{\text{object}} + 1)\lambda_{\text{restframe}}, \tag{3.2}$$

where λs are the wavelengths and the z_{object} is the redshift [Karttunen et al., 2010]. The filter passbands are not fully covering the u, g, r and i bands. The magnitudes of the filters which cover best, or are closest to the bands, are selected. The errorbars in the following plots are not taking the overlap and the misfit of the observed magnitudes to the restframe magnitudes into account. The errors are calculated using standard deviations with the error values given by GALFIT.

3.5.1 Stellar mass and Stellar mass to light relation estimations

The galaxy $(g-i)$ colour can be used to estimate stellar mass-to-light ratio M_*/L [Taylor et al., 2011]. The empirical relation between $(g-i)$ and M_*/L_i has form:

$$\log(M_*/L_i) = -0.68 + 0.70(g-i), \tag{3.3}$$

where L_i is the i band luminosity [Taylor et al., 2011]. The Figure 3.2 shows this relation for the fitted galaxies.

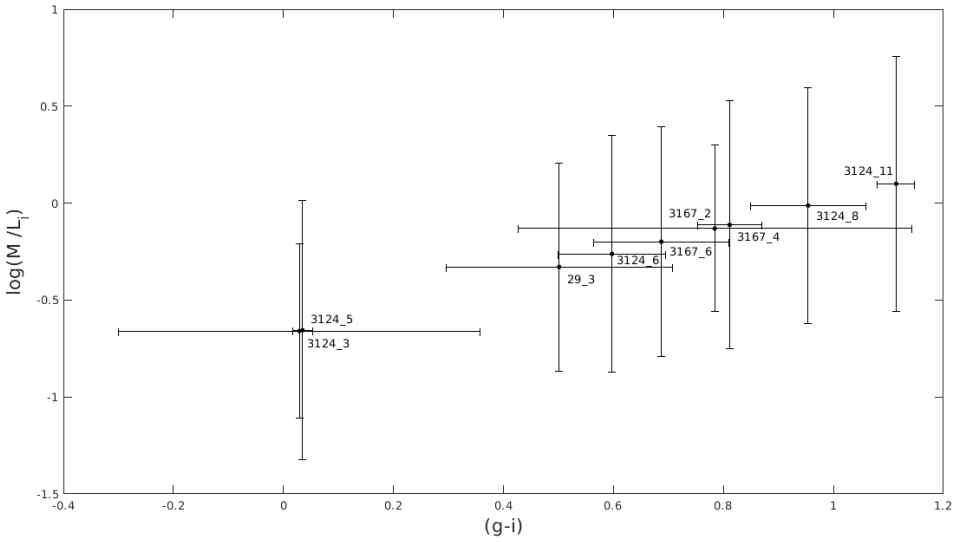

Figure 3.2: The estimation for $\log(M_*/L_i)$ from empirical relation (Eq. 3.3) Taylor et al. [2011] found for galaxies of the Galaxy And Mass Assembly (GAMA) survey catalogue.

Compared to the Figure 12 of Taylor et al. [2011] the $\log(M_*/L_i)$ values in Figure 3.2 are ~ 1.5 smaller than their results for the GAMA catalog galaxies. This difference can be explained by different units. Taylor et al. use the AB magnitude system and the GALFIT model magnitudes are fitted with the ST magnitude system. The conversion between the photometric systems can be calculated with the

information in STSCI website [STSCI, 2012]:

$$\begin{cases} \text{STmag} = -2.5\log_{10}(F_\lambda) - 21.10 \\ \text{ABmag} = -2.5\log_{10}(F_\nu) - 48.60, \end{cases} \tag{3.4}$$

where F_λ is the flux in erg cm^{-2} s^{-1} Å^{-1} and F_ν is the flux in erg cm^{-2} s^{-1} Hz^{-1}.

The galaxy stellar mass can be estimated by rearranging the Eq. 3.3 [Taylor et al., 2011]:

$$\log(M_*/[M_\odot]) = 1.15 + 0.70(g - i) - 0.4M_i, \tag{3.5}$$

where the M_i is the absolute AB magnitude in the restframe i band.

3.5.2 (u-r) colors

The $(u - r)$ colors are used in color classifications of galaxies [Strateva et al., 2001]. The color distribution of galaxies is bimodal and the separation between redder and bluer is at $(u - r) = 2.22$ (in AB system): late morphological type galaxies (Sb, Sc, Irr) have the $(u-r)$ color value less than that separation [Strateva et al., 2001]. The Figure 3.3 shows that the colors of the fitted objects are below 2.22 as expected.

The young hot stars are bluer than the older stars. The regions with high star formation are more prominent in the blue wavelengths. This can be seen in RGB images introduced in section 3.5.3. In order to study galaxy evolution, the amount of star formation traced by the $(u - r)$ colors of galaxies have to be inspected as a function of redshift. This is plotted in Figure 3.4. The $(u-r)$ colors seem to decline towards smaller redshifts. However the 9 objects are not providing enough statistics to make any reliable deductions about redshift's effects to the star formation and the galaxy $(u - r)$ color.

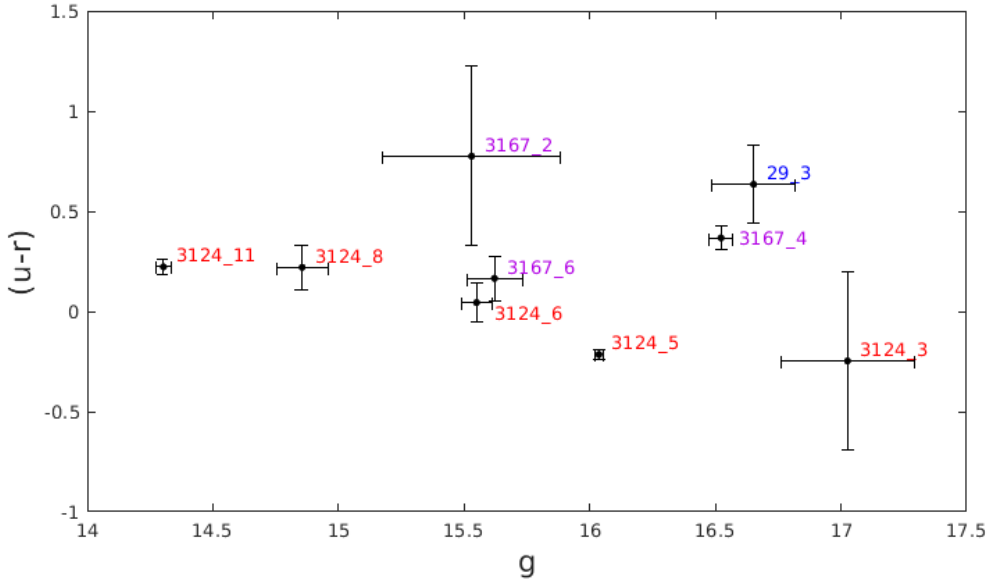

Figure 3.3: Comparing the $(u-r)$ colors versus g band magnitudes. The object marked with blue (29_3) is the only object with data images covering the u, r and g bands. The purple means that the magnitudes of the filters closest to covering the restframe bands was used. The red means that the magnitudes of the filter F606W is used both as u and g magnitudes because it is the closest to u band available and best for g band.

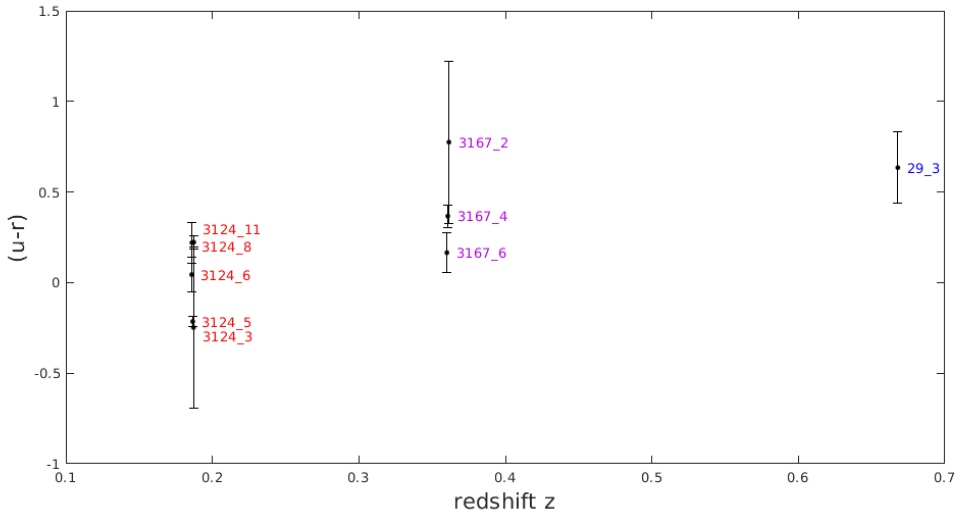

Figure 3.4: The $u-r$ colors are plotted as function of redshift z. The colour coding of the data points is similar to one presented in Figure 3.3.

3.5.3 RGB images

The RGB images are compositions of three images so that the first image is set to red, the second to green and the third to blue. These images display the galaxy structure. The RGB images such as Fig. 3.5 and Fig. 3.6 are made with IRAF and DS9.

The objects' redshifted restframe u, g, r and i bands are calculated with Matlab at first. After this the RGB images are made by IRAF with task `imstack`. The parameters are set manually in PyRAF `epar imstack`. The input image names have to be set in following order: first red, then green and the blue last. The used combination of the images (filters) is written into the title.

The image combination is chosen by comparing the redshifted wavelengths of the u, g, r and i bands to the wavelengths of the filter passbands. The output images resembling best the colours from u to r are named with a label RGB_SF and those with the colours from g to i are named with a label RGB_ML. The best fitting HST filters for the u, g, r and i bands are also checked. These filters are listed in Appendix A.3.3. The observations using these filters would cover the sample and the colors of the galaxies could be calculated reliably.

The .fits images made by `imstack` is opened in DS9. The image scales are adjusted manually so the structure of the galaxy is as clearly visible as possible and the colors are in balance. After being satisfied with the result, the images are saved to .png files.

The RGB images of the GALFIT models are made in a manner described above. The difference of working with extended .fits data cube is that the data image has file extension [1] and the model image in extension [2], and the image names have to have the extension added in `imstack` command. The Figure 3.7 presents the comparison of the RGB images of the data images and the GALFIT model images. Similar images for the other fitted sample galaxies are in Appendix

A.3.1. As seen in Figures 3.7, A.6 and A.7 the fitted models seem to overestimate the blue band.

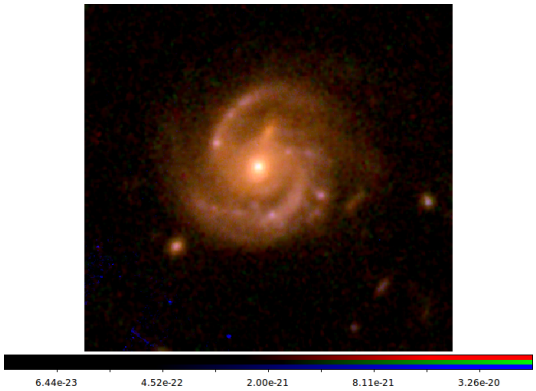

Figure 3.5: The RGB figure which is a composition of three images in different filters: red is F160, green is F125 and blue is F814. Red and blue represent colors closest to restframe i and g colors achieved with available filters.

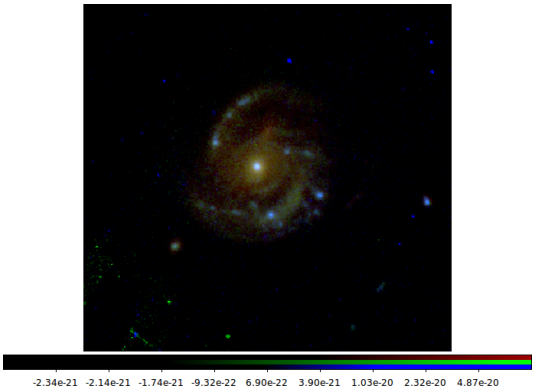

Figure 3.6: The RGB figure which is a composition of three images in different filters: red is F125, green is F814 and blue is F606. Red and blue represent colors closest to restframe r and u colors achieved with available filters.

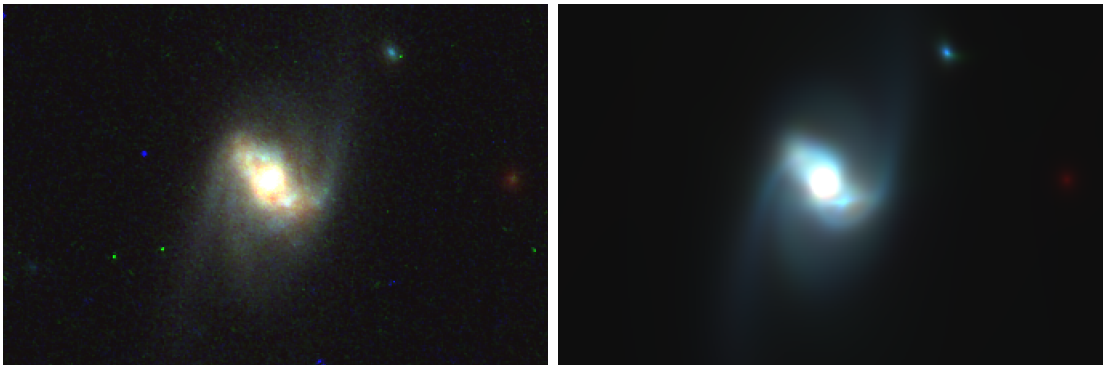

Figure 3.7: The RGB image of the object 3124_8 composed with data images in the left and the GALFIT models in the right. The filters from red to blue are: F160, F814 and F606.

3.6 Results

3.6.1 Magnitudes

The magnitudes of the objects in multiple wavebands are determined using the GALFIT models. The magnitudes can be calculated by combining the integrated

magnitudes of the fitted components. Because of the logarithmic nature of the magnitude scale the magnitudes can't be added together directly. The total apparent magnitude m_{tot} can be calculated by adding the fluxes (F) of the components. From the definition of the apparent magnitude [Karttunen et al., 2010]:

$$m = -2.5\log_{10}(\frac{F}{F_0}) \tag{3.6}$$

$$\rightarrow \frac{F}{F_0} = 10^{-0.4m}, \tag{3.7}$$

where the F_0 is the reference flux. The flux corresponding to the total apparent magnitude:

$$\frac{F_{tot}}{F_0} = \frac{F_1}{F_0} + \frac{F_2}{F_0} + ... + \frac{F_n}{F_0}. \tag{3.8}$$

Replacing the fluxes with Eq. 3.7, the total apparent magnitude comes from

$$10^{-0.4m_{tot}} = 10^{-0.4m_1} + 10^{-0.4m_2} + ... + 10^{-0.4m_n} \tag{3.9}$$

$$\rightarrow m_{tot} = -2.5\log_{10}(10^{-0.4m_1} + 10^{-0.4m_2} + ... + 10^{-0.4m_n}). \tag{3.10}$$

The magnitudes are calculated with a Matlab script using Eq. 3.10. Errors for each component are calculated by GALFIT and total errors per band are calculated using formula

$$\mathrm{Err}_{\mathrm{total}} = \sqrt{\sum_i (\mathrm{Err}_i)^2}, \tag{3.11}$$

where $\mathrm{Err}_{\mathrm{total}}$ is the total error of the magnitude in the band and Err_i is errors of the components' magnitudes [Koppelman, 2005]. The results are presented in Table 3.3.

Some of the analytic functions GALFIT fits have parameter Central surface brightness, instead of Integrated magnitude [Peng, 2002]. For example edge-on disk function (Eq. 2.4) is a component that uses the surface brightness [mag/□"] as the

flux parameter. These components are fitted with multiple Sérsic profiles to get the integrated magnitudes from these components too.

Apparent magnitudes of the objects and the errors of the magnitudes

	F105W	Err105	F125W	Err125	F160W	Err160	F606W	Err606	F814W	Err814	F850LP	Err850
29_3	16.2234	0.1677	16.0845	0.1417	16.1510	0.1223	16.8577	0.1017	16.6523	0.1653	-	-
3124_3	-	-	16.9969	0.1950	17.2063	0.1954	17.0258	0.2643	17.2731	0.3562	-	-
3124_5	-	-	16.0015	0.0092	16.1919	0.0088	16.0364	0.0156	16.2514	0.0214	-	-
3124_6	-	-	14.9520	0.0774	15.0681	0.0500	15.5494	0.0600	15.5053	0.0766	-	-
3124_8	-	-	13.9016	0.0149	13.9427	0.0114	14.8556	0.1031	14.6351	0.0454	-	-
3124_11	-	-	13.1896	0.0185	13.1310	0.0066	14.3034	0.0284	14.0808	0.0246	-	-
3167_2	-	-	14.7458	0.0624	14.6873	0.0500	16.3048	0.2773	15.5298	0.3524	-	-
3167_4	-	-	15.7112	0.0365	15.7076	0.0285	16.8895	0.0403	16.5224	0.0456	-	-
3167_6	-	-	14.9337	0.0531	14.9567	0.0245	15.7861	0.0042	15.6208	0.1110	-	-

Table 3.3: The table shows the total (apparent) magnitudes of the objects based on GALFIT fits and calculated with Eq. 3.10. The errors are based on the error values from GALFIT fits.

Brightnesses in Table 3.3 are several magnitudes higher than expected. The cause of this could be a bad sky estimate or overlapping light contribution from nearby bright sources or hot pixels in the data images. The unexact exposure times discussed in section 3.3.4 could also affect, but for these objects the effect should not be critical: The largest inaccuracy in exposure times are for GOODS-S WFC3/IR objects and 29_3 is the only fitted galaxy in GOODS-S field. All the other fitted objects are in the COSMOS field.

3.6.2 Measurements of asymmetry

The values of A_L, A_E and A_R

Peng et al. [2010a] introduce a method of measuring the asymmetry of galaxy by using the Fourier modes used in the fitting. The method contains three asymmetry parameters: A_L, A_E and A_R. The first is calculated using the amplitude of the

1st Fourier mode. It describes the lopsidedness of the galaxy. A_E measures the deviation from an ellipse and A_R is the characteristic of the rotational asymmetry. The mathematical forms of A_L, A_E and A_R are as follows:

$$A_L = |a_1|, \tag{3.12}$$

where a_1 is the amplitude of the Fourier mode 1,

$$A_E = \sum_{m}^{N} |a_m|, \tag{3.13}$$

where m is the mode, and

$$A_R = \sum_{m=\text{even}} |a_m| \sin^2\left(\pi m \frac{\phi_m}{180°}\right) + \sum_{m=\text{odd}} |a_m| \sin^2\left(\pi m \frac{\phi_m}{90°}\right), \tag{3.14}$$

where ϕ_m is the phase angle in degrees [Peng et al., 2010a].

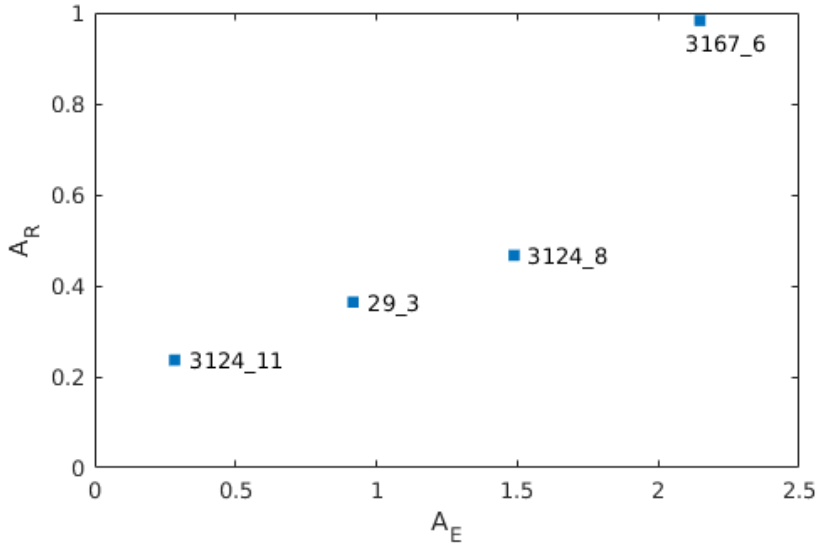

Figure 3.8: The plot compares the total A_R and A_E values of the galaxies. Highly symmetric galaxies would lie near the lower left corner of the figure. Edge-on spirals would lie at lower right corner as they deviate clearly from an ellipse, but have high regularity.

Figure 3.8 shows the comparison of the total A_R and A_E values summed over all of the wavebands. The galaxy 3167_6 stands out as the most asymmetric object of the subsample. Images of this galaxy can be seen in Figure A.16 and the

high A_R and A_E values are easily understood by visual qualitative inspection. Also 3124_8 (in Figure A.12) has values within an expected range.What is surprising in the Figure 3.8, is the location of 29_3 in the plot. The image of the galaxy (Figure 3.1) would intuitively imply slightly higher values. The reason for the low values is that only Fourier mode 1 is used in the fits. This shows that the choice of the fitted components affects significantly to the results.

The right panel of Figure 3.9 shows that the two most asymmetric galaxies from Figure 3.8 (3167_6 and 3124_8) have by far highest A_E values in bluer wavelengths. The 3167_6 shows rise in A_E towards the shorter wavelengths, while other galaxies indicate approximately constant A_E value over the wavebands, at least in the range of available data points.

The comparability of the results is weak, since the fitting process (i.e. the choice of the fitting components) has clear influence to the asymmetry indices A_L, A_E and A_R. It also affects to the subsample size, because all of the galaxies are not fitted using all (or any) Fourier modes. This reduces the statistics of the already small sample. The fitting process should be unified so all of the galaxies have truly comparable A_L, A_E and A_R values.

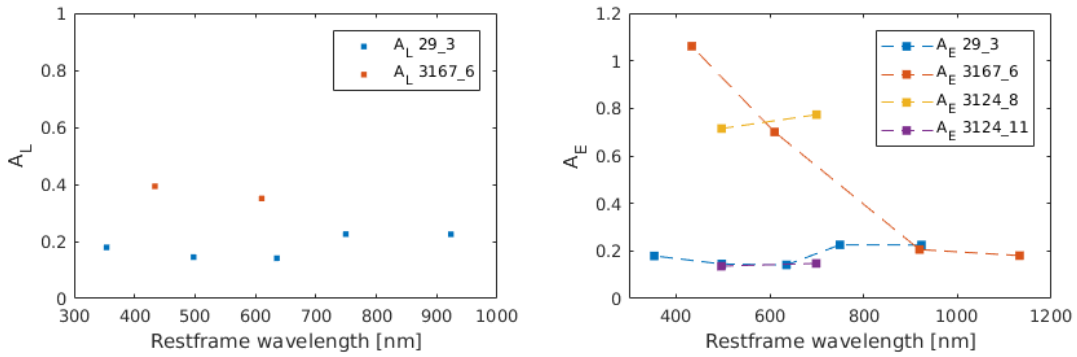

Figure 3.9: Left: The values of A_L presented as a function of restframe wavelength. The wavelengths are calculated using Eq. 3.2. Only two galaxies out of the nine were fitted using Fourier mode 1. Right: A_E is plotted as a function of restframe wavelength.

Figure 3.10 would show possible trends in A_L, A_E and A_R values as a function

of distance from the cluster or group center and as a function of redshift, if the results were reliably comparable and the size of the sample were larger. The asymmetries presumably increase towards the cluster center as the environment is denser and more galaxy-galaxy interactions take place.

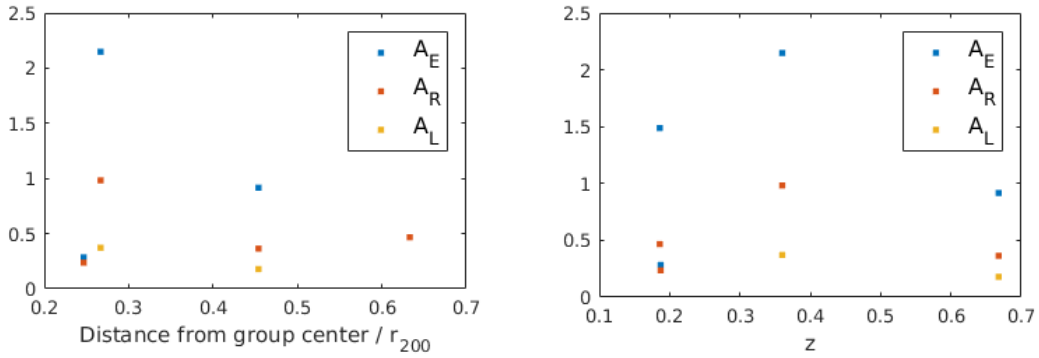

Figure 3.10: Values of asymmetry indices plotted against distance (right) and redshift (left). The blue markers are A_E values while the reds are A_R and the yellows are A_L.

4. Bulge-to-Disk decomposition of LoCuSS cluster galaxies

4.1 Quenching of galaxies

It's well known that galaxy morphology relates strongly with stellar mass, because the most massive galaxies in the Universe are ellipticals. Environment has its effects on morphology as well. By adding morphology-redshift relation, it's been noted that galaxy structure has dependency of its local environment, mass and time [Conselice, 2014].

Some star-forming galaxies cease their star formation and this way produce passive galaxies with quiescent star formation resulting the well known bi-modal distribution of the galaxy population with blue and red galaxies separated by the green valley [Peng et al., 2010b]. The cessation of the star formation is called quenching. Peng et al. found in [2010b] that mass of a galaxy and its environment have clearly separate effects to quenching of galaxies. This result suggest that there are two independent physical processes driving the quenching. Environment quenching is driven by galaxies falling into larger dark matter haloes (satellite-quenching) and mergers, and mass-quenching is a result of feedback processes [Peng et al., 2010b]. However, Peng et al. note that it's possible that some other physical processes can cause similar observational signatures.

Peng et al. define relative environmental quenching ϵ_ρ and mass-quenching ϵ_m efficiencies and show that ϵ_ρ is independent of galactic stellar mass and ϵ_m is independent of environment:

$$\begin{aligned} \epsilon_\rho(\rho, \rho_0) &= (1 - \exp(-(\rho/p_1)^{p_2})) \\ \epsilon_m(m, m_0) &= (1 - \exp(-(m/p_3)^{p_4})), \end{aligned} \tag{4.1}$$

where ρ is density of the environment, ρ_0 is density of a low density reference environment, where environmental effects are expected to be minimum, m is galactic mass, m_0 is very low reference mass at which nearly all galaxies are blue, and $p_1,\ p_2,\ p_3,$ and p_4 are best-fitting parameters to the SDSS and zCOSMOS spectroscopic redshift survey data they used to empirically derive the form of quenching effects. The values for $p_1,\ p_2,\ p_3,$ and p_4 are presented in Table 2 in [Peng et al., 2010b]. By using these relative quenching efficiencies Peng et al. formulate the fraction of red galaxies $f_{\mathrm{red}}(\rho, m)$ as a function of two independent quenching processes [Peng et al., 2010b]:

$$f_{\mathrm{red}}(\rho, m) = \epsilon_\rho + \epsilon_m - \epsilon_\rho \epsilon_m. \tag{4.2}$$

Peng et al. postulate a simple form for mass-quenching:

$$\lambda_m = \mu \mathrm{SFR}, \tag{4.3}$$

where μ is a constant that represents the physics of the quenching process, SFR is galaxy's star formation rate [$\mathrm{M}_\odot\ \mathrm{yr}^{-1}$] and the mass-quenching rate λ_m is a fraction of galaxies that are mass-quenched per unit time [Peng et al., 2010b]. Similar transformation rate for environment quenching has form

$$\lambda_\rho = \frac{1}{(1 - \epsilon_\rho)} \frac{\partial \epsilon_\rho}{\partial \log \rho} \frac{\partial \log \rho}{\partial t}, \tag{4.4}$$

where t is time [Peng et al., 2010b]. Peng et al. use these models in a simulation that evolves galaxy mass functions and red fractions f_{red} over time. The evolving mass functions and red fractions are shown in Figure 4.1.

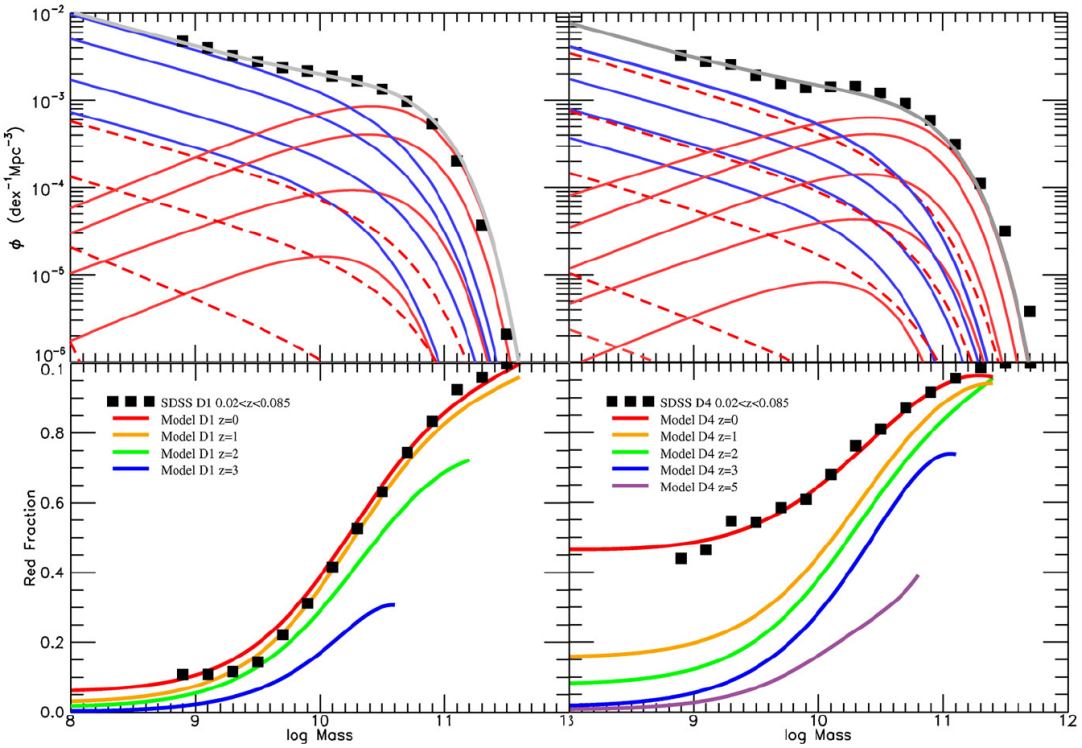

Figure 4.1: Evolution of mass functions (top) and fractions of red galaxies (bottom). The left column shows the model computed for the lowest density region of data Peng et al. used (in $z = 3$, 2, 1, 0), and the right column is computed for the densest quartile of their data (in $z = 5$, 3, 2, 1, 0). Top: The red lines are mass functions of mass-quenched passive galaxies, the dashed red lines represent environment-quenched and merger-quenched passive galaxies, and the solid blue lines show star-forming galaxies [Peng et al., 2010b]. Bottom: The models of evolving red fraction.

4.2 Sample selection and the aim of the study

The Local Cluster Substructure survey (LoCuSS) is targeted to X-ray luminous clusters in range of redshifts $0.15 \leq z \leq 0.30$ and the selected groups are detected to be in the infall regions i.e. the groups are entering, falling, into a halo of a large galaxy cluster [Haines et al., 2017]. These clusters are observed both spectroscopically and photometrically in several bands during multiple surveys as summarised in [Bianconi et al., 2017]. The list of the 23 sample clusters is in the Table 1 of Haines et al. [2017].

The identification of the groups is done by visual inspection of the Subaru

Telescope optical data [Bianconi et al., 2017]. The central group galaxies are identified as they are massive early-type galaxies near the center of the X-ray emission, and the companion galaxies are selected within 3 arcmin and 1000 km s^{-1} from the central galaxy [Bianconi et al., 2017]. A pair of nearby (at $\sim$2 arcmin and $\Delta v < 1000$ km s^{-1}) galaxies is treated as a central object in the cases of no clear central galaxy.

The group member selection is verified by using peculiar velocities

$$|v| = \left| \frac{c(z - \bar{z})}{(1 + \bar{z})} \right| < 500 \text{ km s}^{-1}, \tag{4.5}$$

where $\bar{z}$ is the mean redshift of the group [Harrison and Noonan, 1979], and within the virial radius r_{200} of the group [Bianconi et al., 2017]. The virial radius is estimated by using X-ray luminosity L_X and the scaling relation between the L_X and the virial mass following Leauthaud et al. [2010]. Five groups from [Haines et al., 2017] are excluded as four of them are part of highly disturbed systems and one has mass closer to a cluster than a group [Bianconi et al., 2017].

The work is done in collaboration with Matteo Bianconi from School of Physics and Astronomy, University of Birmingham. The aim of the study is to focus on the environmental effects to the galaxies in the dense infalling groups. The bulge-to-disk decompositions are used in morphological classification of galaxies based on the Sérsic index n. The shape parameters obtained from the fits are used to connect the morphological information with the data from photometry, weak-lensing, X-ray maps and spectral energy distributions.

4.3 Using GALFIT for a large dataset

As described in chapters 2 and 3, GALFIT is basically used for one galaxy at the time. Doing this manually is unreasonable when considering a dataset with hundreds of galaxies in it. The fitting process have to be automated and I do it by a script

that creates an input file and runs GALFIT for each galaxy image in a group or a cluster. The fitting procedure is explained in detail in the next section.

4.3.1 Fitting procedure

Following tools are used in the fitting procedure: text editor, DS9, open terminal window, GALFIT, IRAF, python scripts `galfit_parser.py` and `test_galfit.py` for reading the output parameters, and IDL script `galscript.pro` for running GALFIT for a set of images.

Preparation of the data

In order to work with the script `galscript.pro` the data needs to be sorted according to the galaxy clusters. All images of galaxies in a cluster are placed in the same directory. Fitting can be done one cluster at the time instead of fitting every image one by one.

Lists of the input file names of every cluster are created. Easiest way to do this is 'ls' command in terminal. For example:

`ls cut_*.fits > imagenames.list`,

where 'cut_*.fits' includes all of the data .fits files.

As mentioned before, GALFIT uses some of the .fits header information. The data image headers have to be updated as mentioned in section 3.3.4. Header `GAIN` is set to 2.5, `RDNOISE` to 10 and `EXPTIME` to 1. Values of `GAIN` and `RDNOISE` are from Subaru Telescope's Suprime-Cam instrument parameter web page [Subaru Telescope, NAOJ, 2009].

GALFIT needs a point spread function (PSF) image for fitting. I make PSF images using GALFIT and the information of seeing FWHM found in .fits headers. Seeing FWHM is given in units of arcseconds while GALFIT uses units of pixels, so I convert FWHM to pixels.

GALFIT produces a model image based on parameter values of components given in the input file, when no input data image name is given in the input file. I give GALFIT a Gaussian function component with FWHM equal to the seeing FWHM and a sky component with the sky value of zero. Because the PSF image should be sufficiently large to contain all of the light in PSF profile, I produce 100×100 pixel PSF images. Each cluster has its own PSF image due to different seeing values.

Constraint file is used to fix the center of the exponential disk profile component to the same coordinate as the center of the bulge Sérsic component. This ensures that fitted models represent the bulge and disk components of the same galaxy. Without this constraint, GALFIT could fit these components to different objects. Used constraint files have following form:

```
# Component/    parameter   constraint  Comment
# operation     (see below)   range

  1_2          x          offset        # Hard constraint: Constrains the
                                        # x parameter for components 3, 2,
                                        # 1, and 9 to have RELATIVE
                                        # positions defined by the initial
                                        # parameter file.

  1_2          y          offset        # Hard constraint: Constrains the
                                        # x parameter for components 3, 2,
                                        # 1, and 9 to have RELATIVE
                                        # positions defined by the initial
                                        # parameter file.
```

Scripts

Galscript.pro: The code of this script is in Appendix A.2.1. The IDL script has a variable 'cluster' which is set to correct cluster name. The script needs the path of the file with a list of input image names.

The Figure 4.2 shows schematically the method used in `galscript.pro` to run GALFIT for several images. At the first step, the script reads the names of the input images from a list. Second step is to print GALFIT input parameters to a file

for the first image of the list. After this, the script runs GALFIT and tests if the GALFIT output file is created. These steps are repeated until all images have been fitted. At the end of the script, the output files are created.

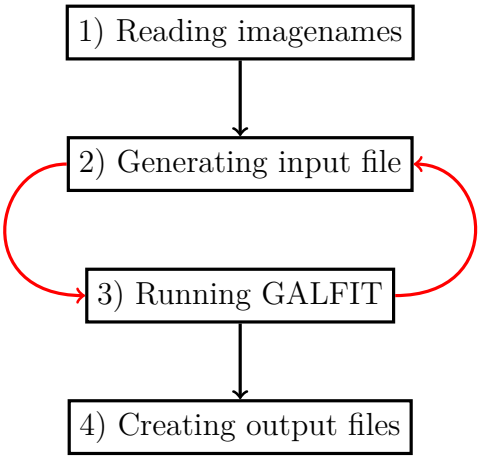

Figure 4.2: The basic principle of the script `galscript.pro`. The red arrows indicate that the steps 2) and 3) are repeated for each image in the cluster before proceeding to the next step.

I used the script in IDL Development Environment: IDL's graphical user interface. When using the script that way it's important to check that IDL console is in the correct directory.

The input file that script produces for GALFIT can be found in Appendix A.1 as an example of GALFIT input file. The zeropoint magnitude parameter value is from data .fits headers and pixel scale is from Suprime-Cam website [Subaru Telescope, NAOJ, 2009]. The size of the convolution box should be sufficiently large. I use box size larger than both PSF image and data image.

Python scripts galfit_parser.py and test_galfit.py: These scripts are used to gather the data from the output .fits files to catalogs. The codes are in Appendices A.2.2 and A.2.3.

The `galfit_parser.py` reads the GALFIT output .fits files. The `test_galfit.py` calls the parser code when it reads the parameter values from the .fits files and saves

them to a text file.

GALFIT marks constrained parameters with braces {}. To remove these braces, lines of code need to be added. Code is presented below. It is added to the IF statement in FOR loop `for param in comp_params`.

```
elif '{' in val: #constrained parameter
val = val.translate(None,'{}*')
          setattr(self,paramsplit[1].lower(),float(val[0]))
          setattr(self,paramsplit[1].lower() + '_err',float(val[1]))
```

The script `test_galfit.py` needs the file path to directories, so they should be updated. It also needs cluster name to be added in the variable 'cluster'. The name of the input file is trimmed. Number of characters to be removed have to be updated. The script leaves only the ID number of the galaxy to the trimmed value to the catalog.

In addition to producing the catalog, the script tests the goodness and the reliability of the fits. The test:

```
for w in range(len(chi2c)):
    Chi2s = np.array(chi2c)
    MAGsErr = np.array(mags_errc)
    nErr = np.array(n_errc)
    MAGexpErr = np.array(mage_errc)
    RsErr = np.array(rs_errc)
    ReErr = np.array(re_errc)
    ArErr = np.array(ar_errc)
    rsc = np.array(rsc)
    rec = np.array(rec)
    if Chi2s[w] > 3000:
        print ID_fc[w],'Chi^2'
    elif nErr[w] > 1:
        print ID_fc[w],'n'
    elif MAGsErr[w] > 1:
        print ID_fc[w],'Mags'
    elif MAGexpErr[w] > 1:
        print ID_fc[w],'Mage'
    elif RsErr[w] > 1:
        print ID_fc[w],'Rs'
    elif ReErr[w] > 1:
        print ID_fc[w],'Re'
    elif ArErr[w] > 1:
        print ID_fc[w],'AR'
```

prints the IDs of those galaxies that have bad initial fits. I use the χ^2 values and

errors of n indices, magnitudes, scale lengths and axis ratios as indicators of the badness of the fit.

Fitting

Running GAFLIT with IDL script: After preparation of the data and the scripts, the fitting can be started. It's simply done by compiling and running the `galscript.pro` IDL script.

Fitting the failed fits: The script saves the file names of the objects for which GALFIT failed to fit the galaxy and crashed without producing an output image block. The list is in the file called `galscript.output`. These objects are first checked with DS9 and then refitted with better initial parameter values.

First the input file created by the IDL script is copied to a new file `test.input`:

```
cp galscript.input test.input
```

The file is opened in the text editor (I use Pico):

```
pico test.input
```

The data image of the object is opened in DS9 for visual inspection. The reason which caused GALFIT to crash is searched and then the GALFIT input file is updated. GALFIT is run by command:

```
./galfit test.input
```

The input and output image names should be updated to the `test.input`.

After fitting the objects listed in `galscript.output`, the list of the fit files is updated:

```
ls gal2_cut_* > fits.lis
```

Python script uses this list to read parameters from all of the fitted images. If this list is not updated after fitting the crashed cases, they are left out of the file which has the parameters saved.

If the data image is contaminated by strong artefacts and fitting can't be done, the name of the file is removed from the `fits.lis` file.

Reading the output parameters: The script `test_galfit.py` is run with command:

```
python test_galfit.py
```

The script saves the fitted parameters to a file and prints to terminal IDs of the objects that have bad fits. The criteria I use are arbitrary, but they reveal large number of fits that can be enhanced. The criteria are $\chi^2 > 3000$ and magnitude, radius, Sérsic index and axis ratio errors greater than 1.

If there is too few objects in the cluster the script is not able to read the parameters. Copying some of the resulting .fits images and adding them also to `fits.lis` helps in this. After running the script, these excessive lines are removed from the result file manually.

Enhancing the fits: Enhancing the fits requires individual inspection of the objects listed by the Python script. By opening the GALFIT result image block in DS9, the data image and the fitted model can be compared visually. This helps determining the way to adjust the input parameters. The GALFIT output .fits files are opened as multiple extension cube in DS9:

`File` → `Open as` → `Multiple Extension Cube`.

The first image is blank, second is the data image, third is the fitted model and the last one is the residual image.

The most usual reasons why χ^2 of the fits are large, are the neighbouring objects, bad initial parameters and in some cases artefacts. Bright objects in the image or highly elliptical objects can cause troubles with getting good fits.

The process consists of adjusting the parameters in a text editor and running GALFIT in terminal. Looking how the parameters evolve during iterations helps to decide which parameters should be adjusted further. Process of getting better fits consists quite a lot of try and error.

Finishing and moving to the next cluster: After all of the initial fits are enhanced, the final check on the parameter values is done before starting with the next cluster. If the final check reveals some parameters standing out as clearly too large or somehow else anomalous, those galaxies need to be refitted. If the fit can't be enhanced further, it will stay as an outlier.

The fitting process is started again from the beginning when advancing to the next cluster. The scripts need to be updated before running them. The fits are done by running the IDL script and the problematic fits need individual fitting.

4.4 Results

The visualizations of data presented in this section are made for an article in preparation [Bianconi et al.]. The result parameters of the fits are combined with the knowledge of the objects obtained using different methods.

The Sérsic indices of the fitted bulge components are used in the morphological classification. The Figure 4.3 shows the classification in three wavebands. The Sérsic indices are presented against the stellar masses of the infalling galaxies. The plots test the Sérsic classification by comparing it to the observed photometry of these galaxies. The blue star-forming galaxies should lie on the left side of the figure, as the low n indicates the disk-like morphology. The ellipticals should lie near the

upper right corner as the high stellar mass, red color and $n \approx 4$ combined indicate the elliptical galaxy type. The plots show this behaviour, so the classification based on the n values is justified.

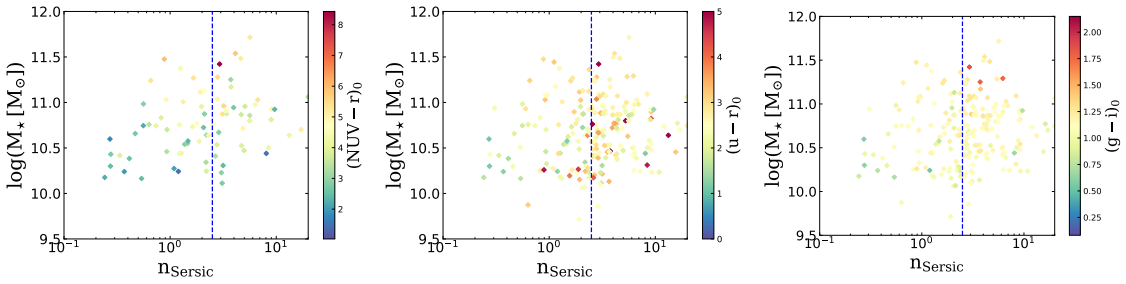

Figure 4.3: The plots show the Sérsic index against the stellar mass of the infalling group galaxies. The color coding is in respect to restframe wavelengths: k-corrected $NUV - r$ (left panel), $u - r$ middle panel and $g - i$ (right panel). The disk-dominated galaxies ($n_{\text{Sérsic}} < 2.5$) and the bulge-dominated galaxies ($n_{\text{Sérsic}} > 2.5$) are separated with the vertical dashed line.

Figure 4.4 compares the star-forming and non star-forming galaxies by their axis ratios (left panel) and the bulge-to-disk ratio (right panel) as functions of clustercentric radii in infalling groups. Studying the morphological information as a function of distance from the center of the cluster gives insight to the effects of the environment. The galaxy-galaxy interactions and mergers increase towards the center. The left panel shows that the star-forming galaxies tend to be slightly more elongated than the passive galaxies. However, the significance is low, so more data is needed to derive definitive conclusions about this tendency.

The right panel of Figure 4.4 shows that the bulge-to-disk ratio of the passive galaxies is constant through the range of clustercentric distance. The star-forming galaxies show tiny increase of bulge luminosity towards the center of the cluster. This also has quite low significance, so more data is needed to conclude if there really is a rise in bulge luminosity near the core or not. The fits of both axis ratios and bulge-to-disk ratios can suffer from projection effects, i.e. the results of the fits can differ if the galaxies are observed from different angle. Some galaxies might

seem more elongated if they are observed edge on instead of face on.

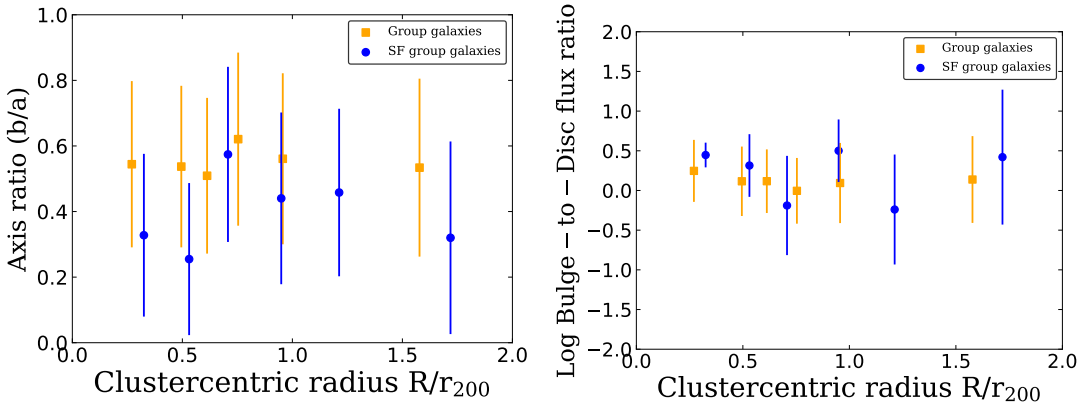

Figure 4.4: The left panel shows the axis ratio versus clustercentric radius in the infalling groups. The right panel has the bulge-to-disk flux ratio against the clustercentric radius in infalling groups. The orange and the blue marks are for non star-forming and star-forming galaxies, respectively.

Figure 4.5 visualizes the stellar mass functions in clusters and in both infalling and isolated groups. The stellar mass functions from the Illustris simulation [Vogelsberger et al., 2014] and isolated field groups are presented for comparison to our sample. The field groups are selected from Chandra Deep Field North and South, COSMOS and AEGIS surveys. The figure tests the Sérsic index based classification presented in Fig. 4.3, whether the classification is visible in stellar mass functions as well.

The bottom panel of Figure 4.5 shows a bump dominated by elliptical galaxies above the stellar mass function of the Illustris simulation. At this regime the difference of stellar mass functions of spirals and ellipticals is significant. The isolated group ellipticals follow nicely the shape of stellar mass function of mass-quenched passive galaxies presented in Figure 4.1. The infalling group galaxies and cluster galaxies in the upper panels lack the difference of spirals and ellipticals, and the bump feature in the total stellar mass function is less prominent, almost non-existing. Deviation from the shape of quenched mass functions by [Peng et al., 2010b] (shown in Figure 4.1) implies that the mass-quenching has no significant

effect in the high mass ellipticals in these clusters and infalling groups.

The other obvious difference in the Figure 4.5 is the lack of low mass spirals in cluster and infalling group galaxies compared to the field galaxies. This can be due to the disrupting interactions these low mass spiral galaxies suffer in the dense environment. However the LoCuSS survey has a magnitude limit $M_{*,K} + 1.5$ that corresponds to a mass limit $M_* \approx 2 \times 10^{10}$ $M_\odot$ below which the survey starts to miss galaxies [Bianconi et al., 2017]. This leads to increasing incompleteness towards the lower masses. The lack of the spirals is affected by the missing of the smaller objects in the survey. Observations targeting these low mass galaxies are needed to confirm the lack of these objects or evince that they are simply not detected by the LoCuSS survey.

The physical process of the mass-quenching is unclear, but the phenomenon is associated with AGNs (Active Galactic Nuclei) or some transient feature in galaxy morphology [Peng et al., 2010b]. The inefficiency of the mass-quenching could imply that the dense environment does not support enough the black hole growth, so the AGN production is insufficient. The spiral galaxies tend to change morphology from disky to elliptical as a result of mergers. This is how the high mass ellipticals are often formed. The low number of small spirals can then cause the low number of ellipticals.

As discussed, the fitting method and the procedure are effective to produce morphological parameters that are significant in the scientific study of galaxy morphology and environmental effects to the galaxies. The Sérsic n values from the fits are used successfully in the morphological classification. Even though the results presented in Figures 4.5 and 4.4 suffer from low statistics, the two component fitting method and the automated fitting of a large number of objects proved to be a practical way of producing scientifically relevant data from the observations.

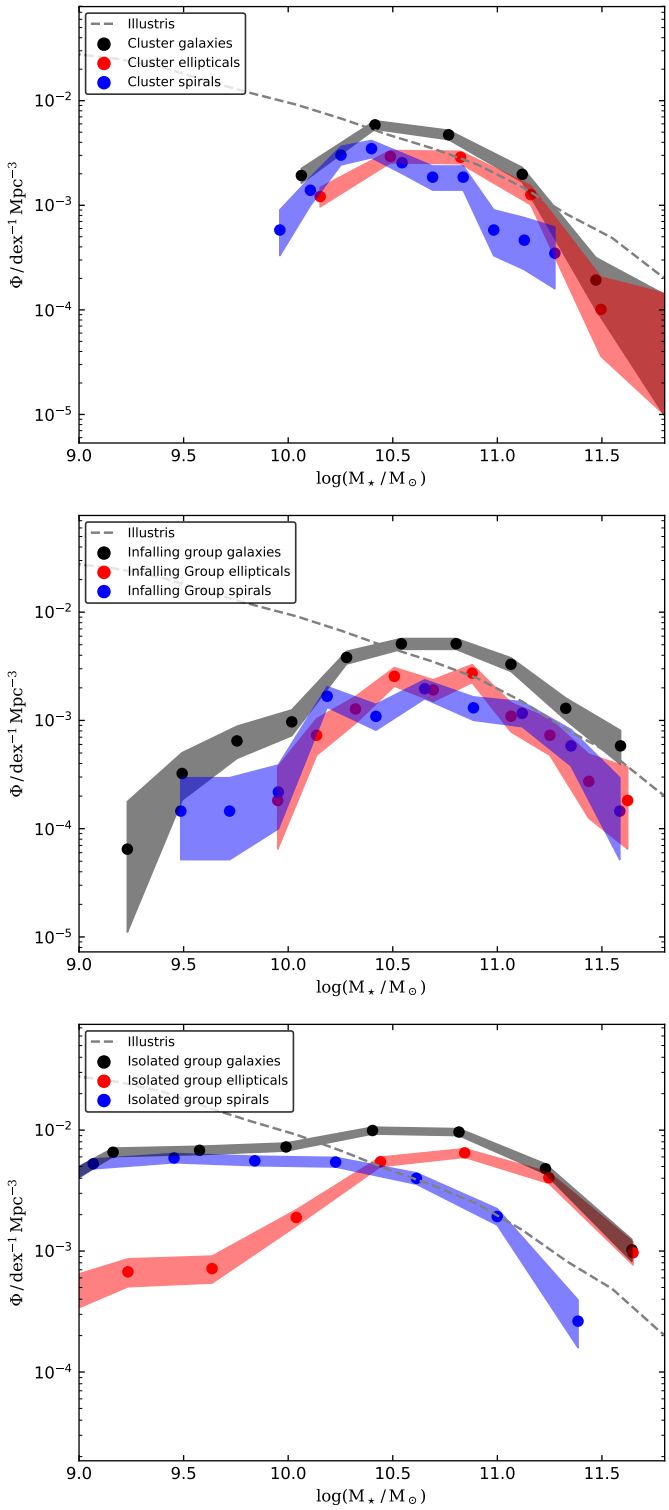

Figure 4.5: The stellar mass functions presented for spiral (blue) and elliptical (red) galaxies in clusters (top), infalling groups (middle) and field groups (bottom). The total stellar masses are presented in black. The shaded areas cover the 1 σ uncertainties computed following Gehrels [1986]. The grey dashed line shows the galaxy stellar mass function from the Illustris simulation [Vogelsberger et al., 2014].

5. Modeling galaxy field images using GALFIT

5.1 Euclid OU SIM Validation Project

Euclid [Laureijs et al., 2011] is a space telescope mission by the European Space Agency (ESA). It's expected to be launched in 2020. It's goal is to gain better understanding of dark energy and the expansion of the Universe [Laureijs et al., 2011].

Euclid will carry a 1.2 m aperture telescope with a near-infrared spectrometer and photometer (NISP) and a visual imager (VIS) [Laureijs et al., 2011]. The NISP photometry will cover the Y, J and H bands according to Laureijs et al.. A group in Helsinki is working with the Organization Unit (OU SIM) responsible of creating simulations to test and validate the data processing pipeline. The group is developing validation tools that are used to validate the test data from the intricate simulations by the OU SIM. The highly realistic OU SIM simulation data is used to test the data reduction pipeline that is planned to be used for the real observational data when the satellite is functional.

My project is part of the near-infrared photometry (NIP) validation. The aim of my project is to simulate observational data with galaxylike objects in it. This simple mock data is used to test independently the data reduction tools that the

Helsinki group is using in the OU SIM validation. I produce galaxy field images with catalogs listing the object coordinates, position angles and magnitudes.

5.2 Methods

The mock images are produced using GALFIT. Instead of fitting a data input image, GALFIT is ran with no input image, so it generates a model image based on initial parameters as mentioned in chapter 2. Each object is constructed with two components. Elliptical galaxies have de Vaucouleurs and Sérsic profiles and spiral galaxies have Sérsic and exponential disk profiles. The components of the objects have common central coordinates.

First I model individually 25 different objects (Fig. 5.1). By adjusting the parameter values and inspecting the result images one object at the time, I make sure that the objects are looking realistic. This helps to understand the reasonable ranges of the parameter values. By this insight the code for random generating large number of objects is easier to implement.

The IDL code `galscript.pro` is modified so that it prints the first 25 objects and then generates and prints given number of objects in random locations with random structural parameter values to a GALFIT input file similar to one in Appendix A.1. The positions are generated by code

```
; Generating random pixel coordinates:
fieldWidth = 2040
fieldHeight = 2040
xcoord = fieldWidth * RANDOMU(Seed, Ntargets)
ycoord = fieldHeight * RANDOMU(Seed, Ntargets)
```

where `Ntargets` is the number of objects and the `xcoord` and `ycoord` are the x and y coordinates in units of pixels. The other structural parameters are calculated by code

```
; Generating random values for Sersic n, position angle, radius, axis ratio, C0
SersicN = 0.5 + 6 * RANDOMU(Seed,Nrandom)
C = FLTARR(2,Nrandom)
```

```
AR = FLTARR(2,Nrandom)
Re = FLTARR(2,Nrandom)

Incl = 10 + 60 * RANDOMU(Seed,Nspirals)     ; Inclination
Nmode = 2 + 2 * FIX(3 * RANDOMU(Seed,Nspirals))
Nmode = STRTRIM(Nmode,2)
Famp = 0.01 + 0.3 * RANDOMU(Seed,Nspirals)  ; Fourier amplitude
Fang = 180 * RANDOMU(Seed,Nspirals)         ; Fourier angle
Bamp = 0.01 + 0.6 * RANDOMU(Seed, Nspirals) ; Bending amplitude
R1 = 5 * RANDOMU(Seed,Nspirals)             ; Bar radius [pix]
R2 = 5 + 50 * RANDOMU(Seed,Nspirals)        ; Asymptotic radius
R3 = 120 + 180 * RANDOMU(Seed, Nspirals)    ; Rotation to r_asympt
R4 = 0.5 + 4 * RANDOMU(Seed,Nspirals)       ; Winding scale radius

FOR j =0,Nrandom-1 DO BEGIN
  C[0,j] = -0.2 + 0.5 * RANDOMU(Seed,1)
  C[1,j] = -0.2 + 0.5 * RANDOMU(Seed,1)

  AR[0,j] = 0.3+0.8*RANDOMU(Seed,1)
  AR[1,j] = 0.3+0.8*RANDOMU(Seed,1)

  Re[0,j] = 2+7*RANDOMU(Seed,1)
  Re[1,j] = 2+7*RANDOMU(Seed,1)
ENDFOR
```

where `RANDOMU` is a function that generates uniform random numbers, `Nspirals` is the number of spiral galaxies to be generated and `Nrandom` is the number of all of the galaxies to be generated randomly, both ellipticals and spirals. The parameters are generated using ranges of values that GALFIT can calculate without numerical errors and the result pleases the eye. For example `Nmode` is the number of the Fourier mode which effectively determines the number of the spiral arms in the spiral galaxy. It is set so that the `Nmode` will be 2, 4 or 6.

After generating the GALFIT input file, the script runs GALFIT using that file and calls Python script `Tablegenarator.py` to print coordinates, magnitudes and position angles to a catalog. The codes of these scripts are in Appendices A.2.4 and A.2.5.

The readout noise and Poisson noise are added afterwards using IRAF task `mknoise`. The value for the readout noise is the same value as Euclid Collaboration uses in the more sophisticated, complex observation data simulation. The same IRAF task is used to produce cosmic rays to the image. The cosmic ray model

of the `mknoise` is ellipsoidal and Gaussian [STSCI, ndb], so the added cosmic rays represent direct hits to a CCD by the high energy cosmic particles. Stripes that are caused by the cosmic rays hitting a CCD in an angle close to the plane of the detector, are not modeled to the images.

5.3 Results

The produced mock data is used at first steps on using Source Extractor (SExtractor) software. The Euclid Collaboration has highly sophisticated OU-SIM simulation data images that are used in the validation of Euclid data analysis software, but my work is useful as an independent test data in the development of the validation tools by the Euclid group in Helsinki to validate the software producing this simulated data.

Figure 5.1 presents the first 25 objects made one by one. There is both elliptical and spiral galaxies with high variety in brightness, size, shape and position angle. The components of the ellipticals are affected by boxyness/diskyness parameter C0. The spiral galaxies have different inclination angles and shapes of the spiral structure.

Figure 5.3 is one of the over 30 images of the produced simulated galaxy fields. The image has 400 objects including the objects in Figure 5.1. The rest of the objects are generated automatically. The ratio of the number of ellipticals and spirals is close to the fraction of massive galaxies based on morphology in low redshifts [Conselice, 2014]: 70% of the randomly generated objects are ellipticals.

The noise added to the model images can be seen in Figure 5.2. The grainy appearance comes from the added Poisson and readout noise. The GALFIT image is completely smooth before the added noise. The image shows also morphologically different ellipticals and three spirals. Some of the objects are overlapping due to the randomed positions.

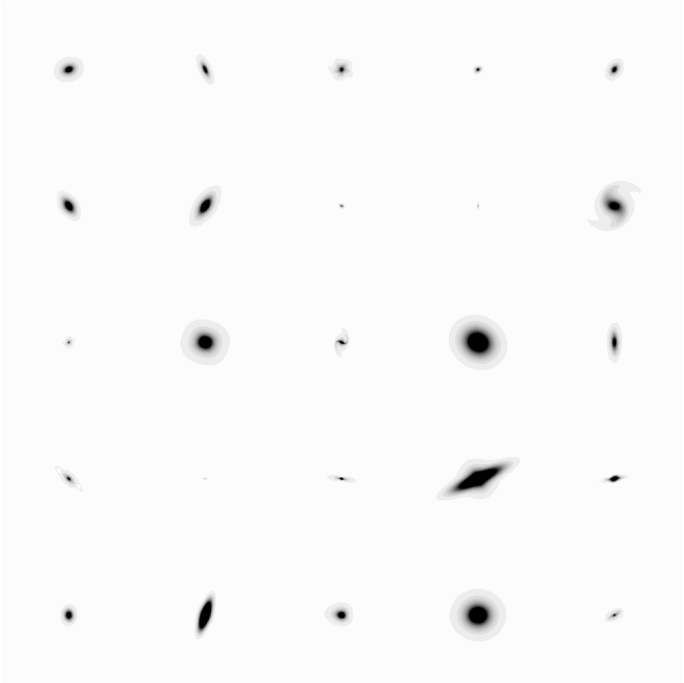

Figure 5.1: The 25 individually generated different galaxies in a grid. The dimmest objects are barely visible.

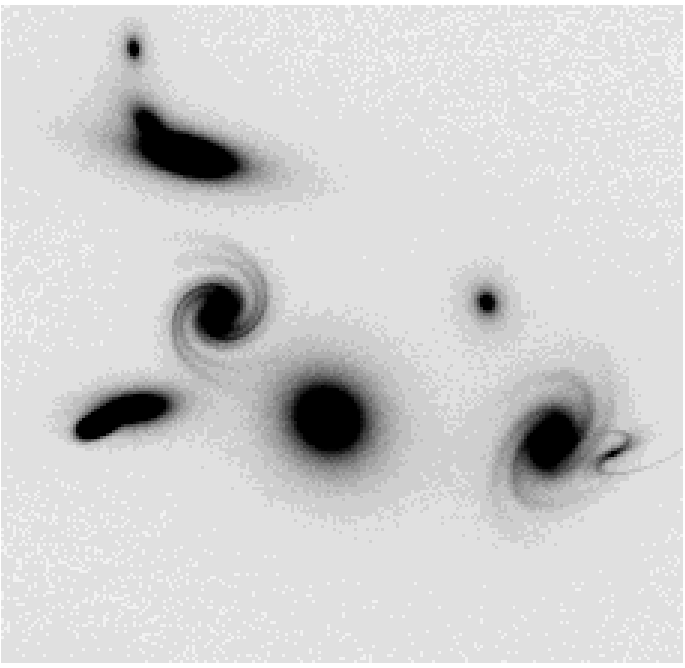

Figure 5.2: The close up from the Fig. 5.3 which shows couple of galaxies with more detail. The noise generated to the image is also more visible.

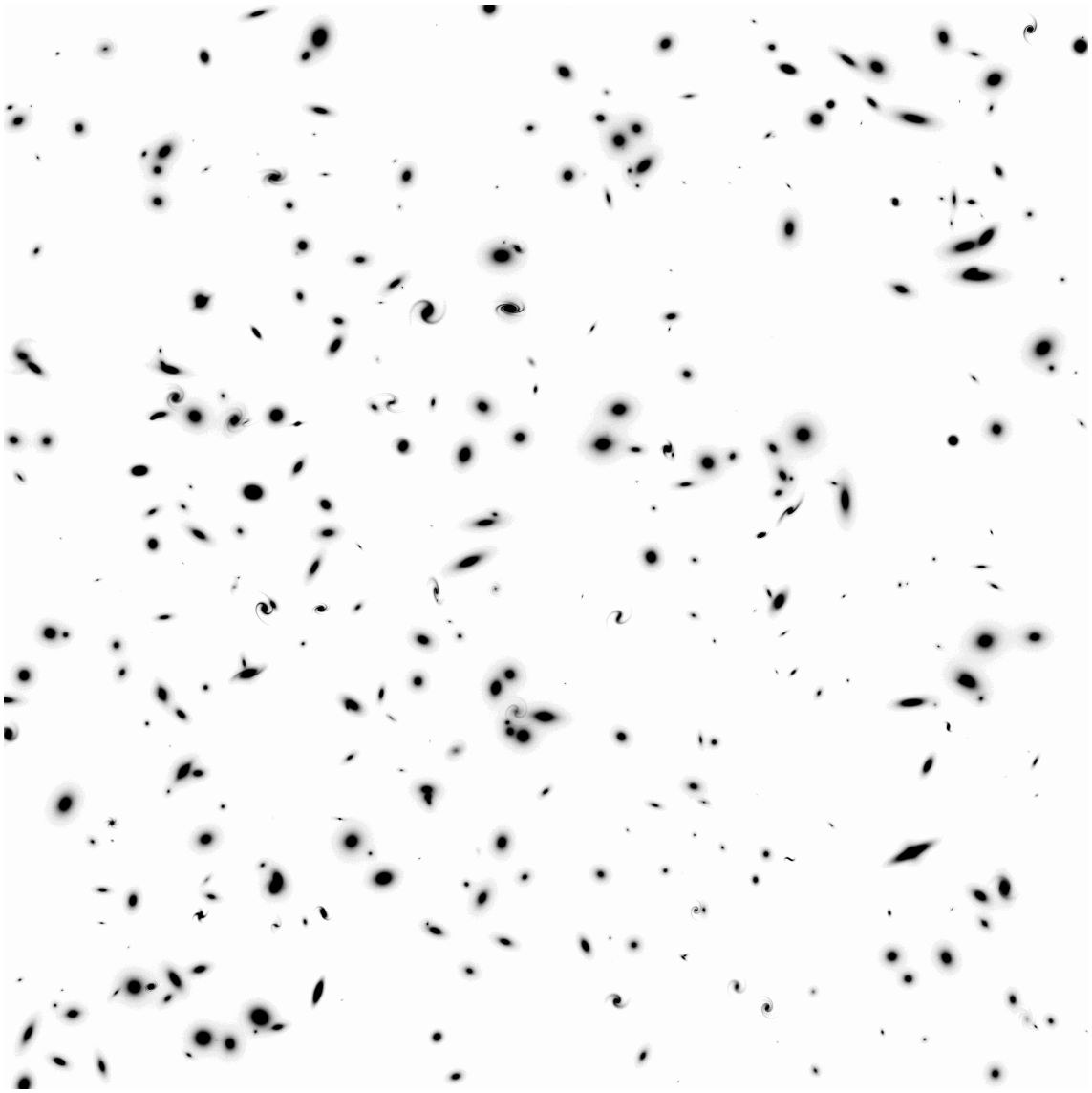

Figure 5.3: Simulated galaxy field image with 400 objects. 375 of them are generated randomly. There can be seen elliptical and spiral galaxies with different shapes, position angles and brightnesses.

6. Conclusions

GALFIT is a versatile tool for galaxy research. It's capable of highly detailed multi-component fitting as well as fits with single or two components. It can be even used for simulating image data as showed above in chapter 5. Even though complicated fits include lots of try and error, simple fits can be implemented for a large sample and run GALFIT for all of them at the same time.

The sample of X-ray group member spiral galaxies in the CANDELS fields is not yet fully fitted and analysed. However, the 9 objects are fitted in all of the available wavebands and various methods are used to study their structure and morphology. The statistics are insufficient for declaring any claims about galaxy evolution. The fitting process needs some improvement to get better and more comparable data from the fits of the every object in the sample. Because the observational data does not cover all of the u, g, r and i bands for every object, I suggest suitable HST filters (Appendix A.3.3) to be used to get them covered.

The large sample of galaxies in the infalling groups in the LoCuSS survey is successfully fitted with bulge and disk components. I run GALFIT with a script, so that all of the galaxies in the same group or cluster is fitted at a single run. The results are used in morphological classification based on the Sérsic index n. The classification is valid as the tests indicate. The analysis indicates that the star-forming galaxies are more elongated than the passive galaxies in these infalling groups. Most curiously results imply that the mass-quenching does not have significant effect in

this kind of environment. However the survey misses objects particularly at the low masses, so we are lacking some information.

My part in the Euclid project include an application of GALFIT to a task it's not particularly designed for. Instead of fitting image data I produce simulated images with galaxylike objects in it. The result images with the catalogs are used as an independent test data in the validation tool development.

Learning to use GALFIT and the insight I gained during the summer 2016 in the project with the CANDELS data were valuable and essential to modify and automate the fitting process to the needs of both projects during the summer 2017. In the future I will use this experience further. Analysis of the sample of the spiral galaxies in the CANDELS fields needs to be finished. For this I will revise the fitting method to gain better and more comparable results. The detailed fits can be used to measure the ratio of symmetrical and asymmetrical components and calculating values for the CAS parameters introduced in the section 1.3. The stellar populations of these galaxies can be studied by SED fitting. I will also take part in the publishing of the intriguing results of the LoCuSS infalling groups. I could also contribute to the Euclid OU SIM validation project by comparing the OU SIM images to the real observational images by fitting them using similar fitting procedure with GALFIT.

A. Appendix

A.1 Example GALFIT input file

```
================================================================================
# IMAGE and GALFIT CONTROL PARAMETERS
A) 'imagename'         # Input data image (FITS file)
B) gal2_'imagename'     # Output data image block
C) none            # Sigma image name (made from data if blank or "none")
D) psf_',cluster,'.fits  # Input PSF image and (optional) diffusion kernel
E) 1                   # PSF fine sampling factor relative to data
F) none                # Bad pixel mask (FITS image or ASCII coord list)
G) constraints.txt     # File with parameter constraints (ASCII file)
H) 1    50   1    50   # Image region to fit (xmin xmax ymin ymax)
I) 160     160         # Size of the convolution box (x y)
J) 33.630              # Magnitude photometric zeropoint
K) 0.20  0.20         # Plate scale (dx dy)   [arcsec per pixel]
O) regular            # Display type (regular, curses, both)
P) 0                # Choose: 0=optimize, 1=model, 2=imgblock, 3=subcomps

# INITIAL FITTING PARAMETERS
#
#   For component type, the allowed functions are:
#       sersic, expdisk, edgedisk, devauc, king, nuker, psf,
#       gaussian, moffat, ferrer, and sky.
#
#   Hidden parameters will only appear when they're specified:
#       Bn (n=integer, Bending Modes).
#       C0 (diskyness/boxyness),
#       Fn (n=integer, Azimuthal Fourier Modes).
#       R0-R10 (coordinate rotation, for creating spiral structures).
#       To, Ti, T0-T10 (truncation function).
#
# ------------------------------------------------------------------------------
#   par)    par value(s)    fit toggle(s)    # parameter description
# ------------------------------------------------------------------------------

# Component number: 1
0) sersic            #  Component type
1) 25  25  1 1       #  Position x, y
3) 21.0     1        #  Integrated magnitude
```

```
4) 6.0237      1     #  R_e (effective radius)   [pix]
5) 2.      1         #  Sersic index n (de Vaucouleurs n=4)
6) 0.0000      0     #     -----
7) 0.0000      0     #     -----
8) 0.0000      0     #     -----
9) 0.843      1      #  Axis ratio (b/a)
10) 0.2400     1     #  Position angle (PA) [deg: Up=0, Left=90]
#C0) 0     1         #  Diskyness(-)/Boxyness(+)
Z) 0                 #  Skip this model in output image?  (yes=1, no=0)

# Component number: 2
0) expdisk           #  Component type
1) 25  25  1 1       #  Position x, y
3) 21.0     1        #  Integrated magnitude
4) 6.5157      1     #  R_s (disk scale-length)   [pix]
5) 0.0000      0     #     -----
6) 0.0000      0     #     -----
7) 0.0000      0     #     -----
8) 0.0000      0     #     -----
9) 0.863      1      #  Axis ratio (b/a)
10) 0.7506     1     #  Position angle (PA) [deg: Up=0, Left=90]
Z) 0                 #  Skip this model in output image?  (yes=1, no=0)

# Component number: 3
0) sky               #  Component type
1) 0.7700      0    #  Sky background at center of fitting region [ADUs]
2) 0.000e+00      1  #  dsky/dx (sky gradient in x)     [ADUs/pix]
3) 0.000e+00      1  #  dsky/dy (sky gradient in y)     [ADUs/pix]
Z) 0                 #  Skip this model in output image?  (yes=1, no=0)

================================================================================
```

A.2 Scripts

A.2.1 Galscript.pro

```
PRO GALscript
; ##################################################################
; This script runs GALFIT for set of FITS files. It first reads the
; input FITS from a list. The script generates a GALFIT input file.
; Then the script runs GALFIT and repeats the process. The script
; checks if the GALFIT's output image exists or not. If GALFIT has
; failed to fit and produce output image, the script writes a report
; of it to its own output file.
; ##################################################################
; Reading the name of the input FITS from a file:

starttime = SYSTIME() ; Start time of the run


CLOSE, 1 ; Closing a file that can possibly be open already.

; # The file with all the names of data images have to be created before this! # ;
```

```
; Cluster  ID
cluster = 'RXJ1720'

; Open the file with input image names.
file = FILEPATH('imagenames.list',ROOT_DIR=['~'],SUBDIRECTORY=['locuss',cluster])
OPENR, lun, file, /GET_LUN

; Read one line at the time and save to array
imagenames = ''
line = ''
WHILE NOT EOF(lun) DO BEGIN & $
  READF, lun, line & $
  imagenames = [imagenames,line] & $
ENDWHILE

; Close the file and free the file unit
FREE_LUN, lun

samplesize = SIZE(imagenames,/N_ELEMENTS) -1 ; Number of the filenames.
                                             ; (minus 1 because of the indexing)

; ####################################################################
; ####################################################################
; Loop for generating GALFIT inputfile and running GALFIT.
; Each iteration contains the inputfile generation and GALFIT run.


  ; Open file for script output. Problems will be saved here.
scriptfile = FILEPATH('galscript.output',ROOT_DIR=['~'],SUBDIRECTORY=['locuss',cluster])
OPENW, lun2, scriptfile, /GET_LUN
; Print date to scripts output file.
PRINTF, lun2, '# '+starttime+' #'


; ####################################################################
; ####################################################################
; Begin a FOR loop for iterating through all the files
;
; ####################################################################

; --------------------------
FOR i =1,samplesize DO BEGIN
; --------------------------

    ; Open the file.
  galfitfile = FILEPATH('galscript.input',ROOT_DIR=['~'],SUBDIRECTORY=['locuss',cluster])
  OPENW, lun, galfitfile, /GET_LUN

  imagename = imagenames[i]

; Generating a GALFIT input file (same parameter values than test.input)
; ###################################################################
PRINTF,lun, '================================================================================'
PRINTF,lun, '# IMAGE and GALFIT CONTROL PARAMETERS'
PRINTF,lun, 'A) ',imagename,'      # Input data image (FITS file)'
PRINTF,lun, 'B) gal2_',imagename,'      # Output data image block'
PRINTF,lun, 'C) none                # Sigma image name (made from data if blank or "none")'
PRINTF,lun, 'D) psf_',cluster,'.fits            # Input PSF image and (optional) diffusion kernel'
PRINTF,lun, 'E) 1                   # PSF fine sampling factor relative to data'
PRINTF,lun, 'F) none                # Bad pixel mask (FITS image or ASCII coord list)'
PRINTF,lun, 'G) constraints.txt               # File with parameter constraints (ASCII file)'
PRINTF,lun, 'H) 1    50   1    50   # Image region to fit (xmin xmax ymin ymax)'
PRINTF,lun, 'I) 160     160           # Size of the convolution box (x y)'
PRINTF,lun, 'J) 33.630              # Magnitude photometric zeropoint'
PRINTF,lun, 'K) 0.20  0.20        # Plate scale (dx dy)   [arcsec per pixel]'
PRINTF,lun, 'O) regular             # Display type (regular, curses, both)'
PRINTF,lun, 'P) 0                   # Choose: 0=optimize, 1=model, 2=imgblock, 3=subcomps'
PRINTF,lun, ' '
```

```
PRINTF,lun, '# INITIAL FITTING PARAMETERS'
PRINTF,lun, '# '
PRINTF,lun, '#   For component type, the allowed functions are:'
PRINTF,lun, '#       sersic, expdisk, edgedisk, devauc, king, nuker, psf,'
PRINTF,lun, '#       gaussian, moffat, ferrer, and sky.'
PRINTF,lun, '# '
PRINTF,lun, '#   Hidden parameters will only appear when they"re specified:'
PRINTF,lun, '#       Bn (n=integer, Bending Modes).'
PRINTF,lun, '#       C0 (diskyness/boxyness),'
PRINTF,lun, '#       Fn (n=integer, Azimuthal Fourier Modes).'
PRINTF,lun, '#       R0-R10 (coordinate rotation, for creating spiral structures).'
PRINTF,lun, '#       To, Ti, T0-T10 (truncation function).'
PRINTF,lun, '# '
PRINTF,lun, '# ------------------------------------------------------------------------------'
PRINTF,lun, '#   par)    par value(s)    fit toggle(s)    # parameter description'
PRINTF,lun, '# ------------------------------------------------------------------------------'
PRINTF,lun, ' '
PRINTF,lun, '# Component number: 1'
PRINTF,lun, '0) sersic                 #  Component type'
PRINTF,lun, '1) 25  25  1 1  #  Position x, y'
PRINTF,lun, '3) 21.0    1          #  Integrated magnitude'
PRINTF,lun, '4) 6.0237      1          #  R_e (effective radius)   [pix]'
PRINTF,lun, '5) 2.      1          #  Sersic index n (de Vaucouleurs n=4)'
PRINTF,lun, '6) 0.0000      0          #     -----'
PRINTF,lun, '7) 0.0000      0          #     -----'
PRINTF,lun, '8) 0.0000      0          #     -----'
PRINTF,lun, '9) 0.843      1          #  Axis ratio (b/a)'
PRINTF,lun, '10) 0.2400     1          #  Position angle (PA) [deg: Up=0, Left=90]'
PRINTF,lun, '#C0) 0     1          #  Diskyness(-)/Boxyness(+)'
PRINTF,lun, 'Z) 0                      #  Skip this model in output image?  (yes=1, no=0)'
PRINTF,lun, ' '
PRINTF,lun, '# Component number: 2'
PRINTF,lun, '0) expdisk                #  Component type'
PRINTF,lun, '1) 25  25  1 1  #  Position x, y'
PRINTF,lun, '3) 21.0     1          #  Integrated magnitude'
PRINTF,lun, '4) 6.5157      1          #  R_s (disk scale-length)   [pix]'
PRINTF,lun, '5) 0.0000      0          #     -----'
PRINTF,lun, '6) 0.0000      0          #     -----'
PRINTF,lun, '7) 0.0000      0          #     -----'
PRINTF,lun, '8) 0.0000      0          #     -----'
PRINTF,lun, '9) 0.863      1          #  Axis ratio (b/a)'
PRINTF,lun, '10) 0.7506     1          #  Position angle (PA) [deg: Up=0, Left=90]'
PRINTF,lun, 'Z) 0                      #  Skip this model in output image?  (yes=1, no=0)'
PRINTF,lun, ' '
PRINTF,lun, '# Component number: 3'
PRINTF,lun, '0) sky                    #  Component type'
PRINTF,lun, '1) 0.7700          0       #  Sky background at center of fitting region [ADUs]'
PRINTF,lun, '2) 0.000e+00       1       #  dsky/dx (sky gradient in x)     [ADUs/pix]'
PRINTF,lun, '3) 0.000e+00       1       #  dsky/dy (sky gradient in y)     [ADUs/pix]'
PRINTF,lun, 'Z) 0                      #  Skip this model in output image?  (yes=1, no=0)'
PRINTF,lun, ' '
PRINTF,lun, '================================================================================'
; ###############################################################

; Close the file and free the file unit
FREE_LUN, lun

; Give command to run GALFIT
command = './galfit '+galfitfile
SPAWN, command & PRINT, imagename, i


; Testing if GALFIT has created the output file.
; If not, print report to script's output file.
result = FILE_TEST('gal2_'+imagename)
  IF result NE 1 THEN BEGIN
    PRINT, 'File gal2_'+imagename+' has not been created.'
    PRINTF, lun2, 'No output image: ', imagename
```

```
  ENDIF

; -------------------------
ENDFOR
; -------------------------
;
; ###################################################################
; ###################################################################


; Print end date to script's output file.
PRINTF, lun2, '# '+SYSTIME()+' #'
endtime = SYSTIME() ; End time of the run.
PRINTF, lun2, '# Remember to update "fits.lis" after fitting these. #'


; Close the script's output file and free the file unit.
FREE_LUN, lun2

PRINT, 'Start: '+starttime
PRINT, 'Finish: '+endtime

; Give command to create a input file for script test_galfit.py
command2 = 'ls gal2_cut* > fits.lis'
SPAWN, command2 & PRINT, 'fits.lis file created'

END
```

A.2.2 Galfit_parser.py

```
# This module will read in the galfit best fit values and uncertainties
#

from astropy.io import fits
'''
  to create an object containing galfit results,
  use obj = GalfitResult('<output block fits file>')
  you can access to the output parameters by:
       obj.component_num.param
'''
class GalfitComponent(object):
    """
    stores results from one component of the fit
    """
    def __init__(self,galfitheader,component_number):
        """
        takes in the fits header from HDU 3 (the galfit model) from a galfit output file
        and the component number to extract
        """
        #checks
        assert component_number > 0
        assert "COMP_" + str(component_number) in galfitheader

        self.component_type = galfitheader["COMP_" + str(component_number)]
        self.component_number = component_number
        headerkeys = [i for i in galfitheader.keys()]
        comp_params = []
        for i in headerkeys:
            if str(component_number) + '_' in i:
                comp_params.append(i)
        for param in comp_params:
            val = galfitheader[param]
            #we know that val is a string formatted as 'result +/- uncertainty'
            #if val is fixed in GalFit, it is formatted as '[result]'
            paramsplit = param.split('_')
```

```
            # If there's some numerical error, should output a warning (*)

            if '[' in val:     #fixed parameter
                val = val.translate(None,'[]*')
                setattr(self,paramsplit[1].lower(),float(val))
                setattr(self,paramsplit[1].lower() + '_err',None)
            else:              #normal variable parameter
                val = val.translate(None,'*').split()
                setattr(self,paramsplit[1].lower(),float(val[0]))
                setattr(self,paramsplit[1].lower() + '_err',float(val[2]))

class GalfitResults(object):
    """
    This class stores galfit results information
    INPUT:
        galfit_fits_file: the block fits file generated by GalFit
    """
    def __init__(self, galfit_fits_file):
        """
        init method for GalfitResults. Take in a string that is the name
        of the galfit output fits file
        """
        hdulist = fits.open(galfit_fits_file)
        #now some checks to make sure the file is what we are expecting
#print len(hdulist)
        assert len(hdulist) == 4
        galfitmodel = hdulist[2]
        galfitheader = galfitmodel.header
        galfit_in_comments = False
        for i in galfitheader['COMMENT']:
            galfit_in_comments = galfit_in_comments or "GALFIT" in i
        assert True == galfit_in_comments
        assert "COMP_1" in galfitheader
        #now we've convinced ourselves that this is probably a galfit file

        self.galfit_fits_file = galfit_fits_file
        #read in the input parameters
        self.input_initfile = galfitheader['INITFILE']
        self.input_datain = galfitheader["DATAIN"]
        self.input_sigma = galfitheader["SIGMA"]
        self.input_psf = galfitheader["PSF"]
        self.input_constrnt = galfitheader["CONSTRNT"]
        self.input_mask = galfitheader["MASK"]
        self.input_fitsect = galfitheader["FITSECT"]
        self.input_convbox = galfitheader["CONVBOX"]
        self.input_magzpt = galfitheader["MAGZPT"]

        #read in the chi-square value
        self.chisq = galfitheader["CHISQ"]
        self.ndof = galfitheader["NDOF"]
        self.nfree = galfitheader["NFREE"]
        self.reduced_chisq = galfitheader["CHI2NU"]

        #find the number of components
        num_components = 1 #already verified above
        while True:
            if "COMP_" + str(num_components + 1) in galfitheader:
                num_components = num_components + 1
            else:
                break
        self.num_components = num_components

        for i in range(1, self.num_components + 1):
            setattr(self,"component_" + str(i),GalfitComponent(galfitheader,i))

        hdulist.close()
```

A.2.3 Test_galfit.py

```
import matplotlib.pyplot as plt
from matplotlib import rc
import matplotlib.ticker as ticker
import sys
sys.path.append('/usr/lib/')  #/Library/Python/2.7/site-packages/') #/usr/lib/python2.7
import os
import subprocess
import numpy as np
from matplotlib.ticker import FuncFormatter
import csv
from matplotlib.patches import Rectangle
from mpl_toolkits.axes_grid1 import make_axes_locatable
from scipy import spatial
from scipy import stats
import pylab
import pyfits
import pandas as pd
from matplotlib.colors import LogNorm
from matplotlib.mlab import griddata
from scipy.ndimage.filters import gaussian_filter
import re
from math import atan2,degrees
from scipy import interpolate
import matplotlib as mpl
import galfit_parser
from galfit_parser import GalfitComponent
from galfit_parser import GalfitResults
import numpy as np


galfit = '/home/antluoma/locuss/'
dir_cat = '/home/antluoma/locuss/catalogs/'
cluster = ['A68']
cat = '_UVMIRgals.v3.gaia'

gc = pd.read_csv(dir_cat+str(cluster[0])+cat, sep='\s+', header='infer', na_values=['nan'],
 skiprows = [1], keep_default_na=False)

ID_cat = gc['ID'].values.tolist()
ra = gc['RA(J2000)'].values.tolist()
dec = gc['DEC(J2000)'].values.tolist()
rr200 = gc['DIST'].values.tolist()

fp1 = file(galfit+str(cluster[0])+'/fits.lis')
rdr = csv.reader(filter(lambda row: row[0]!='#', fp1), delimiter=',', quotechar='|',
 skipinitialspace=True)

ID = []
for row in rdr:
    ID.append(str(row[0]))
fp1.close()


ID_out =[]
for y in ID:

   ID_out.append(y[13:].split(".")[0])


magsc = []
mags_errc = []
magec = []
mage_errc = []
nc = []
n_errc = []
rec = []
```

```
re_errc = []
rsc = []
rs_errc = []
skyc = []
sky_errc = []
arc = []
ar_errc = []
chi2c = []
chi2_redc = []
ID_fc = []


for i in range(len(ID)):
   galfitres = galfit_parser.GalfitResults(ID[i])
   comps = galfitres.num_components
   if comps > 3:
      comps=3

   chi2 = galfitres.chisq
   chi2_red = galfitres.reduced_chisq

   mags = np.array([-99.00] * len(ID))
   mags_err = np.array([-99.00] * len(ID))
   mage = np.array([-99.00] * len(ID) )
   mage_err = np.array([-99.00] * len(ID))
   n = np.array([-99.00] * len(ID) )
   n_err = np.array([-99.00] * len(ID) )
   re = np.array([-99.00] * len(ID) )
   re_err = np.array([-99.00] * len(ID) )
   rs = np.array([-99.00] * len(ID))
   rs_err = np.array([-99.00] * len(ID))
   sky = np.array([-99.00] * len(ID) )
   sky_err = np.array([-99.00] * len(ID))
   ar = np.array([-99.00] * len(ID))
   ar_err = np.array([-99.00] * len(ID) )



   ID_f = [-99.00] * len(ID)
   ID_f = [item for item in ID_out for k in range(comps)]

   for x in range(comps):
      x += 1
      comp_num = getattr(galfitres, 'component_'+str(x))
      comp_type = getattr(comp_num, 'component_type')
# print str(comp_type)
# print x

      if str(comp_type) == "sersic":
         mags[x] = getattr(comp_num, 'mag')
         mags_err[x] = getattr(comp_num, 'mag_err')
         n[x] = getattr(comp_num, 'n')
         n_err[x] = getattr(comp_num, 'n_err')
         re[x] = getattr(comp_num, 're')
         re_err[x] = getattr(comp_num, 're_err')
         ar[x] = getattr(comp_num, 'ar')
         ar_err[x] = getattr(comp_num, 'ar_err')
      elif str(comp_type) == "expdisk":
         mage[x] = getattr(comp_num, 'mag')
         mage_err[x] = getattr(comp_num, 'mag_err')
         rs[x] = getattr(comp_num, 'rs')
         rs_err[x] = getattr(comp_num, 'rs_err')
      elif str(comp_type) == "sky":
         sky[x] = getattr(comp_num, 'sky')
         sky_err[x] = getattr(comp_num, 'sky_err')

      magsc.append(mags[x])
      mags_errc.append(mags_err[x])
```

```
      magec.append(mage[x])
      mage_errc.append(mage_err[x])
      nc.append(n[x])
      n_errc.append(n_err[x])
      rec.append(re[x])
      re_errc.append(re_err[x])
      rsc.append(rs[x])
      rs_errc.append(rs_err[x])
      skyc.append(sky[x])
      sky_errc.append(sky_err[x])
      arc.append(ar[x])
      ar_errc.append(ar_err[x])
   chi2c.append(chi2)
   chi2_redc.append(chi2_red)

   ID_fc.append(ID_f)


magsc = list(filter(lambda x: x > 0, magsc))
mags_errc = list(filter(lambda x: x != -99, mags_errc)) #> 0, mags_errc ))
magec = list(filter(lambda x: x > 0, magec))
mage_errc = list(filter(lambda x: x != -99, mage_errc)) #> 0, mage_errc))
nc = list(filter(lambda x: x > 0, nc))
n_errc = list(filter(lambda x: x != -99, n_errc)) #> 0, n_errc))
rec = list(filter(lambda x: x > 0, rec ))
re_errc = list(filter(lambda x: x != -99, re_errc)) #> 0, re_errc))
rsc = list(filter(lambda x: x > 0, rsc))
rs_errc = list(filter(lambda x: x != -99, rs_errc)) #> 0, rs_errc))
arc = list(filter(lambda x: x > 0, arc))
ar_errc = list(filter(lambda x: x != -99, ar_errc)) #> 0, ar_errc))
ID_fc = ID_fc[0][:][0::3]


for w in range(len(chi2c)):
   Chi2s = np.array(chi2c)
   MAGsErr = np.array(mags_errc)
   nErr = np.array(n_errc)
   MAGexpErr = np.array(mage_errc)
   RsErr = np.array(rs_errc)
   ReErr = np.array(re_errc)
   ArErr = np.array(ar_errc)
   rsc = np.array(rsc)
   rec = np.array(rec)
   if Chi2s[w] > 3000:
      print ID_fc[w],'Chi^2'
   elif nErr[w] > 1:
      print ID_fc[w],'n'
   elif MAGsErr[w] > 1:
      print ID_fc[w],'Mags'
   elif MAGexpErr[w] > 1:
      print ID_fc[w],'Mage'
   elif RsErr[w] > 1:
      print ID_fc[w],'Rs'
   elif ReErr[w] > 1:
      print ID_fc[w],'Re'
   elif ArErr[w] > 1:
      print ID_fc[w],'AR'

np.savetxt("galfit_comps2_"+str(cluster[0])+".txt",  np.c_[map(int,ID_fc), np.array(magsc),
 np.array(mags_errc), np.array(nc), np.array(n_errc), np.array(rec), np.array(re_errc),
 np.array(arc), np.array(ar_errc), np.array(magec), np.array(mage_errc),  np.array(rsc),
 np.array(rs_errc), np.array(chi2c), np.array(chi2_redc)], header='ID MAGsersic
 MAGsersic_ERR  n   n_err   Re    Re_err    AR    AR_err    MAGexp   MAGexp_ERR    Rs
 Rs_err   Chi2   Chi2_Red',delimiter=' ', fmt=" %i " + " %.3f "*14)
```

A.2.4 GalaxyFieldScript.pro

```
PRO GalaxyFieldScript
; ####################################################################
; ####################################################################


; Insert RA DEC coordinates in degrees for pixel in x=0, y=0
InitCoord = FLTARR(1,2)
InitCoord[0,0] = 25.47     ; RA
InitCoord[0,1] = -12.47    ; DEC

; Set background sky level and gradient and Mag_zero
sky = 30.0
skyString = STRTRIM(sky,2)
dx = 0
dy = 0
Mag_zero = 33.63

starttime = SYSTIME() ; Start time of the run
PRINT, 'Start: '+starttime

CLOSE, 1 ; Closing a file that can possibly be open already.

; Work directory
dir = "OUsimValidation"
; Number of galaxies
Ntargets = 200
NtargetsString = STRTRIM(Ntargets, 2)

; Generating random pixel coordinates:
fieldWidth = 2040
fieldHeight = 2040
xcoord = fieldWidth * RANDOMU(Seed, Ntargets)
ycoord = fieldHeight * RANDOMU(Seed, Ntargets)

; Magnitudes of the components
MAG = FLTARR(2,Ntargets)
MAG25 = [ [20,  23],[21,  23],[22.6040,  23.5535],[19.6040,  20.5535],[20.04,  19.74],$
  [19,  17],[25,  25],[19,  18],[17.49,  17.87],[20.24,  21.31],[19,  21],[22,  22],$
  [21,  21],[24,  24],[20.9,  21.46],[18,  17.3],[17,  17],[16.8,  16.7],[24,  24],$
  [22.9,  22.6],[22,  22.5],[21, 21.4],[19.98,  20.8],[19,  19.6],[20.8,  19.7] ]
; Position angles of the components
PA = FLTARR(2,Ntargets)
PA25 = [ [4.0, 4.0 ],[47.04, 47.04 ],[3.5644, 4.4393],[33.5644, 49.4393],[-247.0, -250.0],$
  [-18.0, -18.0],[-87.0,  -87.0],[72.0, 72.0],[146.8, 146.0],[-157.43, -150.8],$
  [98.0, 88.0],[89.0, 89.0],[0.0, 89.0],[78.0,  72.0],[7.04, 0.04],[97.0, 89.0],$
  [297.0, 295.0],[97.0, 97.0],[7,  9],[0.04, 0.04],[119.04, 28.04],[119.04, 9.04],$
  [1.04,1.04],[89.04, 1.04],[7.0, 47.0] ]

; Magnitude values to a single array
FOR k = 0,24 DO BEGIN
    MAG[0,k] = MAG25[0,k]
    MAG[1,k] = MAG25[1,k]
    PA[0,k] = PA25[0,k]
    PA[1,k] = PA25[1,k]
ENDFOR
; Filling rest of the parameters with random values
;
FOR k = 25,Ntargets-1 DO BEGIN
  MAG[0,k] = 17 + 10 * RANDOMU(Seed,1)
  MAG[1,k] = 17 + 10 * RANDOMU(Seed,1)
  PA[0,k] = 180 * RANDOMU(Seed,1)
  PA[1,k] = PA[0,k]+5*RANDOMU(Seed,1)
ENDFOR


; Number of galaxies to randomgenerate
```

```
Nrandom = Ntargets-25
; Number of ellipticals and spirals
Ndens = 0.7   ; Number density of ellipticals as percentage of all targets
Nellipses = FIX(Ndens*Nrandom)
Nspirals = Nrandom - Nellipses


;print, Nrandom, MAG


    ; Open the file.
galfitfile = FILEPATH('galaxyfield.input',ROOT_DIR=['~'],SUBDIRECTORY=['Euclid',dir])
OPENW, lun, galfitfile, /GET_LUN



; Generating a GALFIT input file (same parameter values than test.input)
; ###################################################################
PRINTF,lun, "================================================================================"
PRINTF,lun, "# IMAGE and GALFIT CONTROL PARAMETERS"
PRINTF,lun, "A)       # Input data image (FITS file)"
PRINTF,lun, "B) Sky30.0_randField_",NtargetsString,".fits      # Output data image block"
PRINTF,lun, "C) none                # Sigma image name (made from data if blank or none)"
PRINTF,lun, "D) none          # Input PSF image and (optional) diffusion kernel"
PRINTF,lun, "E) 1                   # PSF fine sampling factor relative to data"
PRINTF,lun, "F) none                # Bad pixel mask (FITS image or ASCII coord list)"
PRINTF,lun, "G) none      # File with parameter constraints (ASCII file)"
PRINTF,lun, "H) 1  ",fieldWidth,"  1  ",fieldHeight," # Image region to fit (xmin xmax ymin ymax)"
PRINTF,lun, "I) 160    160          # Size of the convolution box (x y)"
PRINTF,lun, "J) ",Mag_zero,"              # Magnitude photometric zeropoint"
PRINTF,lun, "K) 0.300  0.300        # Plate scale (dx dy)   [arcsec per pixel]"
PRINTF,lun, "O) regular             # Display type (regular, curses, both)"
PRINTF,lun, "P) 0                   # Choose: 0=optimize, 1=model, 2=imgblock, 3=subcomps"
PRINTF,lun, ""
PRINTF,lun, "# INITIAL FITTING PARAMETERS"
PRINTF,lun, "#"
PRINTF,lun, "#   For component type, the allowed functions are:"
PRINTF,lun, "#       sersic, expdisk, edgedisk, devauc, king, nuker, psf,"
PRINTF,lun, "#       gaussian, moffat, ferrer, and sky."
PRINTF,lun, "#"
PRINTF,lun, "#   Hidden parameters will only appear when they're specified:"
PRINTF,lun, "#       Bn (n=integer, Bending Modes)."
PRINTF,lun, "#       C0 (diskyness/boxyness),"
PRINTF,lun, "#       Fn (n=integer, Azimuthal Fourier Modes)."
PRINTF,lun, "#       R0-R10 (coordinate rotation, for creating spiral structures)."
PRINTF,lun, "#       To, Ti, T0-T10 (truncation function)."
PRINTF,lun, "#"
PRINTF,lun, "# ------------------------------------------------------------------------------"
PRINTF,lun, "#   par)    par value(s)    fit toggle(s)    # parameter description"
PRINTF,lun, "# ------------------------------------------------------------------------------"
PRINTF,lun, ""
PRINTF,lun, "================================================================================"
PRINTF,lun, "# Column 1: x=100"
PRINTF,lun, "================================================================================"
PRINTF,lun, "# Component number: 1"
PRINTF,lun, " 0) sersic                 #  Component type"
PRINTF,lun, " 1) ",xcoord[0]," ",ycoord[0]," 1 1  #  Position x, y"
PRINTF,lun, " 3) 20     1          #  Integrated magnitude"
PRINTF,lun, " 4) 4.     1          #  R_e (effective radius)   [pix]"
PRINTF,lun, " 5) 1.3     1          #  Sersic index n (de Vaucouleurs n=4)"
PRINTF,lun, " 6) 0.0000      0          #     -----"
PRINTF,lun, " 7) 0.0000      0          #     -----"
PRINTF,lun, " 8) 0.0000      0          #     -----"
PRINTF,lun, " 9) 0.79      1          #  Axis ratio (b/a)"
PRINTF,lun, " 10) 4     1          #  Position angle (PA) [deg: Up=0, Left=90]"
PRINTF,lun, " #B1) 0.9 1"
PRINTF,lun, "  Z) 0                      #  Skip this model in output image?  (yes=1, no=0)"
PRINTF,lun, " "
```

```
PRINTF,lun, " # Component number: 1"
PRINTF,lun, " 0) expdisk                #  Component type"
PRINTF,lun, " 1) ",xcoord[0],"  ",ycoord[0],"  1 1  #  Position x, y"
PRINTF,lun, " 3) 23     1          #  Integrated magnitude"
PRINTF,lun, " 4) 8.0      1          #  R_s (disk scale-length)   [pix]"
PRINTF,lun, " 5) 0.0000      0          #     -----"
PRINTF,lun, " 6) 0.0000      0          #     -----"
PRINTF,lun, " 7) 0.0000      0          #     -----"
PRINTF,lun, " 8) 0.0000      0          #     -----"
PRINTF,lun, "  9) 0.856      1          #  Axis ratio (b/a)"
PRINTF,lun, " 10) 4     1          #  Position angle (PA) [deg: Up=0, Left=90]"
PRINTF,lun, "  R0) power                  #  PA rotation func. (power, log, none)"
PRINTF,lun, " R1) 2.     1          #  Spiral inner radius [pixels]"
PRINTF,lun, " R2) 20.     1          #  Spiral outer radius [pixels]"
PRINTF,lun, " R3) 320.    1          #  Cumul. rotation out to outer radius [degrees]"
PRINTF,lun, "R4) 0.03      1          #  Asymptotic spiral powerlaw"
PRINTF,lun, "R9) 5.     1          #  Inclination to L.o.S. [degrees]"
PRINTF,lun, "R10) 94   1          #  Sky position angle"
PRINTF,lun, "B1) 9   1          #  Bending mode 1 amplitude"
PRINTF,lun, "B2) 0.03   1          #  Bending mode 2 amplitude"
PRINTF,lun, " Z) 0                      #  Skip this model in output image?  (yes=1, no=0)"
PRINTF,lun, "################################################################################"
PRINTF,lun, ""
PRINTF,lun, "# Component number: 2"
PRINTF,lun, " 0) sersic                 #  Component type"
PRINTF,lun, " 1) ",xcoord[1]," ",ycoord[1]," 1 1  #  Position x, y"
PRINTF,lun, " 3) 21.     1          #  Integrated magnitude"
PRINTF,lun, " 4) 8.     1          #  R_e (effective radius)   [pix]"
PRINTF,lun, " 5) 4.     1          #  Sersic index n (de Vaucouleurs n=4)"
PRINTF,lun, " 6) 0.0000      0          #     -----"
PRINTF,lun, " 7) 0.0000      0          #     -----"
PRINTF,lun, " 8) 0.0000      0          #     -----"
PRINTF,lun, " 9) 0.59      1          #  Axis ratio (b/a)"
PRINTF,lun, " 10) 47.04     1          #  Position angle (PA) [deg: Up=0, Left=90]"
PRINTF,lun, " #B1) 0.9 1"
PRINTF,lun, "  Z) 0                     #  Skip this model in output image?  (yes=1, no=0)"
PRINTF,lun, " "
PRINTF,lun, "# Component number: 2"
PRINTF,lun, " 0) expdisk                #  Component type"
PRINTF,lun, " 1) ",xcoord[1],"  ",ycoord[1],"  1 1  #  Position x, y"
PRINTF,lun, " 3) 23.     1          #  Integrated magnitude"
PRINTF,lun, " 4) 6.0      1          #  R_s (disk scale-length)   [pix]"
PRINTF,lun, " 5) 0.0000      0          #     -----"
PRINTF,lun, " 6) 0.0000      0          #     -----"
PRINTF,lun, " 7) 0.0000      0          #     -----"
PRINTF,lun, " 8) 0.0000      0          #     -----"
PRINTF,lun, " 9) 0.56      1          #  Axis ratio (b/a)"
PRINTF,lun, " 10) 47.04     1          #  Position angle (PA) [deg: Up=0, Left=90]"
PRINTF,lun, " F2) 0.6 20  1 1         # Az. Fourier mode 2, amplitude and phase angle"
PRINTF,lun, " R0) log                 # PA rotation func. (tanh, sqrt, log, linear, none)"
PRINTF,lun, "R1) 1.        1       # bar radius  [pixels]"
PRINTF,lun, "R2) 2.       1       # 96% asymptotic radius (i.e. at 96% of tanh rotation)"
PRINTF,lun, "R3) 95.   1       # cumul. coord. rotation out to asymp. radius [degrees]"
PRINTF,lun, "R4) 4.         1       # Logarithmic winding scale radius [pixels]"
PRINTF,lun, "R9) 79.   1       # Inclination to L.o.S. [degrees]"
PRINTF,lun, "R10) -45.  1       # Sky position angle"
PRINTF,lun, "B1) 2.9     1           # Bending mode 1 (shear)"
PRINTF,lun, " Z) 0                      #  Skip this model in output image?  (yes=1, no=0)"
PRINTF,lun, "################################################################################"

.
.
.
[All the rest of the 25 individually made objects are added here similarly to the first
two above.]
.
.
.
```

```
; ###################################################################

; If Ntarget GT 25, more galaxies are generated:

IF Nrandom GT 0 THEN BEGIN
  ; Generating random values for Sersic n, position angle, radius, axis ratio, C0
  SersicN = 0.5 + 6 * RANDOMU(Seed,Nrandom)
  C = FLTARR(2,Nrandom)
  AR = FLTARR(2,Nrandom)
  Re = FLTARR(2,Nrandom)

  Incl = 10 + 60 * RANDOMU(Seed,Nspirals)
  Nmode = 2 + 2 * FIX(3 * RANDOMU(Seed,Nspirals))
  Nmode = STRTRIM(Nmode,2)
  Famp = 0.01 + 0.3 * RANDOMU(Seed,Nspirals)  ; Fourier amplitude
  Fang = 180 * RANDOMU(Seed,Nspirals)         ; Fourier angle
  Bamp = 0.01 + 0.6 * RANDOMU(Seed, Nspirals)  ; Bending amplitude
  R1 = 5 * RANDOMU(Seed,Nspirals)              ; Bar radius [pix]
  R2 = 5 + 50 * RANDOMU(Seed,Nspirals)            ; Asymptotic radius
  R3 = 120 + 180 * RANDOMU(Seed, Nspirals)     ; Rotation to r_asympt
  R4 = 0.5 + 4 * RANDOMU(Seed,Nspirals)       ; Winding scale radius


  FOR j =0,Nrandom-1 DO BEGIN
    C[0,j] = -0.2 + 0.5 * RANDOMU(Seed,1)
    C[1,j] = -0.2 + 0.5 * RANDOMU(Seed,1)

    AR[0,j] = 0.3+0.8* RANDOMU(Seed,1)
    AR[1,j] = 0.3+0.8*RANDOMU(Seed,1)

    Re[0,j] = 2+7* RANDOMU(Seed,1)
    Re[1,j] = 2+7*RANDOMU(Seed,1)
  ENDFOR

  print, 'mode: ',Nmode
  print, Nspirals
  ;print, xcoord[25+Nellipses+1]

  FOR m =0,Nellipses-1 DO BEGIN
    PRINTF,lun, "################################################################################"
    PRINTF,lun, "# Component number: N"
    PRINTF,lun, " 0) sersic                 #  Component type"
    PRINTF,lun, " 1) ",xcoord[25+m]," ",ycoord[25+m]," 1 1  #  Position x, y"
    PRINTF,lun, " 3) ",MAG[0,25+m],"     1          #  Integrated magnitude "
    PRINTF,lun, " 4) ",Re[0,m],"     1          #  R_e (effective radius)   [pix]"
    PRINTF,lun, " 5) ",SersicN[m],"     1          #  Sersic index n (de Vaucouleurs n=4) "
    PRINTF,lun, " 6) 0.0000      0          #     ----- "
    PRINTF,lun, " 7) 0.0000      0          #     ----- "
    PRINTF,lun, " 8) 0.0000      0          #     ----- "
    PRINTF,lun, " 9) ",AR[0,m],"      1          #  Axis ratio (b/a)  "
    PRINTF,lun, " 10) ",PA[0,25+m],"     1          #  Position angle (PA) [deg: Up=0, Left=90]"
    PRINTF,lun, "C0) ",C[0,m],"         0      # traditional diskyness(-)/boxyness(+)"
    PRINTF,lun, " Z) 0                      #  Skip this model in output image?  (yes=1, no=0)"
    PRINTF,lun, ""
    PRINTF,lun, " # Component number: N deVaucouleur function"
    PRINTF,lun, " 0) devauc             # Object type"
    PRINTF,lun, " 1) ",xcoord[25+m],"  ",ycoord[25+m],"  1 1    # position x, y        [pixel]"
    PRINTF,lun, " 3) ",MAG[1,25+m],"        1       # total magnitude    "
    PRINTF,lun, " 4) ",Re[1,m],"        1       #     R_e              [Pixels]"
    PRINTF,lun, " 9) ",AR[1,m],"       1       # axis ratio (b/a)   "
    PRINTF,lun, " 10) ",PA[1,25+m],"       1       # position angle (PA)  [Degrees: Up=0, Left=90]"
    PRINTF,lun, " C0) ",C[1,m],"         0      # traditional diskyness(-)/boxyness(+)"
    PRINTF,lun, " Z) 0                  #  Skip this model in output image?  (yes=1, no=0)"
    PRINTF,lun, "################################################################################"
  ENDFOR
```

```
  IF Nspirals GT 0 THEN BEGIN
    FOR w =0,Nspirals-1 DO BEGIN
      ;MAG[0,25+Nellipses+w] = 1 + MAG[0,25+Nellipses+w]
      MAG[1,25+Nellipses+w] = 1 + MAG[1,25+Nellipses+w]
      PRINTF,lun, "################################################################################"
      PRINTF,lun, "# Component number: N+1"
      PRINTF,lun, " 0) sersic                 #  Component type"
      PRINTF,lun, " 1) ",xcoord[25+Nellipses+w]," ",ycoord[25+Nellipses+w]," 1 1 #Position x, y"
      PRINTF,lun, " 3) ",MAG[0,25+Nellipses+w],"     1 #Integrated magnitude"
      PRINTF,lun, " 4) ",Re[0,Nellipses+w],"    1     #R_e (effective radius)   [pix]"
      PRINTF,lun, " 5) ",SersicN[Nellipses+w],"     1 #Sersic index n (de Vaucouleurs n=4)"
      PRINTF,lun, " 6) 0.0000      0          #     -----"
      PRINTF,lun, " 7) 0.0000      0          #     -----"
      PRINTF,lun, " 8) 0.0000      0          #     -----"
      PRINTF,lun, " 9) ",AR[0,Nellipses+w],"      1          #  Axis ratio (b/a)"
      PRINTF,lun, " 10) ",PA[0,25+Nellipses+w],"   1 #Position angle (PA) [deg: Up=0,Left=90]"
;     PRINTF,lun, " B1) 0.9 1"
      PRINTF,lun, "  Z) 0                      #  Skip this model in output image?  (yes=1, no=0)"
      PRINTF,lun, " "
      PRINTF,lun, "# Component number: N+1"
      PRINTF,lun, " 0) expdisk                # Component type"
      PRINTF,lun, " 1) ",xcoord[25+Nellipses+w]," ",ycoord[25+Nellipses+w]," 1 1 #Position x,y"
      PRINTF,lun, " 3) ",MAG[1,25+Nellipses+w]," 1 # Integrated magnitude"
      PRINTF,lun, " 4) ",Re[1,Nellipses+w]," 1 # R_s (disk scale-length) [pix]"
      PRINTF,lun, " 5) 0.0000      0          #     -----"
      PRINTF,lun, " 6) 0.0000      0          #     -----"
      PRINTF,lun, " 7) 0.0000      0          #     -----"
      PRINTF,lun, " 8) 0.0000      0          #     -----"
      PRINTF,lun, " 9) ",AR[1,Nellipses+w],"     1 # Axis ratio (b/a)"
      PRINTF,lun, " 10) ",PA[1,25+Nellipses+w]," 1 # Position angle (PA) [deg: Up=0, Left=90]"
      PRINTF,lun, "F",Nmode[w],") ",STRTRIM(Famp[w],2)," ",STRTRIM(Fang[w],2)," 1 1 # F2,a,phi"
      PRINTF,lun, " R0) log       # PA rotation func. (tanh, sqrt, log, linear, none)"
      PRINTF,lun, "R1) ",R1[w],"  1  # bar radius  [pixels]"
      PRINTF,lun, "R2) ",R2[w],"  1  # 96% asymptotic radius (i.e. at 96% of tanh rotation)"
      PRINTF,lun, "R3) ",R3[w],"  1  # cumul. coord. rotation out to asymp. radius [degrees]"
      PRINTF,lun, "R4) ",R4[w],"  1  # Logarithmic winding scale radius [pixels]"
      PRINTF,lun, "R9) ",Incl[w]," 1 # Inclination to L.o.S. [degrees]"
      PRINTF,lun, "R10) ",90+PA[1,25+Nellipses+w]," 1  # Sky position angle"
      PRINTF,lun, "B1) ",Bamp[w]," 1 # Bending mode 1 (shear)"
      PRINTF,lun, " Z) 0            #  Skip this model in output image?  (yes=1, no=0)"
      PRINTF,lun, "################################################################################"
    ENDFOR
  ENDIF

ENDIF

PRINTF,lun, "================================================================================"
; Close the file and free the file unit
FREE_LUN, lun


; ###################################
; RUN GALFIT
command = './galfit '+galfitfile
SPAWN, command
; ###################################


; # # # # # # # # # # # # # # # # # # # # # # # # # # # # # # # # # # # # # # # # # # #
; Time to generate some CATALOGS!


; Calculating total integrated magnitudes of each object
; Calculating average position angle and its error for each object


TOTALMAG = FLTARR(1,Ntargets)
RA = FLTARR(1,Ntargets)
```

```
DEC = FLTARR(1,Ntargets)
MEANPA = FLTARR(1,Ntargets)
PAerr = FLTARR(1,Ntargets)

FOR z =0,Ntargets-1 DO BEGIN
  TOTALMAG[z] = -2.5 * ALOG10(10^(-0.4*MAG[0,z])+10^(-0.4*MAG[1,z]))

  RA[z] = xcoord[z] * 0.3 /(60*60)  ; RA in degrees: pixel coordinate times pixel scale
                                    ; ["/pix] divided by seconds times minutes.
  DEC[z] = ycoord[z] * 0.3 /(60*60) ; DEC in degrees: pixel coordinate times pixel scale
                                    ; ["/pix] divided by seconds times minutes.
  RA[z] = InitCoord[0,0] - RA[z]    ; RA increases to left
  DEC[z] = InitCoord[0,1] + DEC[z]  ; DEC increases to up

  MEANPA[z] = 0.5 * (PA[0,z] + PA[1,z]) ; Mean position angle of the objects
  PAerr[z] = 1/SQRT(2) * SQRT(0.5*((PA[0,z] - MEANPA[z])^2+(PA[1,z] - MEANPA[z])^2))
ENDFOR


;print, RA,DEC,MEANPA,PAerr


; #  #  #  #  #  #  #  #  #  #  #  #
; Generating txt file with x [pis], y [pix], RA, DEC and Mag
txttablefile = FILEPATH('randField.txt',ROOT_DIR=['~'],SUBDIRECTORY=['Euclid',dir])
OPENW, lun2, txttablefile, /GET_LUN


FOR q =0,Ntargets-1 DO BEGIN
  PRINTF, lun2, STRING(xcoord[q],FORMAT='(D0)')," ",STRING(ycoord[q],FORMAT='(D0)')," ",$
    STRING(RA[q],FORMAT='(D0)')," ",STRING(DEC[q],FORMAT='(D0)')," ",$
    STRING(TOTALMAG[q],Format='(D0)')," ",STRING(MEANPA[q],Format='(D0)')," ",$
    STRING(PAerr[q],Format='(D0)')
ENDFOR
; Close the script's output file and free the file unit.
FREE_LUN, lun2
; #  #  #  #  #  #  #  #  #  #  #  #

;Generating txt file containing information to fits header
txtheaderfile = FILEPATH('headerinfo.txt',ROOT_DIR=['~'],SUBDIRECTORY=['Euclid',dir])
OPENW, lun3, txtheaderfile, /GET_LUN

PRINTF, lun3, STRING(sky,FORMAT='(D0.2)')," ",STRING(dx,FORMAT='(E11.2)')," ",$
  STRING(dy,FORMAT='(E11.2)')," ",NtargetsString," 0.3 1.0 1.0"


FREE_LUN, lun3
; #  #  #  #  #  #  #  #  #  #  #  #
; Generating FITS table file

command2 = 'rm randField_catalog.fits'  ; Remove existing output .fits table
SPAWN, command2
command3 = 'python tablegenerator.py'   ; run Python script to produce output .fits table
SPAWN, command3                         ; 'randField_catalog.fits'


endtime = SYSTIME() ; End time of the run.
PRINT, 'Start: '+starttime
PRINT, 'Finish: '+endtime

END
```

A.2.5 Tablegenerator.py

```
from astropy.io import fits
import numpy as np
```

```
import pandas as pd
import csv

path = '/home/antluoma/Euclid/OUsimValidation/'

inputfile = open(path+'randField.txt','r+')
headerfile = open(path+'headerinfo.txt','r+')

xcoord=[]
ycoord=[]
RA=[]
DEC=[]
TOTALMAG=[]
MEANPA=[]
PAerr=[]
data=[]
x=[]
y=[]
r=[]
d=[]
m=[]
pa=[]
paerr=[]



for line in inputfile:
   line = line.split()
   xcoord = line[0]
   ycoord = line[1]
   RA = line[2]
   DEC = line[3]
   TOTALMAG = line[4]
   MEANPA = line[5]
   PAerr = line[6]

   x.append(float(xcoord))
   y.append(float(ycoord))
   r.append(float(RA))
   d.append(float(DEC))
   m.append(float(TOTALMAG))
   pa.append(float(MEANPA))
   paerr.append(float(PAerr))

a1 = np.array(x)
a2 = np.array(y)
a3 = np.array(r)
a4 = np.array(d)
a5 = np.array(m)
a6 = np.array(pa)
a7 = np.array(paerr)

col1 = fits.Column(name='XCOORD',format='D',array=a1)
col2 = fits.Column(name='YCOORD',format='D',array=a2)
col3 = fits.Column(name='RA',format='D',array=a3)
col4 = fits.Column(name='DEC',format='D',array=a4)
col5 = fits.Column(name='MAG',format='D',array=a5)
col6 = fits.Column(name='PA',format='D',array=a6)
col7 = fits.Column(name='PAERR',format='D',array=a7)

cols = fits.ColDefs([col1,col2,col3,col4,col5,col6,col7])

tbhdu = fits.BinTableHDU.from_columns(cols)

tbhdu.writeto('randField_catalog.fits')
```

A.3 Results of the fits of the CANDELS sample

A.3.1 RGB images of data and GALFIT models

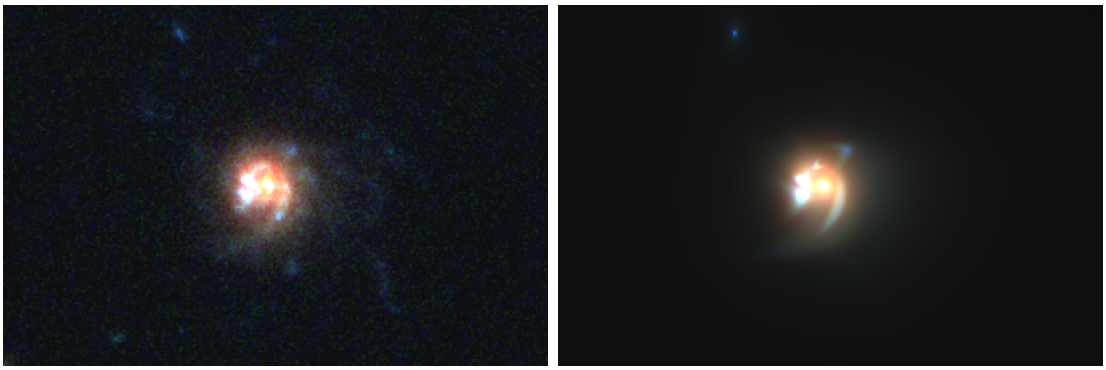

Figure A.1: The RGB image of the object 29_3 composed with data images in the left and the GALFIT models in the right. The filters from red to blue are: F160, F814 and F606.

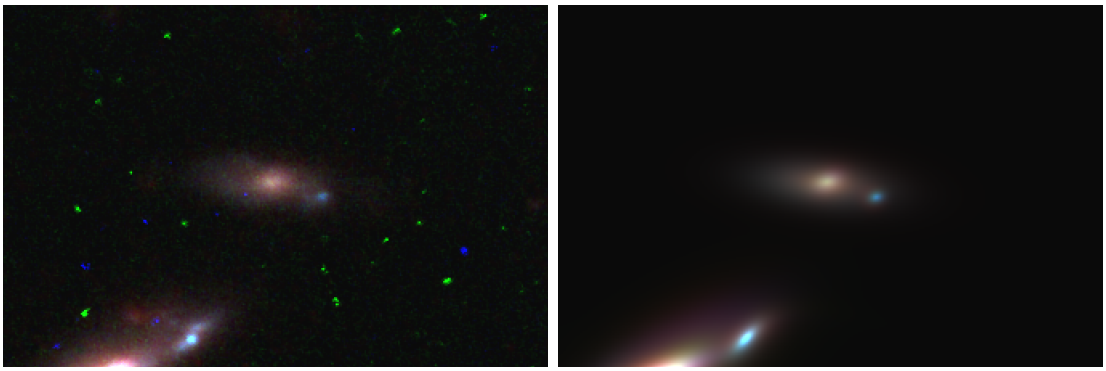

Figure A.2: The RGB image of the object 3124_3 composed with data images in the left and the GALFIT models in the right. The filters from red to blue are: F160, F814 and F606.

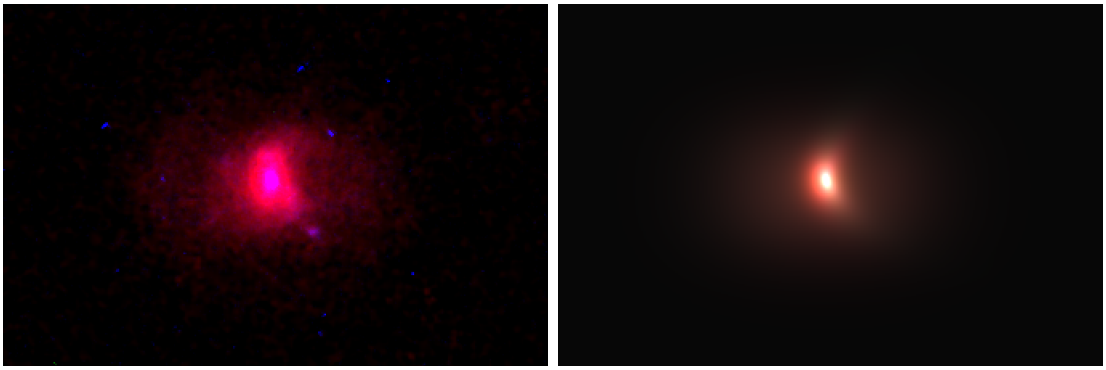

Figure A.3: The RGB image of the object 3124_5 composed with data images in the left and the GALFIT models in the right. The filters from red to blue are: F160, F814 and F606.

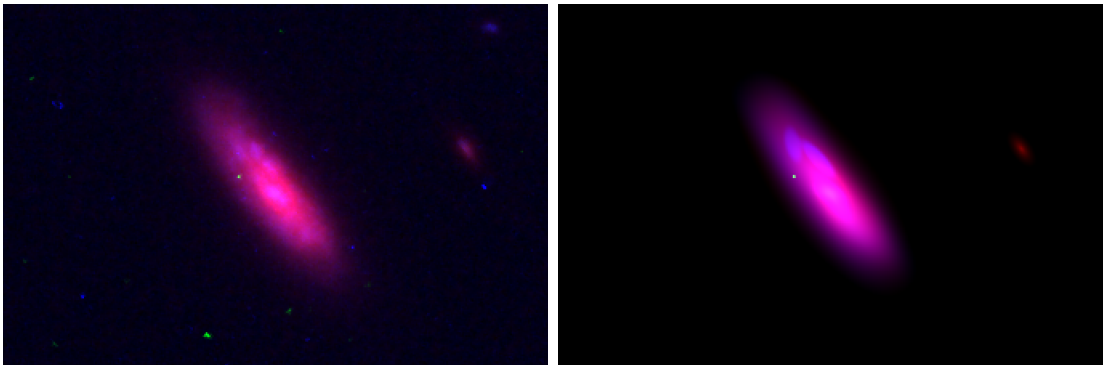

Figure A.4: The RGB image of the object 3124_6 composed with data images in the left and the GALFIT models in the right. The filters from red to blue are: F160, F814 and F606.

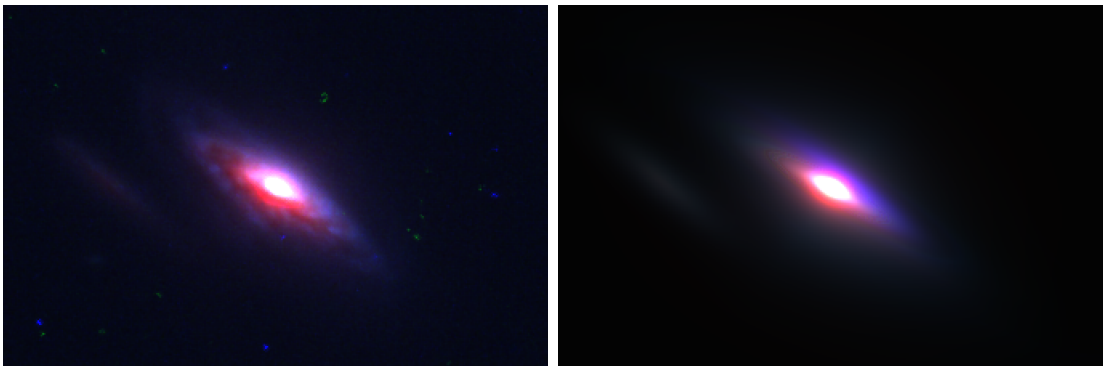

Figure A.5: The RGB image of the object 3124_11 composed with data images in the left and the GALFIT models in the right. The filters from red to blue are: F160, F814 and F606.

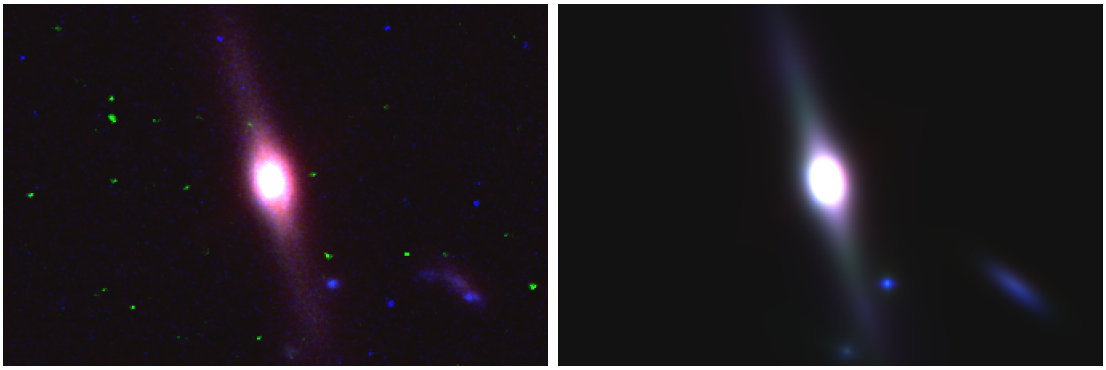

Figure A.6: The RGB image of the object 3167_2 composed with data images in the left and the GALFIT models in the right. The filters from red to blue are: F160, F814 and F606.

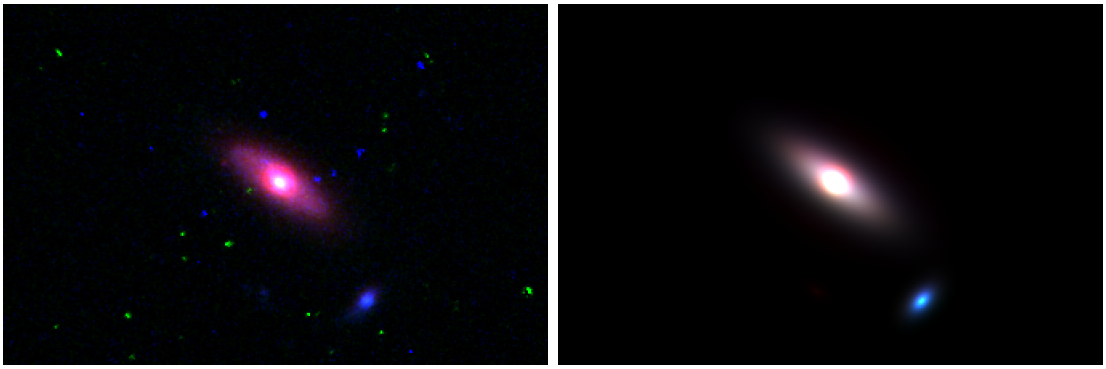

Figure A.7: The RGB image of the object 3167_4 composed with data images in the left and the GALFIT models in the right. The filters from red to blue are: F160, F814 and F606.

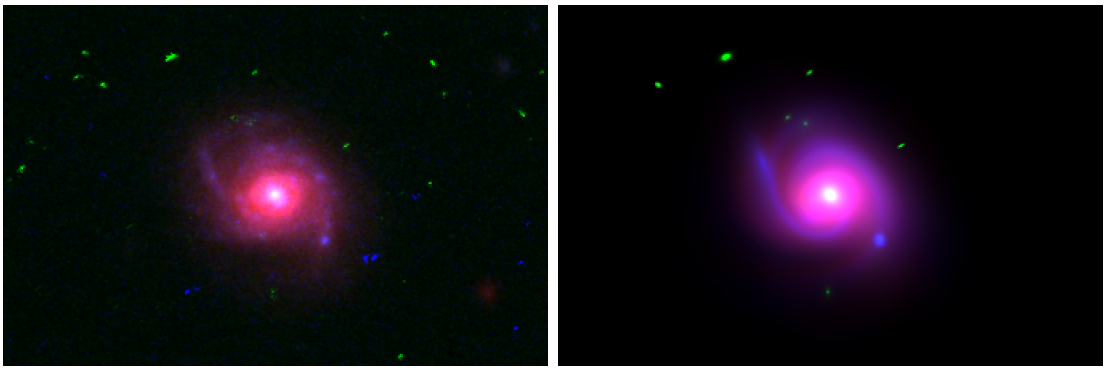

Figure A.8: The RGB image of the object 3167_6 composed with data images in the left and the GALFIT models in the right. The filters from red to blue are: F160, F814 and F606.

A.3.2 Images of the GALFIT models

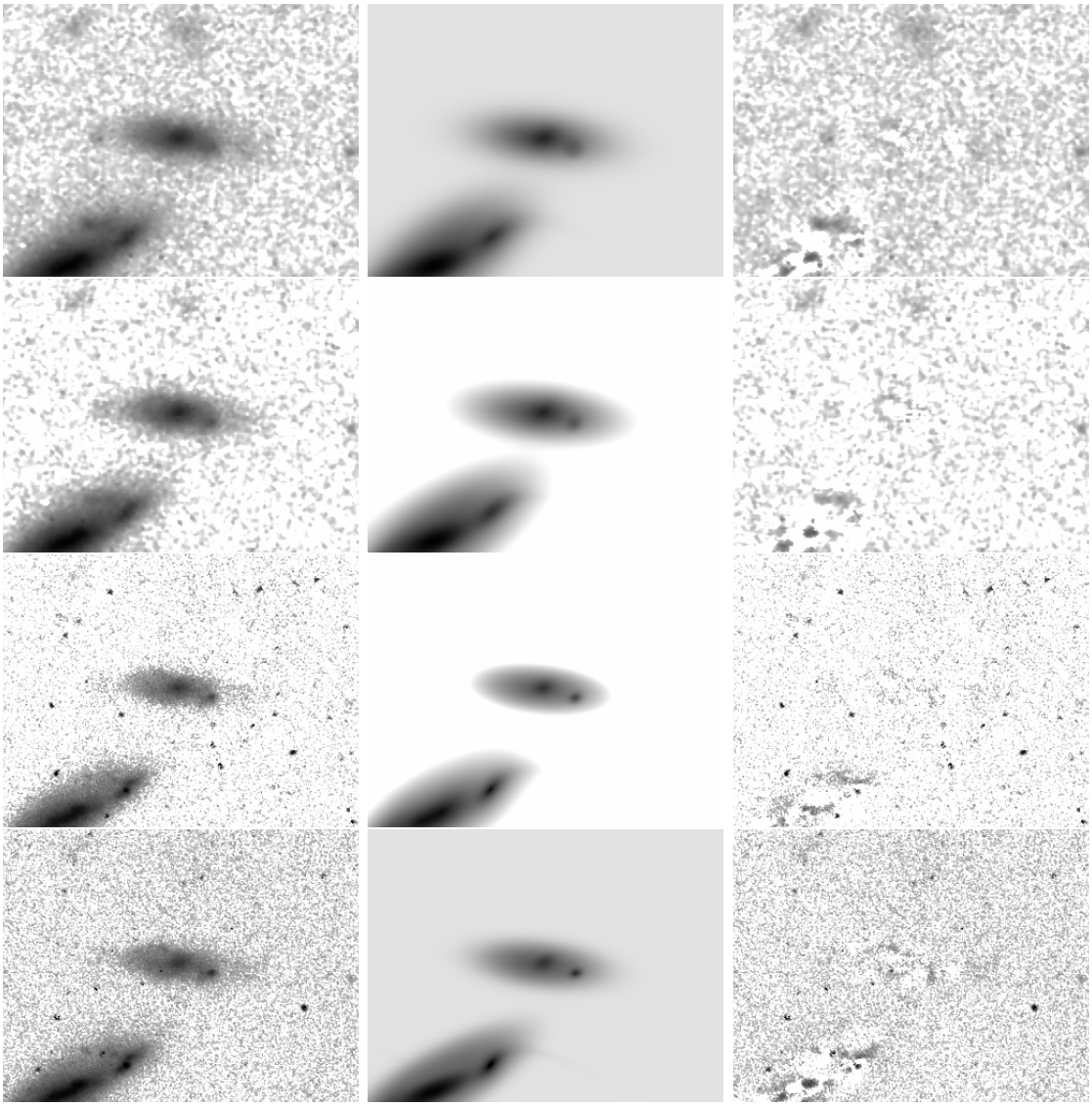

Figure A.9: The observed images of the object 3124_3 are displayed in the left column. The middle column is the GALFIT models obtained with Sersic components and the sky estimate. The right column shows the residual image. The used filters are in order from top to bottom: F160W, F125W, F814W and F606W.

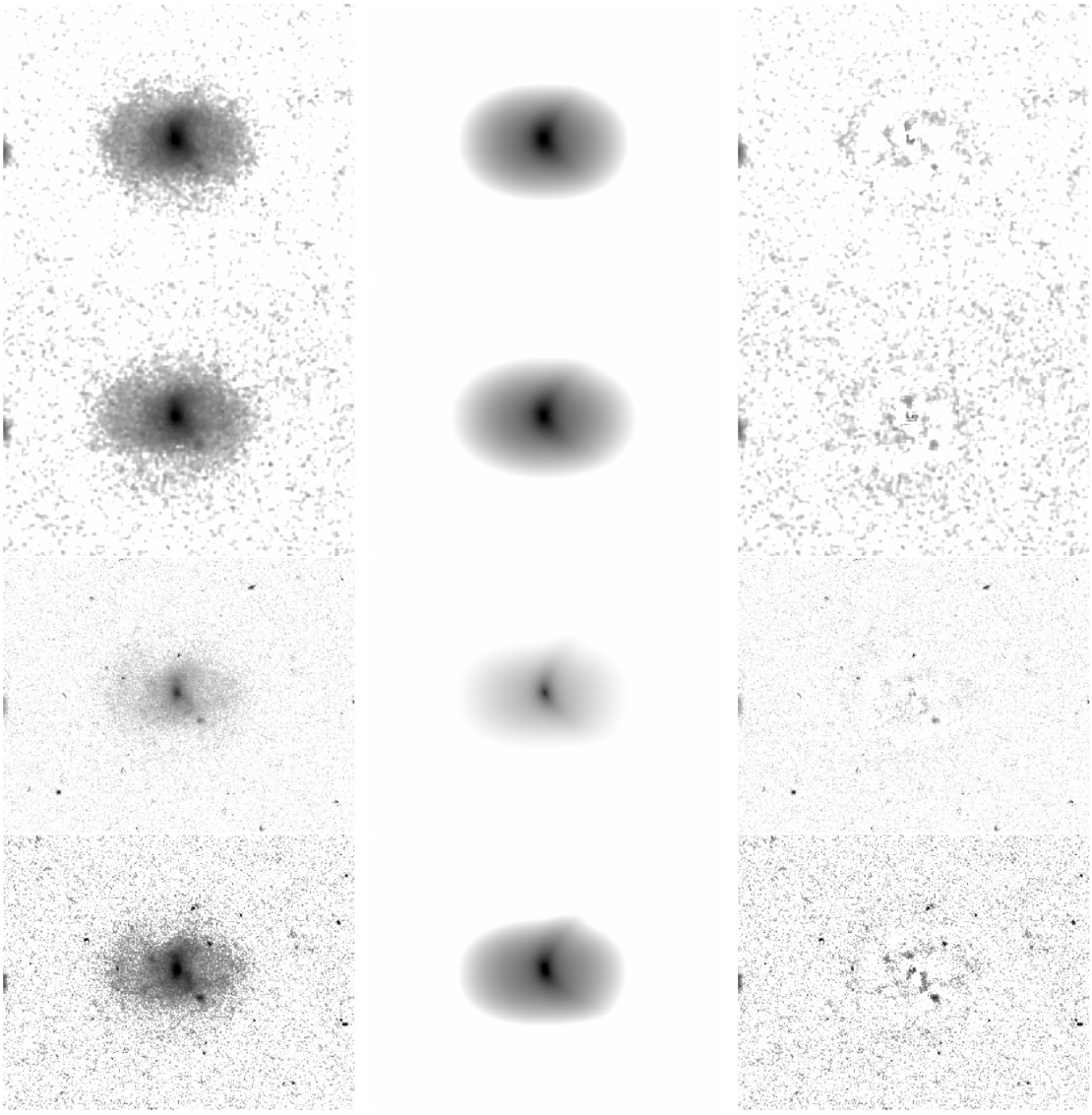

Figure A.10: The observed images of the object 3124_5 are displayed in the left column. The middle column is the GALFIT models obtained with 2 Sersic components and the sky estimate. The right column shows the residual image. The used filters are in the following order from top to bottom: F160W, F125W, F814W and F606W.

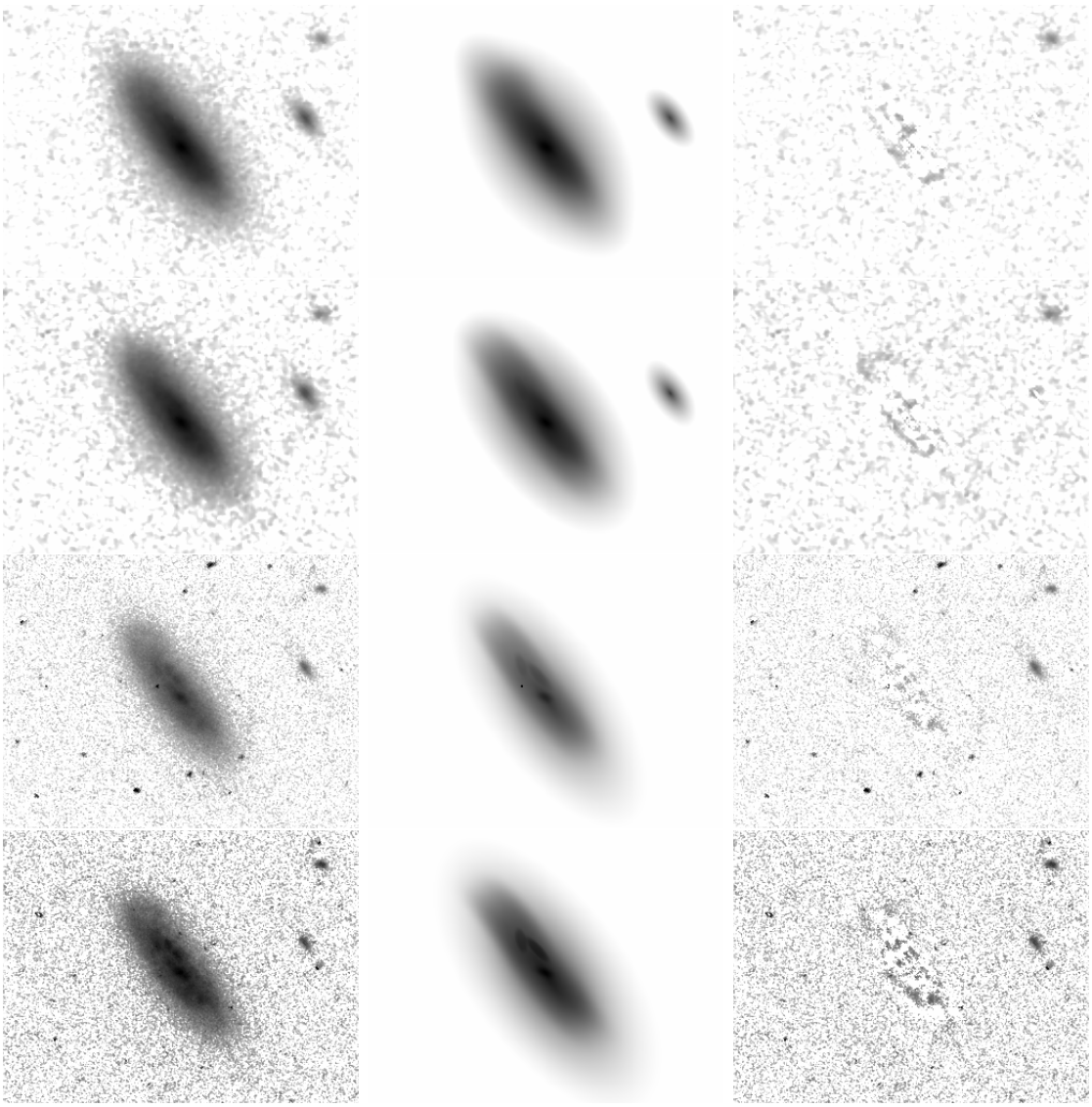

Figure A.11: The observed images of the object 3124_6 are displayed in the left column. The middle column is the GALFIT models obtained with 4 Sersic components, an exponential disk component, gaussian central component and the sky estimate. The right column shows the residual image. The used filters are in the following order from top to bottom: F160W, F125W, F814W and F606W.

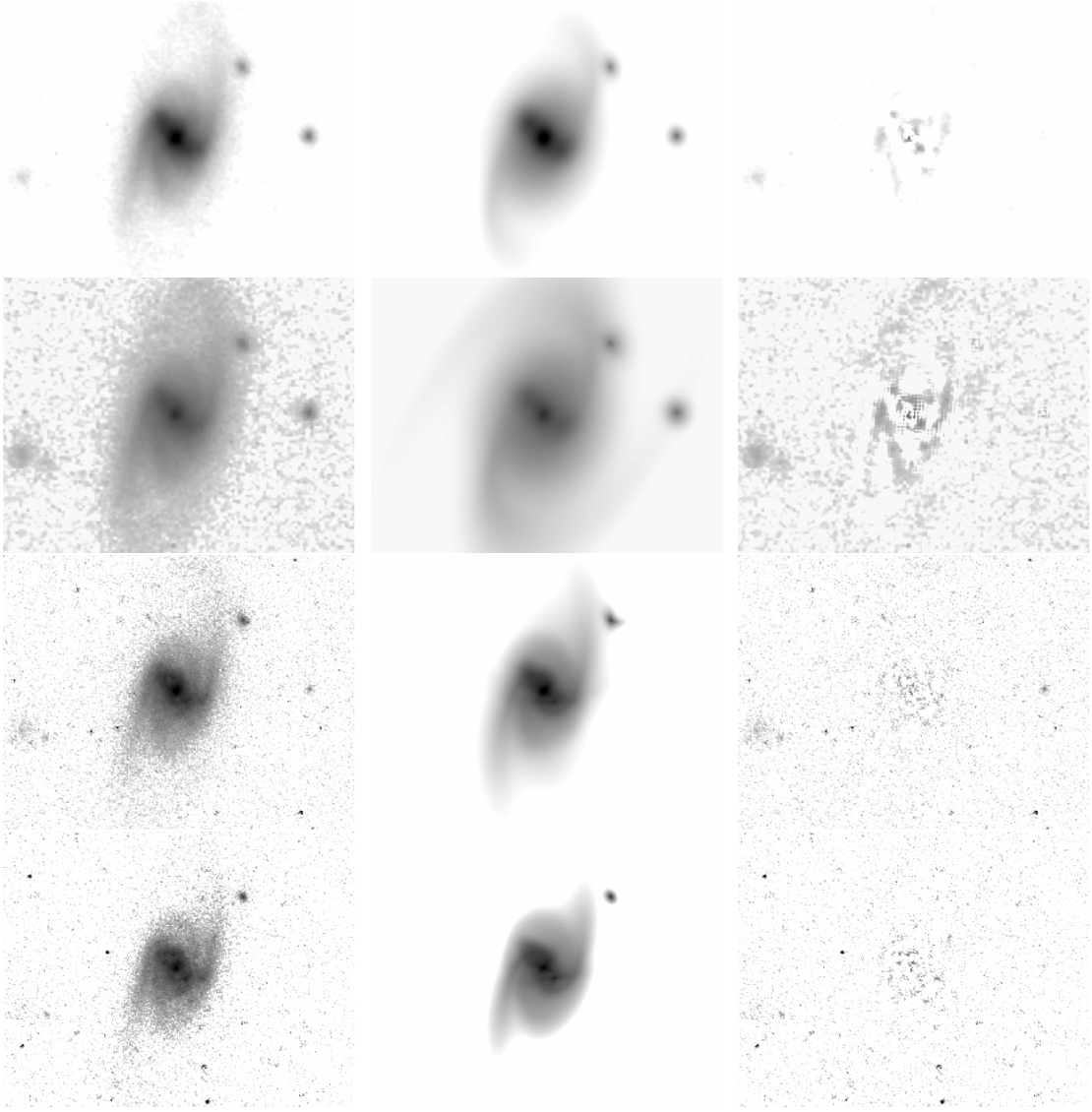

Figure A.12: The observed images of the object 3124_8 are displayed in the left column. The middle column is the GALFIT models obtained with 5 Sersic components, an exponential disk component and the sky estimate. The right column shows the residual image. The used filters are in the following order from top to bottom: F160W, F125W, F814W and F606W.

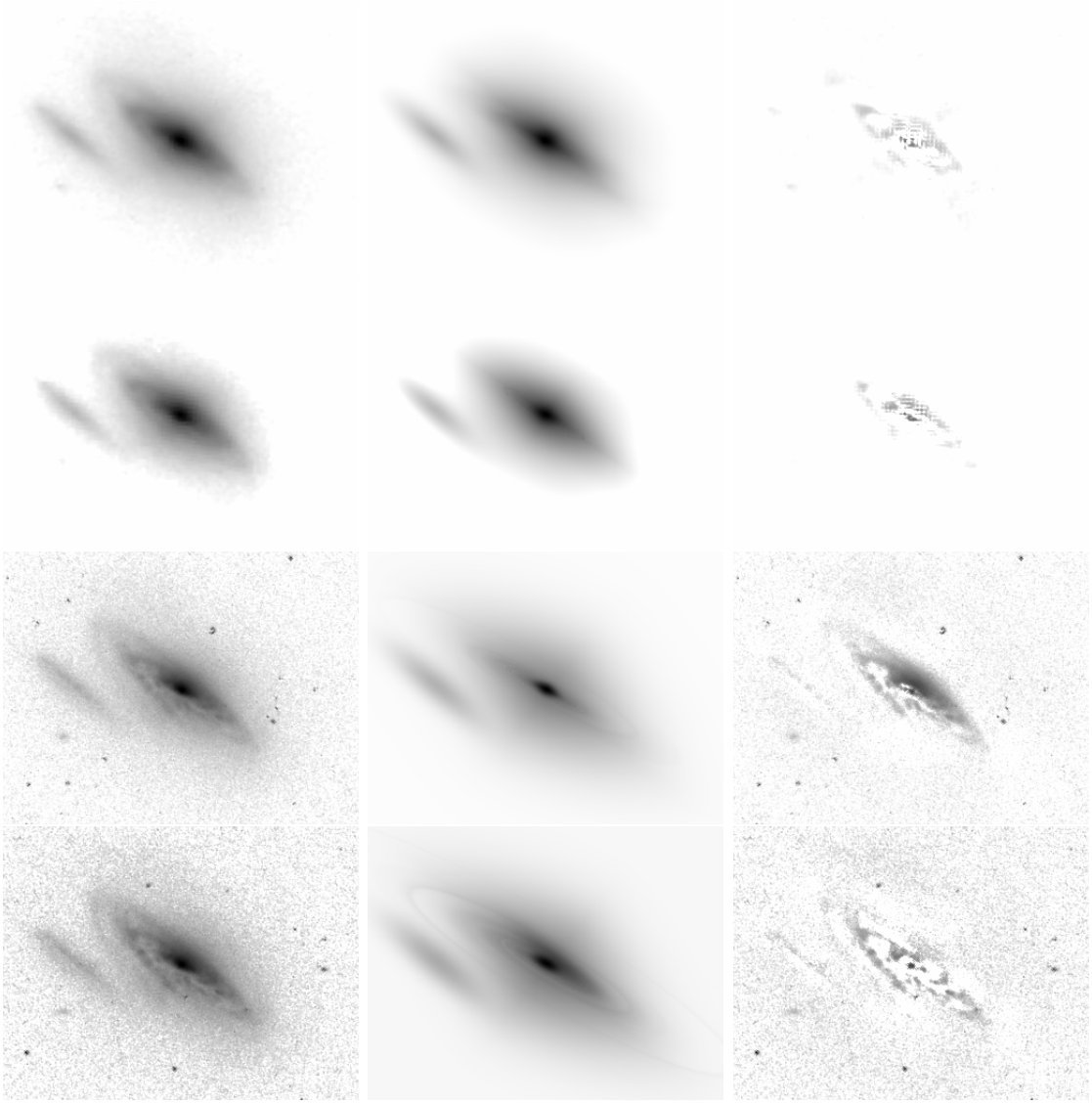

Figure A.13: The observed images of the object 3124_11 are displayed in the left column. The middle column is the GALFIT models obtained with 4 Sersic components, an exponential disk component and the sky estimate. The right column shows the residual image. The used filters are in the following order from top to bottom: F160W, F125W, F814W and F606W.

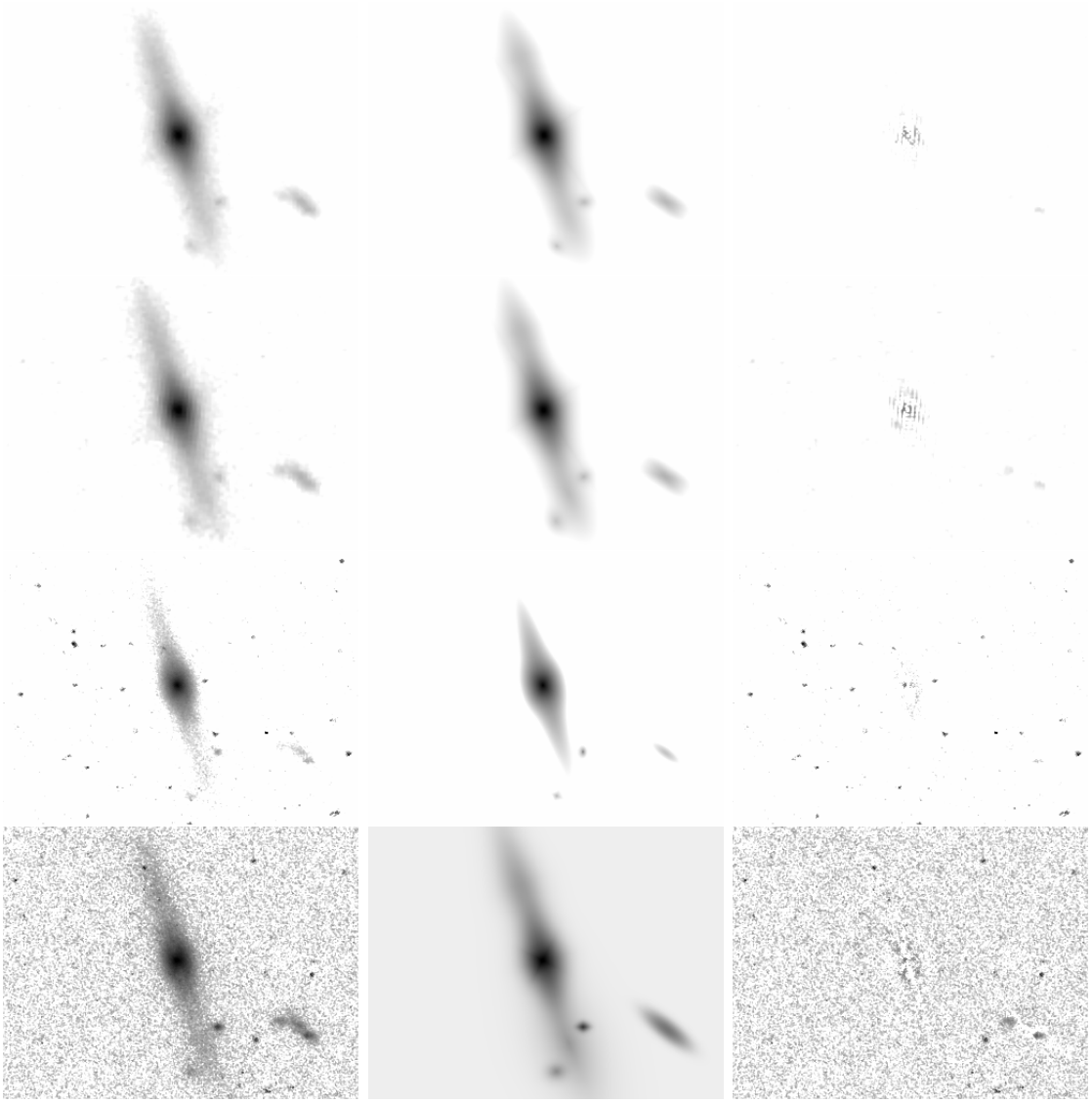

Figure A.14: The observed images of the object 3167_2 are displayed in the left column. The middle column is the GALFIT models obtained with multiple Sersic components, an edge-on exponential disk components and the sky estimate. The right column shows the residual image. The used filters are in the following order from top to bottom: F160W, F125W, F814W and F606W.

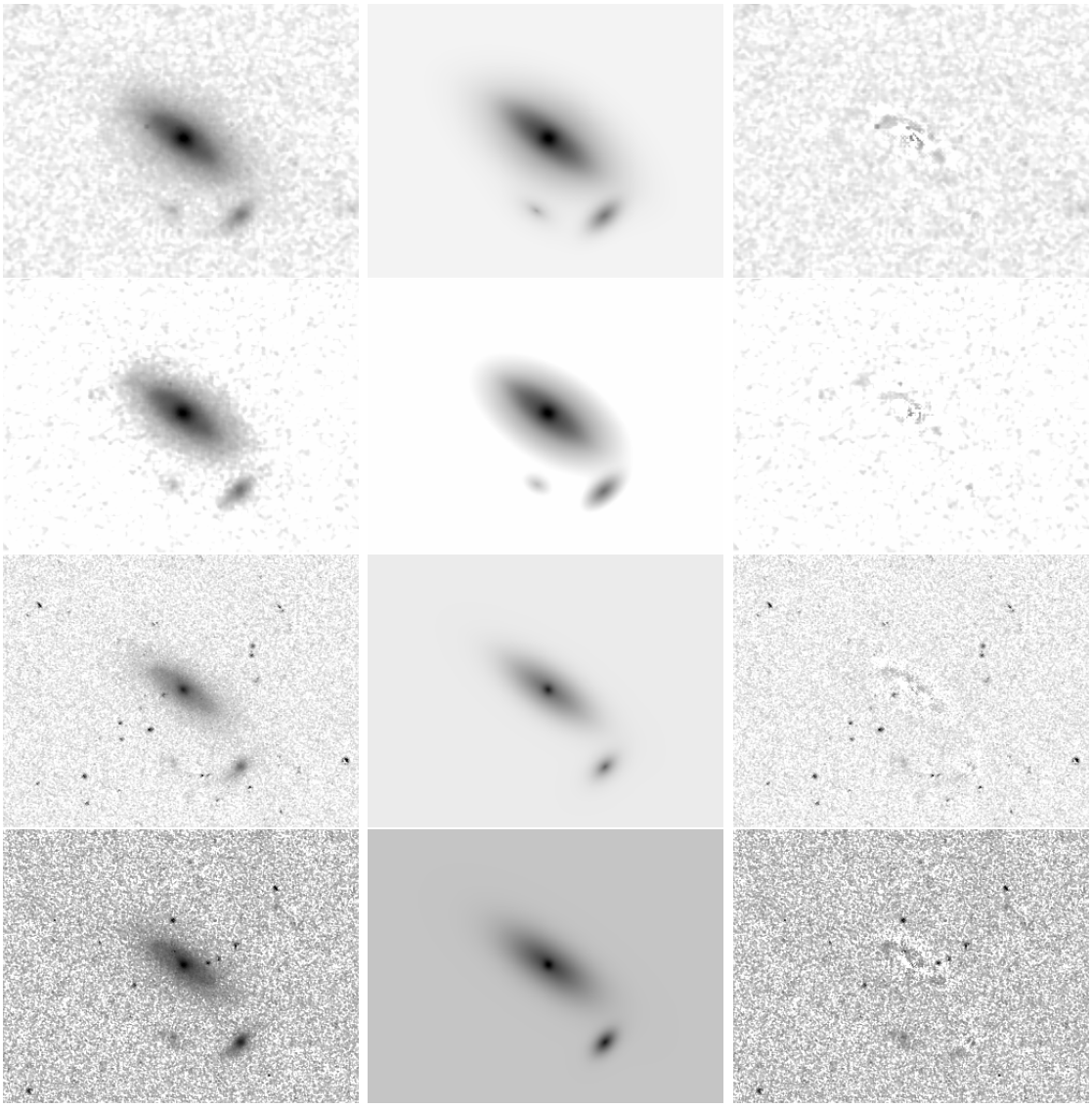

Figure A.15: The observed images of the object 3167_4 are displayed in the left column. The middle column is the GALFIT models obtained with multiple Sersic components and the sky estimate. The right column shows the residual image. The used filters are in the following order from top to bottom: F160W, F125W, F814W and F606W.

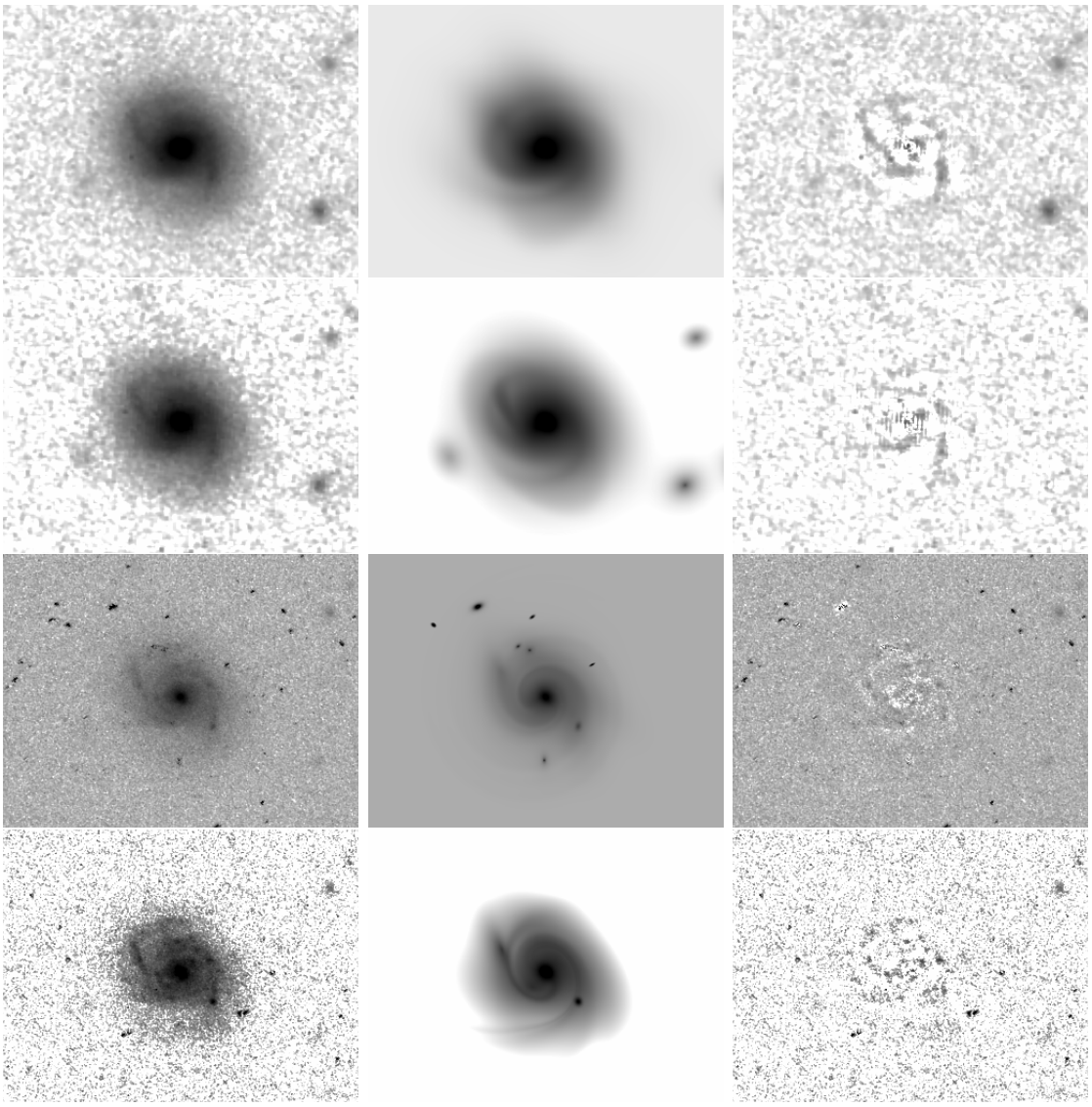

Figure A.16: The observed images of the object 3167_6 are displayed in the left column. The middle column is the GALFIT models obtained with multiple Sersic components, exponential disk component with spiral structure and the sky estimate. The right column shows the residual image. The used filters are in the following order from top to bottom: F160W, F125W, F814W and F606W.

A.3.3 Filters that cover *ugri* colors of the sample galaxies

Object ID	u	g	r	i
113_16[2]	F775W/F814W	F105W	F130N	F160W[1]
113_18[2]	F775W/F814W[1]	F105W	F130N	F160W[1]
113_19[2]	F775W/F814W[1]	F105W	F130N	F160W[1]
113_20[2]	F775W/F814W[1]	F105W	F130N	F160W[1]
131_10[2]	F606W[1]/F350LP	F845M/F814W[1]	F105W[1]	F132N
131_9[2]	F606W[1]/F350LP	F845M/F814W[1]	F105W[1]	F132N
16_9[2]	F475W/F467M	F680N/F689M	F845M/F814W[1]	F105W
17_13	F555W/F200LP	F850LP	F098M	F110W
18_24[2]	F680N/F689M	F098M	F125W[1]	F140W
18_38[2]	F680N/F689M	F098M	F125W[1]	F140W
18_40[2]	F680N/F689M	F098M	F125W[1]	F140W
210_10	F625W/F606W	F850LP	F125W/F110W	F140W
210_3[2]	F625W/F606W	F850LP	F125W/F110W	F140W
227_3[2]	F547M/F606W	F814W[1]	F105W[1]	F140W
229_1[2]	F625W/F606W	F850LP	F125W[1]/F110W	F140W
229_23[2]	F625W/F606W[1]	F850LP	F125W/F110W	F140W
229_5[2]	F625W/F606W[1]	F850LP	F125W/F110W	F140W
229_6[2]	F625W/F606W	F850LP[1]	F125W[1]/F110W	F140W
229_7[2]	F625W/F606W[1]	F850LP[1]	F125W/F110W	F140W
229_9[2]	F625W/F606W[1]	F850LP[1]	F125W[1]/F110W	F140W
28_1[2]	F606W/F350LP	F845M/F814W[1]	F105W	F140W
28_4[2]	F606W/F350LP	F845M/F814W[1]	F105W	F140W
29_10[2]	F606W[1]/F350LP	F814W[1]	F105W[1]	F140W
29_1[2]	F606W[1]/F350LP	F814W[1]	F105W[1]	F140W
29_2[2]	F606W/F350LP	F814W[1]	F105W[1]	F140W
29_3[2]	F606W[1]/F350LP	F814W[1]	F105W[1]	F140W

Object ID	u	g	r	i
3124_11[2]	F438W	F625W/F606W	F775W/F814W	F105W
3124_3[2]	F438W	F625W/F606W[1]	F755W/F814W[1]	F105W
3124_5[2]	F438W	F625W/F606W[1]	F755W/F814W[1]	F105W
3124_6[2]	F438W	F625W/F606W[1]	F755W/F814W[1]	F105W
3124_8[2]	F438W	F625W/F606W	F755W/F814W	F105W
3167_2[2]	F475W	F600LP	F850LP	F105W
3167_4[2]	F475W	F600LP	F850LP	F105W
3167_6[2]	F475W	F600LP	F850LP	F105W
3167_7[2]	F475W	F600LP	F850LP	F105W
3210_15[2]	F625W/F606W[1]	F850LP	F125W[1]/F110W	F140W
3210_18[2]	F625W/F606W[1]	F850LP	F125W[1]/F110W	F140W
3227_7	F438W/F475W	F600LP	F814W	F105W
3289_10	F475X/F555W	F600LP	F098M	F125W
3289_9	F475X/F555W	F600LP	F098M	F125W
392_4	F475X/F555W	F600LP	F850LP	F125W/F105W
392_8	F475X/F555W	F600LP	F850LP	F125W/F105W
432_12	F475X/F555W	F600LP	F850LP	F105W/F105W
432_13	F475X/F555W	F600LP	F850LP	F105W/F105W
438_3[2]	F606W[1]/F350LP	F850LP	F105W	F140W
438_5[2]	F606W[1]/F350LP	F850LP	F105W	F140W
438_6[2]	F606W[1]/F350LP	F850LP	F105W	F140W
438_8[2]	F606W[1]/F350LP	F850LP	F105W	F140W
447_1	F625W/F606W	F850LP	F125W/F110W	F140W
447_4	F625W/F606W	F850LP	F125W/F110W	F140W
447_5	F625W/F606W	F850LP	F125W/F110W	F140W
447_7	F625W/F606W	F850LP	F125W/F110W	F140W
447_8	F625W/F606W	F850LP	F125W/F110W	F140W
455_16	F625W/F606W	F850LP	F125W/F110W	F140W

Object ID	u	g	r	i
455_4	F625W/F606W	F850LP	F125W/F110W	F140W
458_2[2]	F625W/F606W[1]	F600LP	F105W	F110W
458_6[2]	F625W/F606W[1]	F600LP	F105W	F110W
459_11	F438W	F625W/F606W	F775W/F814W	F105W
459_12	F438W	F625W/F606W	F775W/F814W	F105W
459_17	F438W	F625W/F606W	F775W/F814W	F105W
459_18	F438W	F625W/F606W	F775W/F814W	F105W
459_19	F438W	F625W/F606W	F775W/F814W	F105W
459_24	F438W	F625W/F606W	F775W/F814W	F105W
459_25	F438W	F625W/F606W	F775W/F814W	F105W
459_27	F438W	F625W/F606W	F775W/F814W	F105W
459_2	F438W	F625W/F606W	F775W/F814W	F105W
459_3	F438W	F625W/F606W	F775W/F814W	F105W
459_5	F438W	F625W/F606W	F775W/F814W	F105W
459_8	F438W	F625W/F606W	F775W/F814W	F105W
460_13	F438W	F625W/F606W	F775W/F814W	F105W
460_15	F438W	F625W/F606W	F775W/F814W	F105W
460_17	F438W	F625W/F606W	F775W/F814W	F105W
460_19[2]	F438W	F625W/F606W[1]	F775W/F814W[1]	F105W

Table A.1: The HST filters that cover best the restframe u, g, r and i bands. The Object ID has form: [group ID]_[galaxy], where the group ID is unique number of the galaxy group which member the object is and galaxy is the ordinal number of the object in its group. Columns u, g, r and i are the name(s) of the filter(s) that cover the corresponding band. The filter coverages [Rodrigo et al., nd] are compared with the calculated redshifts of the restframe bands.

[1]The filter is used in making the RGB images of the object.

[2]The object has a RGB image.

Bibliography

Abraham, R. G., van den Bergh, S., Glazebrook, K., Ellis, R. S., Santiago, B. X., Surma, P., and Griffiths, R. E. (1996). The Morphologies of Distant Galaxies. II. Classifications from the Hubble Space Telescope Medium Deep Survey. *The Astrophysical Journal, Supplement Series*, 107:1.

Athanassoula, E., Morin, S., Wozniak, H., Puy, D., Pierce, M. J., Lombard, J., and Bosma, A. (1990). The shape of bars in early-type barred galaxies. *Monthly Notices of the Royal Astronomical Society*, 245:130–139.

Bailey, M. E., Butler, C. J., and McFarland, J. (2005). Bailey, Butler, McFarland: Discovery of Spiral Nebulae: Unwinding the discovery of spiral nebulae. *Astronomy and Geophysics*, 46(2):2.26–2.28.

Bevington, P. and Robinson, D. (2003). *Data reduction and error analysis for the physical sciences*. McGraw-Hill Higher Education. McGraw-Hill, 3rd edition.

Bianconi, M., Luoma, A. J. I., Finoguenov, A., Smith, G. P., Haines, C. P., and McGee, S. L. (In preparation). Structural properties of galaxies in the LoCuSS survey.

Bianconi, M., Smith, G. P., Haines, C. P., McGee, S. L., Finoguenov, A., and Egami, E. (2017). LoCuSS: Pre-processing in galaxy groups falling into massive galaxy clusters at z=0.2. *ArXiv e-prints*.

Binney, J. and Tremaine, S. (1987). *Galactic dynamics*. Princeton, NJ, Princeton University Press, 1987, 747 p.

Bundy, K., Ellis, R. S., Conselice, C. J., Cooper, M., Weiner, B., Taylor, J., Willmer, C., and DEEP2 Team (2005). The Mass-Dependent Evolution of Field Galaxies. In *American Astronomical Society Meeting Abstracts*, volume 37 of *Bulletin of the American Astronomical Society*, page 1235.

CANDELS (2013). Latest CANDELS Data Release. http://candels.ucolick.org/data_access/Latest_Release.html. Last accessed on Dec 8, 2017.

Conselice, C. J. (2014). The Evolution of Galaxy Structure Over Cosmic Time. *Annual Review of Astronomy & Astrophysics*, 52:291–337.

Conselice, C. J. (2003). The Relationship between Stellar Light Distributions of Galaxies and Their Formation Histories. *The Astrophysical Journal, Supplement Series*, 147:1–28.

Conselice, C. J., Bershady, M. A., and Jangren, A. (2000). The Asymmetry of Galaxies: Physical Morphology for Nearby and High-Redshift Galaxies. *The Astrophysical Journal*, 529:886–910.

de Vaucouleurs, G. (1948). Recherches sur les Nebuleuses Extragalactiques. *Annales d'Astrophysique*, 11:247.

Elmegreen, D. M. and Elmegreen, B. G. (1987). Arm classifications for spiral galaxies. *The Astrophysical Journal*, 314:3–9.

Erfanianfar, G., Popesso, P., Finoguenov, A., Wuyts, S., Wilman, D., Biviano, A., Ziparo, F., Salvato, M., Nandra, K., Lutz, D., Elbaz, D., Dickinson, M., Tanaka, M., Mirkazemi, M., Balogh, M. L., Altieri, M. B., Aussel, H., Bauer, F., Berta, S., Bielby, R. M., Brandt, N., Cappelluti, N., Cimatti, A., Cooper, M., Fadda,

D., Ilbert, O., Le Floch, E., Magnelli, B., Mulchaey, J. S., Nordon, R., Newman, J. A., Poglitsch, A., and Pozzi, F. (2014). The evolution of star formation activity in galaxy groups. *Monthly Notices of the Royal Astronomical Society*, 445:2725–2745.

Freeman, P. E., Izbicki, R., Lee, A. B., Newman, J. A., Conselice, C. J., Koekemoer, A. M., Lotz, J. M., and Mozena, M. (2013). New image statistics for detecting disturbed galaxy morphologies at high redshift. *Monthly Notices of the Royal Astronomical Society*, 434:282–295.

Gehrels, N. (1986). Confidence limits for small numbers of events in astrophysical data. *The Astrophysical Journal*, 303:336–346.

Grogin, N. A., Kocevski, D. D., Faber, S. M., Ferguson, H. C., Koekemoer, A. M., Riess, A. G., Acquaviva, V., Alexander, D. M., Almaini, O., Ashby, M. L. N., Barden, M., Bell, E. F., Bournaud, F., Brown, T. M., Caputi, K. I., Casertano, S., Cassata, P., Castellano, M., Challis, P., Chary, R.-R., Cheung, E., Cirasuolo, M., Conselice, C. J., Cooray, A. R., Croton, D. J., Daddi, E., Dahlen, T., Davé, R., de Mello, D. F., Dekel, A., Dickinson, M., Dolch, T., Donley, J. L., Dunlop, J. S., Dutton, A. A., Elbaz, D., Fazio, G. G., Filippenko, A. V., Finkelstein, S. L., Fontana, A., Gardner, J. P., Garnavich, P. M., Gawiser, E., Giavalisco, M., Grazian, A., Guo, Y., Hathi, N. P., Häussler, B., Hopkins, P. F., Huang, J.-S., Huang, K.-H., Jha, S. W., Kartaltepe, J. S., Kirshner, R. P., Koo, D. C., Lai, K., Lee, K.-S., Li, W., Lotz, J. M., Lucas, R. A., Madau, P., McCarthy, P. J., McGrath, E. J., McIntosh, D. H., McLure, R. J., Mobasher, B., Moustakas, L. A., Mozena, M., Nandra, K., Newman, J. A., Niemi, S.-M., Noeske, K. G., Papovich, C. J., Pentericci, L., Pope, A., Primack, J. R., Rajan, A., Ravindranath, S., Reddy, N. A., Renzini, A., Rix, H.-W., Robaina, A. R., Rodney, S. A., Rosario, D. J., Rosati, P., Salimbeni, S., Scarlata, C., Siana, B., Simard, L., Smidt, J.,

Somerville, R. S., Spinrad, H., Straughn, A. N., Strolger, L.-G., Telford, O., Teplitz, H. I., Trump, J. R., van der Wel, A., Villforth, C., Wechsler, R. H., Weiner, B. J., Wiklind, T., Wild, V., Wilson, G., Wuyts, S., Yan, H.-J., and Yun, M. S. (2011). Candels: The cosmic assembly near-infrared deep extragalactic legacy survey. *The Astrophysical Journal Supplement Series*, 197(2):35.

Haines, C. P., Finoguenov, A., Smith, G. P., Babul, A., Egami, E., Mazzotta, P., Okabe, N., Pereira, M. J., Bianconi, M., McGee, S. L., Ziparo, F., Campusano, L. E., and Loyola, C. (2017). LoCuSS: The infall of X-ray groups onto massive clusters. *ArXiv e-prints*.

Harrison, E. R. and Noonan, T. W. (1979). Interpretation of extragalactic redshifts. *The Astrophysical Journal*, 232:18.

Hubble, E. P. (1926). Extragalactic nebulae. *The Astrophysical Journal*, 64.

Hubble, E. P. (1936). *Realm of the Nebulae*. New Haven: Yale University Press, 1936. ISBN 9780300025002.

Karttunen, H., Donner, K. J., Kröger, P., Oja, H., and Poutanen, M. (2010). *Tähtitieteen Perusteet*. Tähtitieteellinen yhdistys Ursa.

Kepple, G. R. and Sanner, G. W. (1998). *The Night Sky Observer's Guide Vol. 1*. Richmond, VA: Willmann-Bell.

King, I. (1962). The structure of star clusters. I. an empirical density law. *The Astronomical Journal*, 67:471.

Koekemoer, A. M., Faber, S. M., Ferguson, H. C., Grogin, N. A., Kocevski, D. D., Koo, D. C., Lai, K., Lotz, J. M., Lucas, R. A., McGrath, E. J., Ogaz, S., Rajan, A., Riess, A. G., Rodney, S. A., Strolger, L., Casertano, S., Castellano, M., Dahlen, T., Dickinson, M., Dolch, T., Fontana, A., Giavalisco, M., Grazian, A., Guo, Y.,

Hathi, N. P., Huang, K.-H., van der Wel, A., Yan, H.-J., Acquaviva, V., Alexander, D. M., Almaini, O., Ashby, M. L. N., Barden, M., Bell, E. F., Bournaud, F., Brown, T. M., Caputi, K. I., Cassata, P., Challis, P. J., Chary, R.-R., Cheung, E., Cirasuolo, M., Conselice, C. J., Cooray, A. R., Croton, D. J., Daddi, E., Davé, R., de Mello, D. F., de Ravel, L., Dekel, A., Donley, J. L., Dunlop, J. S., Dutton, A. A., Elbaz, D., Fazio, G. G., Filippenko, A. V., Finkelstein, S. L., Frazer, C., Gardner, J. P., Garnavich, P. M., Gawiser, E., Gruetzbauch, R., Hartley, W. G., Häussler, B., Herrington, J., Hopkins, P. F., Huang, J.-S., Jha, S. W., Johnson, A., Kartaltepe, J. S., Khostovan, A. A., Kirshner, R. P., Lani, C., Lee, K.-S., Li, W., Madau, P., McCarthy, P. J., McIntosh, D. H., McLure, R. J., McPartland, C., Mobasher, B., Moreira, H., Mortlock, A., Moustakas, L. A., Mozena, M., Nandra, K., Newman, J. A., Nielsen, J. L., Niemi, S., Noeske, K. G., Papovich, C. J., Pentericci, L., Pope, A., Primack, J. R., Ravindranath, S., Reddy, N. A., Renzini, A., Rix, H.-W., Robaina, A. R., Rosario, D. J., Rosati, P., Salimbeni, S., Scarlata, C., Siana, B., Simard, L., Smidt, J., Snyder, D., Somerville, R. S., Spinrad, H., Straughn, A. N., Telford, O., Teplitz, H. I., Trump, J. R., Vargas, C., Villforth, C., Wagner, C. R., Wandro, P., Wechsler, R. H., Weiner, B. J., Wiklind, T., Wild, V., Wilson, G., Wuyts, S., and Yun, M. S. (2011). Candels: The cosmic assembly near-infrared deep extragalactic legacy survey—the hubble space telescope observations, imaging data products, and mosaics. *The Astrophysical Journal Supplement Series*, 197(2):36.

Koppelman, M. (2005). Uncertainty Analysis in Photometric Observations. *Society for Astronomical Sciences Annual Symposium*, 24:107.

Lauer, T. R., Ajhar, E. A., Byun, Y.-I., Dressler, A., Faber, S. M., Grillmair, C., Kormendy, J., Richstone, D., and Tremaine, S. (1995). The Centers of Early-Type Galaxies with HST.I.An Observational Survey. *The Astronomical Journal*, 110:2622.

Laureijs, R., Amiaux, J., Arduini, S., Augueres, J. ., Brinchmann, J., Cole, R., Cropper, M., Dabin, C., Duvet, L., Ealet, A., and et al. (2011). Euclid Definition Study Report. *ArXiv e-prints*.

Leauthaud, A., Finoguenov, A., Kneib, J.-P., Taylor, J. E., Massey, R., Rhodes, J., Ilbert, O., Bundy, K., Tinker, J., George, M. R., Capak, P., Koekemoer, A. M., Johnston, D. E., Zhang, Y.-Y., Cappelluti, N., Ellis, R. S., Elvis, M., Giodini, S., Heymans, C., Le Fèvre, O., Lilly, S., McCracken, H. J., Mellier, Y., Réfrégier, A., Salvato, M., Scoville, N., Smoot, G., Tanaka, M., Van Waerbeke, L., and Wolk, M. (2010). A Weak Lensing Study of X-ray Groups in the Cosmos Survey: Form and Evolution of the Mass-Luminosity Relation. *The Astrophysical Journal*, 709:97–114.

Levenberg, K. (1944). A method for the solution of certain non-linear problems in least squares. *Quarterly of Applied Mathematics*, 2:164–168.

Lotz, J. M., Primack, J., and Madau, P. (2004). A New Nonparametric Approach to Galaxy Morphological Classification. *The Astronomical Journal*, 128:163–182.

Marquardt, D. W. (1963). An algorithm for least-squares estimation of nonlinear parameters. *Journal of the Society for Industrial and Applied Mathematics*, 11(2):431–441.

Moffat, A. F. J. (1969). A Theoretical Investigation of Focal Stellar Images in the Photographic Emulsion and Application to Photographic Photometry. *Astronomy & Astrophysics*, 3:455.

Mortlock, A., Conselice, C. J., Bluck, A. F. L., Bauer, A. E., Grützbauch, R., Buitrago, F., and Ownsworth, J. (2011). A deep probe of the galaxy stellar mass functions at $z \sim$ 1-3 with the GOODS NICMOS Survey. *Monthly Notices of the Royal Astronomical Society*, 413:2845–2859.

Peng, C. Y. (2014). GALFIT Home Page. https://users.obs.carnegiescience.edu/peng/work/galfit/galfit.html. Last accessed on Nov 29, 2017.

Peng, C. Y., Ho, L. C., Impey, C. D., and Rix, H.-W. (2002). Detailed Structural Decomposition of Galaxy Images. *The Astronomical Journal*, 124:266–293.

Peng, C. Y., Ho, L. C., Impey, C. D., and Rix, H.-W. (2010a). Detailed Decomposition of Galaxy Images. II. Beyond Axisymmetric Models. *The Astronomical Journal*, 139:2097–2129.

Peng, C., Y. (2002). *GALFIT USER'S MANUAL*. https://users.obs.carnegiescience.edu/peng/work/galfit/README.pdf.

Peng, Y.-j., Lilly, S. J., Kovač, K., Bolzonella, M., Pozzetti, L., Renzini, A., Zamorani, G., Ilbert, O., Knobel, C., Iovino, A., Maier, C., Cucciati, O., Tasca, L., Carollo, C. M., Silverman, J., Kampczyk, P., de Ravel, L., Sanders, D., Scoville, N., Contini, T., Mainieri, V., Scodeggio, M., Kneib, J.-P., Le Fèvre, O., Bardelli, S., Bongiorno, A., Caputi, K., Coppa, G., de la Torre, S., Franzetti, P., Garilli, B., Lamareille, F., Le Borgne, J.-F., Le Brun, V., Mignoli, M., Perez Montero, E., Pello, R., Ricciardelli, E., Tanaka, M., Tresse, L., Vergani, D., Welikala, N., Zucca, E., Oesch, P., Abbas, U., Barnes, L., Bordoloi, R., Bottini, D., Cappi, A., Cassata, P., Cimatti, A., Fumana, M., Hasinger, G., Koekemoer, A., Leauthaud, A., Maccagni, D., Marinoni, C., McCracken, H., Memeo, P., Meneux, B., Nair, P., Porciani, C., Presotto, V., and Scaramella, R. (2010b). Mass and Environment as Drivers of Galaxy Evolution in SDSS and zCOSMOS and the Origin of the Schechter Function. *The Astrophysical Journal*, 721:193–221.

Petrosian, V. (1976). Surface brightness and evolution of galaxies. *The Astrophysical Journal, Letters*, 209:L1–L5.

Richmond, M. (2010). CCD Gain. http://spiff.rit.edu/classes/phys445/

lectures/gain/gain.html Rochester Institute of Technology Dept. of Physics. Last accessed on Jan 2, 2018.

Rodrigo, C., Solano, E., and Bayo, A. (n.d.). The SVO Filter Profile Service. http://svo2.cab.inta-csic.es/svo/theory/fps3/index.php?mode=browse&gname=HST Spanish Virtual Observatory. Last accessed on Nov 25, 2017.

Sandage, A. (1961). *The Hubble atlas of galaxies*. Washington: Carnegie Institution, 1961.

Sérsic, J. L. (1963). Influence of the atmospheric and instrumental dispersion on the brightness distribution in a galaxy. *Boletin de la Asociacion Argentina de Astronomia La Plata Argentina*, 6:41.

Simard, L. (1998). GIM2D: an IRAF package for the Quantitative Morphology Analysis of Distant Galaxies. In Albrecht, R., Hook, R. N., and Bushouse, H. A., editors, *Astronomical Data Analysis Software and Systems VII*, volume 145 of *Astronomical Society of the Pacific Conference Series*, page 108.

Strateva, I., Ivezić, Ž., Knapp, G. R., Narayanan, V. K., Strauss, M. A., Gunn, J. E., Lupton, R. H., Schlegel, D., Bahcall, N. A., Brinkmann, J., Brunner, R. J., Budavári, T., Csabai, I., Castander, F. J., Doi, M., Fukugita, M., Győry, Z., Hamabe, M., Hennessy, G., Ichikawa, T., Kunszt, P. Z., Lamb, D. Q., McKay, T. A., Okamura, S., Racusin, J., Sekiguchi, M., Schneider, D. P., Shimasaku, K., and York, D. (2001). Color Separation of Galaxy Types in the Sloan Digital Sky Survey Imaging Data. *The Astronomical Journal*, 122:1861–1874.

STSCI (2012). Hubble Space Telescope ACS Flux Calibration and Zeropoints. http://www.stsci.edu/hst/acs/analysis/zeropoints The Space Telescope Science Institute / Association of Universities for Research in Astronomy. Last accessed on Nov 28, 2017.

STSCI (n.d.a). Hubble Space Telescope WFC3 Flight Detectors. http://www.stsci.edu/hst/wfc3/ins_performance/detectors The Space Telescope Science Institute / Association of Universities for Research in Astronomy. Last accessed on Jun 16, 2016.

STSCI (n.d.b). mknoise noao.artdata. http://stsdas.stsci.edu/cgi-bin/gethelp.cgi?mknoise The Space Telescope Science Institute. Last accessed on Nov 7, 2017.

Subaru Telescope, NAOJ (2000–2009). https://www.naoj.org/Observing/Instruments/SCam/parameters.html. Last accessed Jul 3. 2017.

Taylor, E. N., Hopkins, A. M., Baldry, I. K., Brown, M. J. I., Driver, S. P., Kelvin, L. S., Hill, D. T., Robotham, A. S. G., Bland-Hawthorn, J., Jones, D. H., Sharp, R. G., Thomas, D., Liske, J., Loveday, J., Norberg, P., Peacock, J. A., Bamford, S. P., Brough, S., Colless, M., Cameron, E., Conselice, C. J., Croom, S. M., Frenk, C. S., Gunawardhana, M., Kuijken, K., Nichol, R. C., Parkinson, H. R., Phillipps, S., Pimbblet, K. A., Popescu, C. C., Prescott, M., Sutherland, W. J., Tuffs, R. J., van Kampen, E., and Wijesinghe, D. (2011). Galaxy And Mass Assembly (GAMA): stellar mass estimates. *Monthly Notices of the Royal Astronomical Society*, 418:1587–1620.

van den Bergh, S. (1960). A Preliminary Luminosity Clssification of Late-Type Galaxies. *The Astrophysical Journal*, 131:215.

van den Bergh, S. (1976). A new classification system for galaxies. *The Astrophysical Journal*, 206:883–887.

van der Kruit, P. C. and Searle, L. (1981). Surface photometry of edge-on spiral galaxies. I - A model for the three-dimensional distribution of light in galactic disks. *Astronomy & Astrophysics*, 95:105–115.

Vogelsberger, M., Genel, S., Springel, V., Torrey, P., Sijacki, D., Xu, D., Snyder, G., Nelson, D., and Hernquist, L. (2014). Introducing the Illustris Project: simulating the coevolution of dark and visible matter in the Universe. *Monthly Notices of the Royal Astronomical Society*, 444:1518–1547.